Contract No:

This document was prepared in conjunction with work accomplished under Contract No. DE-AC09-08SR22470 with the U.S. Department of Energy (DOE) Office of Environmental Management (EM).

Disclaimer:

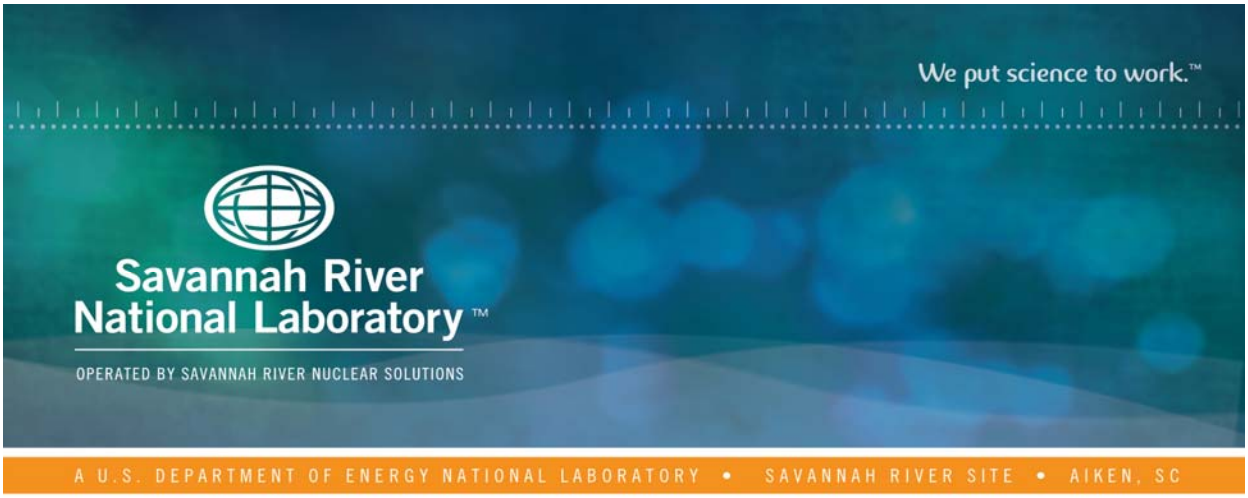

Nitric-Glycolic Flowsheet Testing for Maximum Hydrogen Generation Rate

C.J. Martino

J.D. Newell

M.S. Williams

March 2016

SRNL-STI-2015-00130, Revision 0

DISCLAIMER

Printed in the United States of America

Prepared for
U.S. Department of Energy

SRNL-STI-2015-00130
Revision 0

Keywords: *Alternate Reductant, DWPF, CPC, Catalytic Hydrogen*

Retention: *Permanent*

Nitric-Glycolic Flowsheet Testing for Maximum Hydrogen Generation Rate

C.J. Martino
J.D. Newell
M.S. Williams

March 2016

Prepared for the U.S. Department of Energy under contract number DE-AC09-08SR22470.

Savannah River National Laboratory™
OPERATED BY SAVANNAH RIVER NUCLEAR SOLUTIONS

REVIEWS AND APPROVALS

AUTHORS:

_____
C.J. Martino, Process Technology Programs Date

_____
J.D. Newell, Process Technology Programs Date

_____
M.S. Williams, Process Technology Programs Date

TECHNICAL REVIEW:

_____
T.E. Smith, Separation & Actinide Science, Reviewed per E7 2.60 Date

APPROVAL:

_____
F.M. Pennebaker, Manager Date
Process Technology Programs

_____
D.E. Dooley, Manager Date
Environmental & Chemical Process Technology Research Programs

_____
E.J. Freed, Manager Date
DWPF/Saltstone Facility Engineering

EXECUTIVE SUMMARY

The Defense Waste Processing Facility (DWPF) at the Savannah River Site is developing for implementation a flowsheet with a new reductant to replace formic acid. Glycolic acid has been tested over the past several years and found to effectively replace the function of formic acid in the DWPF chemical process. The nitric-glycolic flowsheet reduces mercury, significantly lowers the chemical generation of hydrogen and ammonia, allows purge reduction in the Sludge Receipt and Adjustment Tank (SRAT), stabilizes the pH and chemistry in the SRAT and the Slurry Mix Evaporator (SME), allows for effective adjustment of the SRAT/SME rheology, and is favorable with respect to melter flammability.

The objective of this work was to perform DWPF Chemical Process Cell (CPC) testing at conditions that would bound the catalytic hydrogen production for the nitric-glycolic flowsheet. Four 4-L scale CPC simulations were performed using a Sludge Batch 8 simulant with 125% of HM (H-area Modified) sludge levels of noble metals and 1% mercury on a total solids basis. The simulant runs were performed using 110% acid stoichiometric ratio and various boil-up rate schemes. The tests were designed to be conducive to catalytic hydrogen generation (high concentration of noble metals, high stoichiometric excess acid) with the objective of producing a maximum process-representative hydrogen generation during the CPC processing with the glycolic acid flowsheet.

The following are key observations from this work:

1. When compared to the nitric-formic flowsheet, hydrogen production remained very low for these nitric-glycolic flowsheet tests. For laboratory results converted to the DWPF scale but without including measurement uncertainty, the maximum hydrogen production and release rate for the current runs was 0.0028 lb/hr in the SRAT and 0.0024 lb/hr in the SME. For this testing, the maximum hydrogen production and release rate was 0.43% of the current SRAT limit of 0.65 lb/hr and 1.1 % of the current SME limit of 0.223 lb/hr.

2. Reviewing current and previous nitric-glycolic flowsheet runs for which formic acid was not added and heat transfer or heating rod temperature issues were not encountered, the highest peak DWPF-scale hydrogen generation rate in the SRAT cycle including measurement uncertainty was 0.0066 lb/hr (at the upper bound of the 95% confidence interval) in three separate tests (GN41, GN70, and GN82). Similarly, the highest peak DWPF-scale hydrogen generation rate in the SME cycle including measurement uncertainty was 0.0087 lb/hr (at the upper bound of the 95% confidence interval) for 220-L scaled run GN79. Run GN36 produced the highest valid hydrogen generation rate in the SME (0.0111 lb/hr), but formic acid was added with the frit addition and difficulties with the measurement prevent estimation of the measurement uncertainty.

3. Run GN79 had the highest overall peak hydrogen concentration measured for the runs that did not have formic acid addition in the SRAT or the SME and that did not have temperature excursions or heat transfer issues. The SME cycle of GN79 had a peak hydrogen concentration of 0.038 vol% (including measurement uncertainty), which is only 0.95% of the lower flammability limit of hydrogen in air. The peak levels of hydrogen produced during the nitric-glycolic flowsheet testing were reliably and significantly less than 25% of the lower flammability limit of hydrogen in air.

4. For two runs in this testing, additional glycolic acid was introduced at the end of the SME cycle. The glycolic acid dump appeared to lower the rate of hydrogen generation that was occurring at the end of the SME cycle. The biggest impact of the glycolic acid dump was the increase in the amount of metal cations in solution, specifically iron, aluminum, and nickel. After the glycolic

acid dump, the oxalate in the SME product became nearly fully soluble. An increase in rheological properties and foaming during processing were encountered after the glycolic acid dump.

5. The pH measurements of the SRAT products were approximately 4.5 and remained at nearly this level through the SME cycle. The additional glycolic acid dump performed on two of the runs further reduced the pH of the SME material to approximately 3.

6. The loss of glycolate in the SRAT cycles was ranged from 13% to 19% and the nitrite-to-nitrate conversion ranged from 51% to 64%. These values are in line with previous nitric-glycolic flowsheet testing.

7. The largest peak in hexamethyldisiloxane concentration from the decomposition of diluted antifoam was 2020 ppmv for a very short duration during a SRAT cycle. This concentration corresponds to a peak generation or release rate of 14.0 mol/hr on the DWPF scale.

TABLE OF CONTENTS

LIST OF TABLES

LIST OF FIGURES

LIST OF ABBREVIATIONS

ACTL	Aiken County Technology Laboratory
ARP	Actinide Removal Process
CC_{hot}	Closed (Sealed) Crucible with Hot insertion
CC_{ramp}	Closed (Sealed) Crucible with Ramped heat treatment
CEF	Cold-cap Evaluation Furnace
CETL	Clemson Environmental Technologies Laboratory
CQ	Caustic Quench
CPC	Chemical Process Cell
DI	Deionized
DWPF	Defense Waste Processing Facility
ELN	Electronic Laboratory Notebook
FAVC	Formic Acid Vent Condenser
FTIR	Fourier Transform Infrared
GC	Gas Chromatography
GF	Nitric-Glycolic-Formic Flowsheet
GN	Nitric-Glycolic Flowsheet
HM	H-area Modified
HMDSO	Hexamethyldisiloxane
IC	Ion Chromatography
ICP-ES	Inductively Coupled Plasma – Emission Spectroscopy
KMA	Koopman Minimum Acid
M&TE	Measurement & Test Equipment
MCU	Modular Caustic-Side Solvent Extraction Unit
MS	Mass Spectroscopy
MWWT	Mercury Water Wash Tank
NCR	Non-Conformance Report
NIST	National Institute of Standards and Technology
n.m.	Not measured
PEG	Polyethylene Glycol
PSAL	Process Science and Analytical Laboratory
REDOX	REDuction/OXidation
SB	Sludge Batch
scfm	Standard cubic feet per minute
SE	Strip Effluent
SME	Slurry Mix Evaporator
SRAT	Sludge Receipt and Adjustment Tank
SRNL	Savannah River National Laboratory
SRR	Savannah River Remediation
SRS	Savannah River Site
TTQAP	Task Technical and Quality Assurance Plan
TTR	Technical Task Request

1.0 Introduction

1.1 Background

The Defense Waste Processing Facility (DWPF) at the Savannah River Site (SRS) is developing for implementation a flowsheet with a new reductant to replace formic acid. Glycolic acid has been tested over the past several years and found to effectively replace the function of formic acid in the DWPF chemical process. The nitric-glycolic flowsheet reduces mercury, significantly lowers the chemical generation of hydrogen and ammonia (which allows purge reduction in the Sludge Receipt and Adjustment Tank (SRAT)), stabilizes the pH and chemistry in the SRAT and the Slurry Mix Evaporator (SME), allows for effective adjustment of the SRAT/SME rheology, and is favorable with respect to melter flammability. As part of process implementation into the facility, Savannah River Remediation (SRR) has identified testing necessary to provide additional data for safety basis evaluations. SRR issued a Technical Task Request (TTR) covering the scope of demonstration of the bounding hydrogen generation in the SRAT/SME, the development of a model for the REDuction/OXidation (REDOX) for the nitric-glycolic flowsheet, and further understanding of the chemistry related to the flowsheet.[1] Savannah River National Laboratory (SRNL) issued a task Technical and Quality Assurance Plan (TTQAP) that addresses the bounding hydrogen generation test scope.[2] Reports addressing the REDOX and chemistry portions of the TTR will be issued separately from the bounding hydrogen generation work presented here.

1.2 Objectives

The major objective of this testing was to demonstrate the maximum flammable gas generation to provide input into the DWPF safety basis documents for the nitric-glycolic flowsheet. Other objectives included the solubility of key chemical components and the demonstration of maximum throughput performance.

1.3 Approach

SRNL issued a white paper detailing and justifying the approach for carrying out the bounding hydrogen generation runs.[3] Due to the uncertainty in how the boil-up rates impact the generation of hydrogen, it was recommended that four SRAT/SME cycles be completed to determine the bounding hydrogen generation for the nitric-glycolic flowsheet.

Table 1-1 contains the matrix of testing that was performed using two different heating rates. The boil-up rates have the possibility of impacting the hydrogen production. Lower boil-up rates are closer to matching the DWPF facility and extends the length of processing. For the nitric-formic flowsheet, higher boil-up rates allow for more catalytic hydrogen production in the SME, where the purge rate is lower. The upper boiling rate is scaled to the design basis of 5000 lb/hr of steam. The lower boiling rate was accomplished by alternating periods of design basis boiling and simmering with minimal overheads production to result in an average heating rate of 2500 lb/hr of steam. Table 1-2 contains additional test plan details from the white paper developed to bound hydrogen formation in the SRAT and SME.[3] A glycolic acid dump, which simulates an inadvertent transfer of glycolic acid at the end of the SME cycle, was performed with an additional hour at boiling for two of the runs. Tests were performed on the four-liter scale.

Table 1-1. Test matrix for bounding hydrogen generation tests (heating to DWPF scale steam flow in the SRAT and SME)

Test Name	Test Description	SRAT Heating Rate (lb/hr of steam)	SME Heating Rate (lb/hr of steam)
GN80	Fast SRAT/Fast SME	5000	5000
GN81	Fast SRAT/Slow SME	5000	2500
GN82	Slow SRAT/Fast SME	2500	5000
GN83	Slow SRAT/Slow SME	2500	2500

Table 1-2. Details of test conditions

Scale: 4 liter vessel

Purge: Scaled air purge of 93.7 scfm (standard ft^3 per min.) in SRAT and 74 scfm in the SME

Sludge Volume: Scaled 6000 gallons of Sludge Batch 8 simulant

Noble Metals: Level of noble metals at 25% higher than HM sludge, 1% mercury.

Actinide Removal Process (ARP): ARP slurry not added

Acid Stoichiometry: 110% Koopman Minimum Acid stoichiometry is recommended (as was used in GN73, GN75, GN77, GN78).[4] The molar acid split is 54.2 mol % glycolic acid. REDOX target is 0.14.

Dewater: Concentrate the slurry to 28 wt % total solids in SRAT product. For high dewater rates, heat at a scaled 5000 lb/hr steam flow. For low dewater rates, dewater in four segments; two having a scaled 5000 lb/hr steam flow equivalent and two simmering the SRAT, for an average of a scaled 2500 lb/hr steam flow equivalent.

Modular Caustic-Side Solvent Extraction Unit (MCU) Strip Effluent (SE): Add a scaled 18,000 gallons of 0.0125 M boric acid solution without solvent to SRAT at 10 gallons per minute.

Reflux: The boiling time is far in excess of time required to steam strip the mercury concentration below 0.45 wt %, assuming 750 lb steam per lb Hg stripped.

Canister Decontamination Addition: In the SME cycle, add six 1000 gallon additions of water followed by a boil off of 1,000 gallons of water after each addition to simulate the addition of water generated during decontamination of canisters. For high dewater rates, heat at a scaled 5000 lb/hr steam flow. For low dewater rates, the first three of the additions will be simmered and the final three additions will have a scaled 5000 lb/hr steam flow equivalent, for an average of a scaled 2500 lb/hr steam flow equivalent.

Process Frit Addition: In the SME cycle, add two process frit slurry additions of 50 wt% frit each followed by boil off of water. Frit additions will not include formic acid. The target waste loading is 36 wt % and the target final concentration of 48 wt % total solids.

The planned data collection during this study included at a minimum the following items:

- SRAT and SME product anion and cation data, physical property data, and pH profile
- SME product rheology, before and after glycolic acid dump
- REDOX of glass produced from SME product, prior to and after the acid dump
- SRAT and SME condensate anion and cation data
- SRAT and SME offgas data

2.0 Experimental Procedure

Four lab-scale SRAT/SME runs were performed with Tank 40H sludge slurry simulants based on the composition of Sludge Batch 8. The sludge was the same simulant blend used in the nitric-glycolic flowsheet scaled demonstration.[4] Testing was completed at the Aiken County Technology Laboratory (ACTL). The four SRAT/SME runs were performed in pairs, with the first pair performed during the week of January 26 through 30, 2015 and the second pair performed during the week of February 9 through 13, 2015. All runs were performed using around-the-clock operations.

The SRAT cycles were coupled, including a dilute boric acid addition and boil-off to emulate strip effluent from MCU. However, ARP product and the solvent component of MCU strip effluent were not added during these tests. On the DWPF scale, 6000 gallons of sludge and 18000 gallons of strip effluent were added during SRAT processing for all tests. The only change from run-to-run was the heating rates during the SRAT and SME cycles.

An additional glycolic acid dump was performed at the end of the SME cycle of tests GN80 and GN81. The acid dump involved bringing the SME product temperature to 93 °C, adding the same quantity of glycolic acid as was added at the beginning of the SRAT, and boiling for at least one hour.

2.1 Process and Sample Analytical Methods

The automated data acquisition system developed for the 4-L lab-scale SRAT/SME was used to collect electronic data on a computer. Collected data included SRAT slurry temperature, bath temperatures for the cooling water to the SRAT condenser and Formic Acid Vent Condenser (FAVC), slurry pH, SRAT mixer speed and torque, air and helium purge flows (helium is used as an internal standard and is set to 0.5% of the nominal SRAT air purge flow), temperatures in the SRAT condenser, FAVC, and ammonia scrubber, the individual temperatures of the two heating rods, the total rod current draw, and the total rod power consumption (used for calculation of a time-dependent heat transfer coefficient between the rods and slurry). Gas sampling, taken off of the vent of the FAVC, is discussed in Section 2.4.

Process samples (liquid, solid, or slurry) were analyzed by various methods. Slurry and supernate elemental compositions were determined by inductively coupled plasma – emission spectroscopy (ICP-ES). Slurry samples were calcined at 1100 °C and then digested prior to analysis by either lithium metaborate and/or sodium peroxide fusions at the Process Science and Analytical Laboratory (PSAL). The main advantage of this approach is to permit easier comparisons between SRAT product elements and sludge elements. Noble metals and mercury are added at the beginning of each SRAT test. Trimming a known concentration into each SRAT batch is preferred because the resulting material balance is more accurate than measuring these components by ICP-ES. Analysis for mercury in slurry is by aqua regia digestion followed by ICP-ES analysis, and analysis for mercury in supernate and condensate is by water dilution followed by ICP-ES analysis.

Water soluble slurry anions were determined by ion chromatography (IC) on caustic quench (CQ)

preparations of slurry followed by 100-fold weighted dilutions with water and filtration to remove the remaining insoluble solids.[5] IC results were obtained on a sample of the SRAT products, the SME product slurries and the post-glycolic acid dump products. SRAT product and SME product slurry samples were submitted to PSAL for mercury analysis by ICP-ES. Simulants, SRAT products, and SME products were analyzed by PSAL for slurry and supernate density using the Anton-Parr DMA-4500 density instrument. The base equivalents for input into the stoichiometric acid equation were determined for the starting sludge simulants by titrating to pH 7 using the PSAL Mettler-Toledo auto-titrator.

Flow curves for the SRAT and SME products were obtained by using a Haake RS600 rheometer and the current DWPF simulant rheology protocol.[6] The up and down curves were fit to a Bingham plastic model to determine yield stress and consistency. Down flow curve data are the generally preferred choice for comparisons between systems.

2.2 Simulant Preparation and Characterization

The simulant prepared for this testing was from the simulant batch prepared for the nitric-glycolic flowsheet scaled demonstration.[4] In 2007, three generic simulants designated A, B, and C were prepared at the Clemson Environmental Technologies Laboratory (CETL) [7]. The simulants were designed to be blended in order to achieve a desired chemical composition. Other chemicals could then be added to supply missing elements. In order to make a simulant similar in composition to Sludge Batch 8, the base simulant was prepared by blending 87 liters of simulant B with 156 liters of simulant C and 293 liters of deionized (DI) water. Soluble supernate species and insoluble trim chemicals were added. The resulting BC blended simulant composition and comparison to SB8-Tank 40 are shown in Table 2-1.

Table 2-1: Elemental composition of SRAT feeds calcined at 1100° C, wt%

	A	B	C	SB8 Tk40	BC Blend +supernate
Al	13.60	6.3	13.2	9.51	10.3
Ba	0.24	0.2	0.2	0.12	0.2
Ca	4.26	3.7	2.5	1.44	1.7
Cu	0.09	0.1	0.1	0.05	0.1
Fe	36.45	37.6	35.5	22.15	25.2
K	0.15	0.2	0.2	0.11	0.2
Mg	0.16	0.1	0.2	0.31	0.3
Mn	3.87	12.1	4.1	7.18	7.9
Na	4.16	4.8	3.4	17.39	15.0
Ni	0.34	0.3	4.9	2.18	2.4
S	0.41	0.3	0.3	0.55	0.4
Si	1.28	1.4	1.3	1.36	1.8
Ti	0.03	0.0	0.0	0.02	<0.100
Zn	0.05	0.1	0.1	0.04	<0.100
Zr	0.55	0.5	0.2	0.13	0.2

Table 2-2 presents results for total, insoluble, soluble and calcined wt.% solids, slurry and supernate density, and the slurry anion results from IC.

Table 2-2. Simulant and Radioactive Feed Properties

	A	B	C	SB8 Tk40	BC Blend +supernate
Total solids, wt.%	17.63	17.54	22.94	17.20	16.94
Insoluble solids, wt.%	16.21	15.88	21.62	11.50	11.77
Soluble solids, wt.%	1.42	1.66	1.32		5.17
Calcined solids, wt.%	13.48	13.85	17.74		12.33
Slurry density, g/mL		1.11	1.18		1.14
Supernate density, g/mL	1.01	1.02	1.01	1.06	1.04
Nitrite, mol/L	0.094	0.094	0.123	0.2927	0.279
Nitrate, mol/L	0.038	0.042	0.048	0.1530	0.157
Sulfate, mol/L	0.024	0.020	0.018	0.0193	0.021
Oxalate, mol/L	0.004	0.012	0.012	0.0248	0.027
Chloride, mol/L	0.018	0.018	0.025	0.0018	0.011

The level of mercury used in this testing was 1 wt% on a total dry solids basis. The levels of noble metals were based on 125% of the HM levels. Targets for mercury and noble metals for the test simulant are presented in Table 2-3. Compared with the scaled testing runs GN70 through GN79,[4] the runs of this report have a lower initial mercury concentration (1.00 wt% versus 2.142 wt%).

Table 2-3. Noble metal and mercury, wt% in total solids

	GN80-GN83 feed slurry
Hg, wt%	1.000
Rh, wt%	0.0475
Ru, wt%	0.2713
Pd, wt%	0.0034
Ag, wt%	0.0164

Rhodium was trimmed as a solution of $Rh(NO_3)_3$ containing 4.93 wt.% Rh. Ruthenium was added as the dry trivalent chloride salt at a purity of 41.74 wt.% Ru. Palladium was trimmed as a solution of $Pd(NO_3)_2$ containing 15.27 wt.% Pd. Silver was added as the dry nitrate salt $AgNO_3$. Mercury was trimmed as dry HgO (yellow mercuric oxide, which is more finely ground than red mercuric oxide).

SME product REDOX was targeted using the results of the previous nitric-glycolic scaled testing.[4]

2.3 Chemical Process Cell

The 4-L lab-scale SRAT equipment was used for these tests. A photo of a typical 4-L rig is shown in Figure 2-1. The SRAT vessel was insulated when at processing temperatures. The trimmed SRAT receipt volume was about 3.0 L.

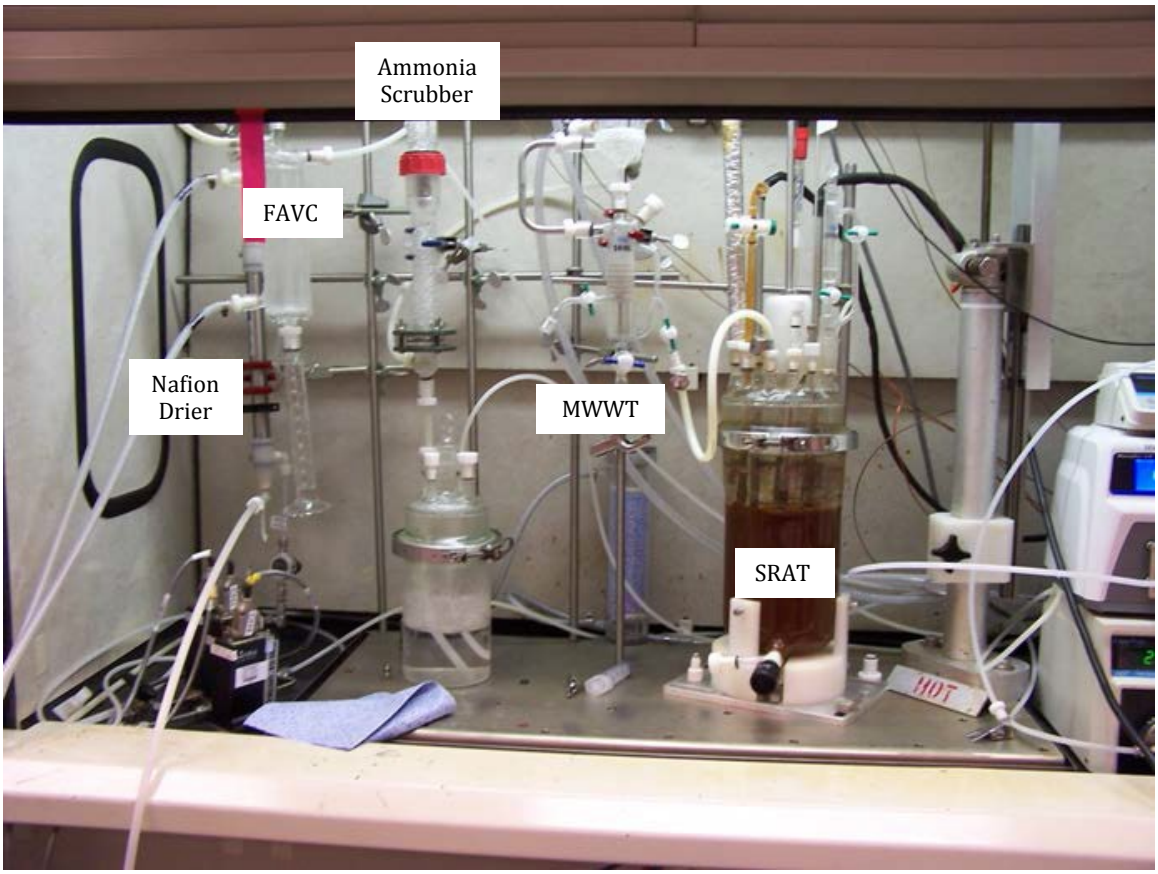

Figure 2-1. Laboratory-scale SRAT apparatus

The modified lab-scale SRAT rig design was used (off-center agitation, heating rods). More details about the new design are in the CPC equipment set-up document.[8] An air drier on the air supply line to the rig equipment removes moisture from the compressed air used for process purges.

The reservoir below the ammonia scrubber was charged with 750 mL of a 0.014 M nitric acid solution. Condensates from the SRAT and SME were not drained into this reservoir. The dilute acid reservoir solution was recirculated by a MasterFlex driven Micropump gear pump at about 300 mL per minute to a spray nozzle at the top of the packed section.

Initial simulant acid calculations were based on the Koopman minimum acid (KMA) requirement equation (all terms have units of moles/L slurry).

$$\frac{\text{mol acid}}{\text{L slurry}} = [\text{base equivalents}] + [\text{Hg}] + [\text{soluble TIC}] + [\text{NO}_2] + 1.5[\text{Ca} + \text{Mg} + \text{Mn}] \quad [1]$$

where concentrations in brackets are in mol/L of slurry

Parallel acid calculations were also performed using the current DWPF algorithm (Hsu equation) for comparison:[7]

$$\frac{\text{mol acid}}{\text{L slurry}} = [\text{base equivalents}] + 2[\text{total TIC}] + 0.75[NO_2] + 1.2[\text{Mn}] + [\text{Hg}] \quad [2]$$

where concentrations in brackets are in mol/L of slurry

For this testing stoichiometric factor of 110% of KMA was used, 1.63 moles of acid per liter of slurry were added with a KMA requirement of 1.48 moles of acid per liter of slurry. This corresponds to a stoichiometric factor of 118% using the Hsu equation, with the Hsu minimum acid requirement of 1.38 moles of acid per liter of slurry. The KMA and Hsu equations were both developed for the nitric-formic flowsheet. A stoichiometric minimum acid equation tailored for the nitric-glycolic flowsheet is under development.

Experimental parameters sought to mimic scaled, design basis DWPF SRAT/SME processing conditions. SRAT and SME cycles did not have a heel from a prior batch and all vessels were clean. Research and development directions were prepared for each run and used to supplement SRNL L29 Manual Procedure ITS-0094 for non-radioactive Chemical Process Cell (CPC) simulations[9]. The following parameters were used for the CPC simulations:

SRAT Cycle

- Sludge, mercuric oxide, and noble metal trim chemicals were added to the vessel while the agitator was in operation.
- The SRAT air purge was scaled to 93.7 scfm in DWPF.
- A 200 ppm antifoam addition was made and heating was initiated. All antifoam additions were 1:10 dilutions of IIT Antifoam 747 in water, followed by an equal amount of water to flush the addition port.
- Nitric acid was added at 2 gpm scaled (initiating addition at near room temperature) and the temperature ultimately reached 93 °C by the end of nitric acid addition.
- A 100 ppm antifoam addition was made and glycolic acid was added at 93 °C at 2 gpm scaled.
- A 100 ppm antifoam addition was made prior to going to boiling following acid addition and every 12 hours after.
- Boiling during initial dewater assumed a condensate production rate of 5000 lb/hr at DWPF scale.
- A scaled 18000 gallons of 0.0125 M boric acid was added as Strip Effluent. For runs GN80 and GN81, boiling for dewatering of SE assumed a condensate production rate of 5000 lb/hr at DWPF scale. In runs GN82 and GN83, boiling for dewatering of SE assumed alternating periods of simmering at 100 °C (with little condensate production) and boiling at a condensate production rate of 5000 lb/hr at DWPF scale, for an overall condensate production rate of 2500 lb/hr at DWPF scale.

SME Cycle

- The SME air purge was scaled to 74 scfm in DWPF.
- A 100 ppm antifoam addition was made at the start of the SME cycle and approximately every 12 hours thereafter.
- 6 canister decontamination water additions and dewaterings were simulated to a scaled DWPF volume of 1000 gallons. For runs GN80 and GN82, boiling for canister decontamination dewatering assumed a condensate production rate of 5000 lb/hr at DWPF scale. In runs GN81 and GN83, boiling for canister decontamination dewatering assumed an initial period of simmering at 100 °C (with little condensate production) and followed by a period of boiling at a condensate production rate of 5000 lb/hr at DWPF scale, for an overall condensate production rate of 2500 lb/hr at DWPF scale.
- Two frit 418-water additions were made targeting 36% waste loading.

- The SME was dewatered following each frit slurry addition.
- The final SME solids target was 48 wt%.
- For runs GN80 and GN81, a 100 ppm antifoam addition was made and an additional glycolic acid "dump" of a scaled 279 gallons was added at 93 °C at 2 gpm scaled. This addition corresponds to the same volume of glycolic acid added during the SRAT cycle.
- After the acid dump, the material was boiled at reflux for at least one hour.

The SRAT and SME product slurries were sampled similarly once they had cooled to 90 °C while the vessel contents were still mixing. Additional SRAT product samples were taken for compositional and solids analyses after the product had cooled further. The Mercury Water Wash Tank (MWWT) and FAVC were drained and the condensates weighed after both the SRAT and SME cycles.

2.4 Offgas Analysis

Gas samples were taken from the exit of the FAVC for analysis by GC, mass spectrometry (MS), and Fourier transform infrared (FTIR) spectroscopy.

The chilled off-gas leaving the FAVC was passed through a Nafion dryer in counter-current flow with a dried air stream to reduce the moisture content of the gases to the analyzers. The GC internal pump pulled a sample at approximately 4.5 minute intervals from this offgas line. A separate sample pump was used to transport samples from the offgas line to the MS and FTIR. Mass flow controllers were used to regulate the amount of gases sent to the MS (~50 mL/min) and FTIR (~150 mL/min). The FTIR sampled only one of each pair of 4-L runs (GN80 and GN82).

The one MS was setup to alternately sample each stream. The MS measured each SRAT/SME system for about 110 sec with a 28 sec delay in between to flush out the other system's sample. The sampling rate was about one sample per 8-9 seconds. The presence of N_2O in the process gas samples introduces error in the measurements of CO_2, NO, and N_2 because it has isobaric fragment ions at the measurement masses of each of these gases. The total sample flow pumped from the offgas system had to be maintained below the total offgas flow from the SRAT/SME equipment so that ambient air would not be drawn into the system and give erroneous results.

Raw chromatographic data were acquired by the GC using separate computers interfaced to the data acquisition computer. Each experiment had a dedicated Agilent (or Inficon) 3000A dual column micro GC. Column-A can collect data related to He, H_2, O_2, N_2, NO, and CO, while column-B can collect data related to CO_2, N_2O, and water. Data for NO, CO, and water are only qualitative. The GCs were calibrated with a standard calibration gas containing He, H_2, O_2, N_2, CO_2 and N_2O. The calibration was verified prior to starting the SRAT cycle and after completing the SME cycle. Room air was used to give a two point calibration for N_2.

An Extrel CMS MAX300LG MS was used to measure H_2, He, N_2, O_2, NO, NO_2, CO_2, and Ar. The MS is calibrated by a series of gas mixtures that are used to measure background intensity, ion fragmentation, and sensitivity. All gases used were National Institute of Standards and Technology (NIST) traceable; the certificates of analysis are documented in the SRNL Electronic Lab Notebook (ELN). In addition, qualitative intensity measurements of specific ion masses that might be expected from antifoam degradation products were also measured. Hexamethyldisiloxane (HMDSO) was monitored at masses 148, 147, 131, and 73; trimethylsilanol was monitored at mass 75; propylene was monitored at masses 41 and 42; and poly(ethylene)glycol (PEG) fragments were monitored at masses 58, 59, and 89. Measurements of H_2 by MS were somewhat inaccurate due to the extremely low values that were subject

to error due to drift in the MS background signal. For some runs, the He calibration drifted and was corrected by a linear interpolation between the calibration value and the post-calibration check value.

An MKS MG2030 FTIR spectrometer was used for runs GN80 and GN82. The FTIR is connected to the two SRAT/SME off-gas systems like the MS, but it is manually valved into one or the other for the duration of the run. The FTIR measures CO, CO_2, NO, NO_2, N_2O, H_2O, and HMDSO concentrations. The FTIR obtained data roughly every 15 seconds.

After the runs were complete, an extensive data review was completed of all the offgas data from the GCs, MS and FTIR. The most reliable data for each offgas component was used but data from all three offgas analyzers was included in the analysis. Since all three analyzers sampled at a different frequency, the data was interpolated to allow a comparison with all data for each run.

3.0 Results

3.1 Simulant Preparation and Characterization

The same base simulant was used as the sludge feed for this testing as was used in the alternate reductant scaled demonstration tests. No new simulant was created for this testing. See Section 2.2 above for a summary and Reference 4 for complete analytical results of the base simulant.

3.2 SRAT/SME Processing Data

3.2.1 SRAT/SME pH

The pH was measured throughout the SRAT and SME cycles using a probe installed in the vessel. The amount of nitric and glycolic acid added to each run is summarized in Table 3-1. The pH is impacted by the moles of acid added, the amount of condensed acids returned to the SRAT during dewater, and the amount of nitric and glycolic acid consumed during processing. The boric acid is a weak acid added to simulate strip effluent was 2.5 % of the total acid added. The final pH of the SRAT and SME products is summarized in Table 3-1. The pH measurements of the SRAT products were consistent (4.44 to 4.68) and remained at nearly this level through the SME cycle, with SME product pH measuring 4.43 to 4.78. For runs GN80 and GN81, the additional glycolic acid dump further reduced the pH of the SME material to 2.92 to 2.96.

Table 3-1. pH of SRAT and SME Products

	GN80	GN81	GN82	GN83
Nitric Acid, mols	1.962	1.962	1.963	1.963
Glycolic Acid, mols	2.350	2.352	2.352	2.351
% Acid as Glycolic Acid (mol%)*	54.5%	54.5%	54.5%	54.5%
Boric Acid, mols	0.110	0.110	0.110	0.110
% Acid as Strip Effluent (mol%)	2.5%	2.5%	2.5%	2.5%
SRAT Product pH	4.44	4.50	4.68	4.60
SME Product pH	4.43	4.78	4.76	4.66
Glycolic Acid Dump, mols	1.368	1.368	0	0
Acid Dump Product pH	2.92	2.96	N/A	N/A

* % reducing acid during initial nitric-glycolic acid addition only. After SE was added, % acid as glycolic acid reduced to 53.1%

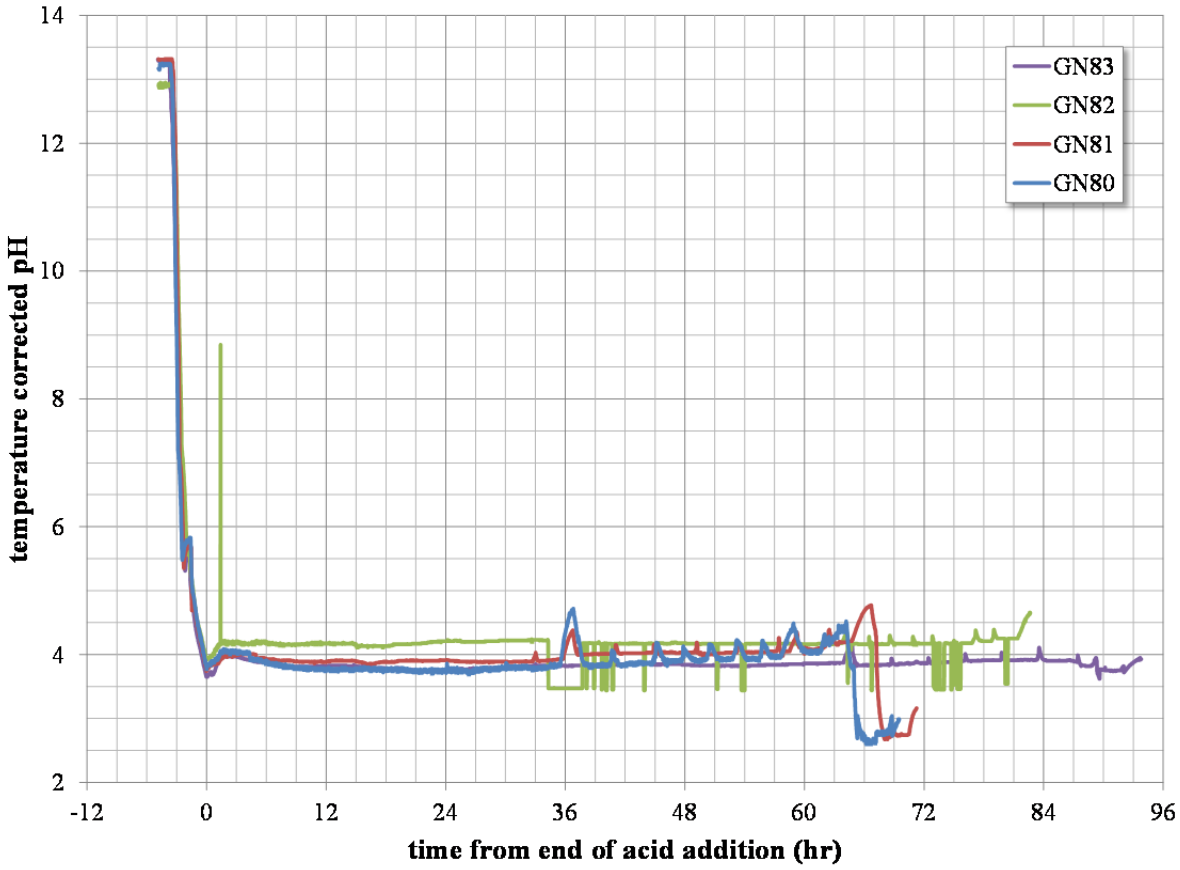

Figure 3-1. pH Trends for SRAT and SME cycles

Table 3-2. End of test pH probe check

pH buffer	GN80	GN81	GN82	GN83
pH 4.0	3.74	2.88	3.10	2.51
pH 7.0	6.15	5.82	6.02	5.45
pH 10.0	8.95	8.97	9.02	8.67

The pH trend for the four runs is summarized in Figure 3-1. All four runs had similar trends, where the pH lowered to just below 4 after the addition of nitric and glycolic acid, increased slightly and reduced slightly again during dewatering, stayed nearly constant at approximately 4 throughout the remainder of the SRAT and SME cycles, and lowered again to a pH less than 3 after the glycolic acid dump. Periods where the temperature is lowered have pH measurements that are slightly higher, approximately 0.5 pH units higher when the temperature is decreased to below 40 °C. Taking into account this temperature effect, the pH measurements from the trends in Figure 3-1 are consistent with the pH of the SRAT and SME products in Table 3-1. The increase in pH by approximately half of a pH unit that occurred approximately 2.5 hours before the end of acid addition corresponds to the period between the end of nitric acid addition and the start of glycolic acid addition. During GN82, there are periods where the pH probe gave erroneous readings as evident by discontinuities in the trend shown in Figure 3-1.

The pH probes were checked prior to use on the first day of each test and after use on the last day of each test. Pre-test checks with buffers of pH = 4.0, 7.0, and 10.0 matched the buffer values within 0.1 pH units. Table 3-2 contains the results for the post-test pH checks. The pH readings during the post-test check average approximately 1 pH unit low over the range of the pH buffers, with reasonable consistency between tests. Thus, portions of the pH trends in Figure 3-1 may be biased low by up to 1 pH unit.

3.2.2 SRAT/SME Heat Transfer

Figure 3-2 shows the heat transfer coefficient during processing to fall within the expected range of 0.15 to 0.20 $W/cm^2 \cdot °C$.

There are two rods that supply heat to the slurry (Watlow heating rods, ½" diameter, 4" heated length). The heat transfer coefficient is calculated from process data (heat input to rods, temperature difference between the rods and slurry) along with the calculated surface area of the heated section of the rod. A two controller cascade system is used to control either the power to the rod directly (during boiling) or the bulk fluid temperature (during acid addition) by supplying the power needed to both heating rods without allowing the temperature of the heating rods to exceed 164 °C, the maximum temperature of 85 psig steam in DWPF. The actual power supplied to each heating rod is not measured and it is expected that both heating rods would be the same temperature (within a few degrees centigrade).

Based on the steady heat transfer and small temperature differential between heating rods (typically <2 °C), significant fouling was not encountered in these runs. This was consistent with observations at the end of the run where buildup was not noted on the heating rods.

During run GN81, a temporary problem with one connection for a thermocouple embedded in one of the heating rods necessitated not using that heating rod during short periods of the acid addition and early in the reflux cycle.

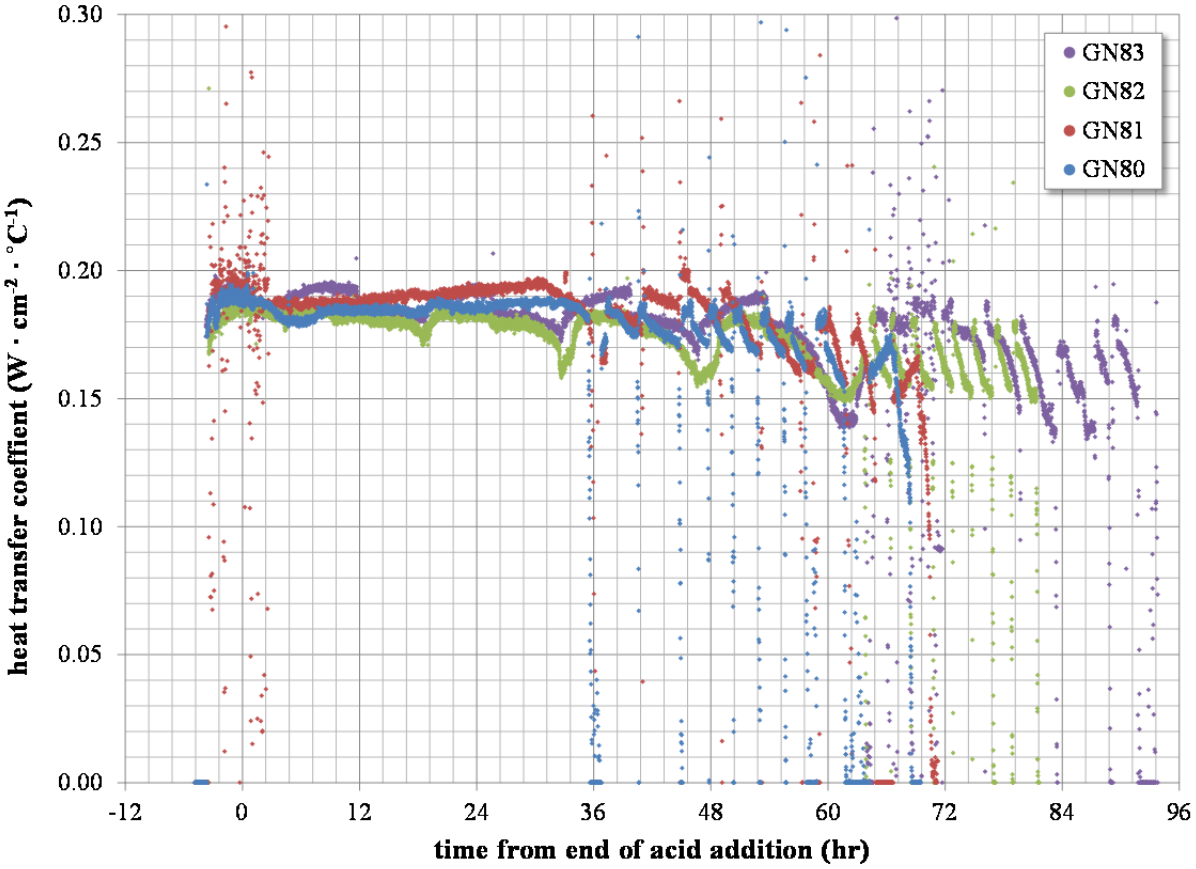

Figure 3-2. Calculated Heat Transfer Coefficient Trends for SRAT and SME Cycles

For run GN80, the measured temperature difference between the two heating rods varied around 8 °C. It was subsequently determined that a heating rod thermocouple for run GN80 was not being read properly and the actual temperature difference between heating rods was likely much less than 8 °C. At the same time, it was determined that the M&TE thermocouple readers used during runs GN80 and GN81 had exceeded their M&TE calibration expiration date. A Non-Conformance Report (NCR, 2015-NCR-11-0002) was issued on the calibration deficiency. Subsequent as-found calibration check of the thermocouple readers revealed that the instruments were within the calibration specification for all channels and there was no negative impact to data quality in this report. The calibration deficiency was resolved prior to performing runs GN82 and GN83.

3.2.3 SRAT/SME Foaming

No appreciable foaming was noted during the duration of the SRAT processing, SME canister decontamination dewater, and SME frit dewater. During the glycolic acid dump at the completion of the SME cycles for GN80 and GN81, however, foaming was encountered. The foam appeared as very fine bubbles that did not appear greatly different from the appearance of the slurry. However, the bulk volume increased greatly, approximately doubling before being countered with a 100 ppm antifoam addition.

This foaming period after the additional glycolic acid dump corresponds to a lower pH, a higher soluble metal content, and a different rheology from the other periods. In the 125% KMA excess stoichiometry run GN71 performed during the scaled demonstration, a higher viscosity and increased foaming were also noted.[4] Thus, increased glycolic acid (or possibly total acid) may correlate with high viscosity and a greater foaming potential in the CPC.

3.3 SRAT/SME Product Sample Results

In comparison to the sample strategy for the recent scaled demonstrations, analysis for a more limited, targeted set of samples was performed for these runs. The slurry samples from the end of the SRAT, SME, and post-acid dump were analyzed by the standard PSAL SRAT and SME product analytical suite. Condensate composite samples from the end of SRAT dewater, SME canister decontamination dewater, and SME frit dewater were also analyzed. The results and a discussion of the sample results are included in the subsections below.

3.3.1 SRAT/SME Product Solids and Density

Table 3-3 and Table 3-4 contain results for the solids and density measurements for the SRAT and SME product samples, respectively. Total solids at the end of the SRAT and SME ranged from 28.8 to 29.8 and 47.4 to 50.0, respectively. Solids levels were within the targeted ranges (27% for SRAT products and 48% SME products), slightly at the high end of the range. The solids levels and densities obtained compare favorably with those from the previous scaled runs GN73, GN75, GN77 and GN78.[10] The glycolic acid dump performed on the SME products from GN80 and GN81 increased the supernate densities and soluble/dissolved solids.

Table 3-3. Solids and Density of SRAT Product Samples

property	GN80	GN81	GN82	GN83
slurry density (g/mL)	1.223	1.230	1.227	1.221
supernatant density (g/mL)	1.128	1.131	1.126	1.140
total solids (wt% in slurry)	28.9	29.8	29.0	28.8
dissolved solids (wt% in supernatant)	18.7	19.2	18.5	18.1
insoluble solids (wt% in slurry)	12.5	13.1	12.9	13.0
soluble solids (wt% in slurry)	16.4	16.6	16.1	15.8
calcined solids (wt% in slurry)	16.3	16.8	16.3	15.9

Table 3-4. Solids and Density of SME Product Samples, With and Without the Acid Dump (for GN80 and GN81)

analyte	GN80		GN81		GN82	GN83
	SME product	acid dump	SME product	acid dump		
slurry density (g/mL)	1.390	1.388	1.420	1.401	1.445	1.396
supernatant density (g/mL)	1.142	1.168	1.148	1.172	1.123	1.136
total solids (wt% in slurry)	48.7	48.5	49.4	49.3	50.0	47.4
dissolved solids (wt% in supernatant)	20.6	23.8	21.4	24.3	20.5	19.8
insoluble solids (wt% in slurry)	35.4	32.4	35.6	33.0	37.1	34.3
soluble solids (wt% in slurry)	13.3	16.1	13.8	16.3	12.9	13.0
calcined solids (wt% in slurry)	38.1	36.2	38.5	36.8	39.5	36.7

3.3.2 SRAT/SME Product Calcined Elemental Composition

Calcined elemental results for the SRAT and SME product slurries from GN80 through GN83 are given in Table 3-5 and Table 3-6. There is excellent agreement from run to run, as expected for runs where the same feed slurry and acid additions were used. The additional glycolic acid dump performed on the SME products did not influence the calcined elemental results.

Table 3-5. Calcined Elemental Results of SRAT Product Samples (wt% calcined solids)

analyte	GN80	GN81	GN82	GN83
Al	9.56E+00	9.48E+00	9.16E+00	9.05E+00
B	3.97E-01	3.79E-01	< 1.0E-01	< 1.0E-01
Ba	1.46E-01	1.47E-01	1.57E-01	1.53E-01
Ca	1.44E+00	1.42E+00	1.51E+00	1.49E+00
Cr	9.48E-02	9.31E-02	1.05E-01	9.99E-02
Cu	< 1.0E-01	< 1.0E-01	< 1.0E-01	< 1.0E-01
Fe	2.16E+01	2.12E+01	2.28E+01	2.27E+01
K	1.54E-01	1.52E-01	1.43E-01	1.38E-01
Li	1.27E-01	1.32E-01	< 1.0E-01	< 1.0E-01
Mg	3.03E-01	3.03E-01	3.01E-01	2.96E-01
Mn	7.03E+00	6.95E+00	6.67E+00	6.68E+00
Na	1.72E+01	1.73E+01	1.61E+01	1.67E+01
Ni	2.13E+00	2.10E+00	2.19E+00	2.17E+00
P	< 1.0E-01	< 1.0E-01	< 1.0E-01	< 1.0E-01
Pd	< 1.0E-01	< 1.0E-01	< 1.0E-01	< 1.0E-01
Rh	n.m.	n.m.	< 1.0E-01	< 1.0E-01
Ru	n.m.	n.m.	< 1.0E-01	< 1.0E-01
S	3.92E-01	3.91E-01	3.69E-01	3.52E-01
Si	2.95E+00	3.00E+00	3.06E+00	2.89E+00
Sn	< 1.0E-01	< 1.0E-01	< 1.0E-01	< 1.0E-01
Ti	< 1.0E-01	< 1.0E-01	< 1.0E-01	< 1.0E-01
Zn	< 1.0E-01	< 1.0E-01	< 1.0E-01	< 1.0E-01
Zr	1.62E-01	2.13E-01	2.55E-01	2.34E-01

n.m. = not measured

Table 3-6. Calcined Elemental Results of SME Product Samples (wt% calcined solids)

analyte	GN80		GN81		GN82	GN83
	SME product	acid dump	SME product	acid dump		
Al	3.48E+00	3.45E+00	3.60E+00	3.39E+00	3.34E+00	3.56E+00
B	1.57E+00	1.60E+00	1.73E+00	1.84E+00	1.46E+00	1.42E+00
Ba	< 1.0E-01	< 1.0E-01	< 1.0E-01	< 1.0E-01	6.40E-02	6.37E-02
Ca	5.07E-01	4.52E-01	5.15E-01	4.74E-01	4.38E-01	4.81E-01
Cr	3.99E-02	3.96E-02	4.12E-02	3.92E-02	4.06E-02	4.46E-02
Cu	< 1.0E-01	< 1.0E-01	< 1.0E-01	< 1.0E-01	< 1.0E-01	< 1.0E-01
Fe	7.50E+00	7.36E+00	8.02E+00	7.35E+00	7.37E+00	8.20E+00
K	1.17E-01	1.16E-01	1.16E-01	1.08E-01	1.07E-01	1.13E-01
Li	2.23E+00	2.26E+00	2.20E+00	2.33E+00	2.18E+00	2.07E+00
Mg	1.14E-01	1.11E-01	1.16E-01	1.11E-01	1.11E-01	1.21E-01
Mn	2.35E+00	2.32E+00	2.53E+00	2.33E+00	2.25E+00	2.46E+00
Na	9.77E+00	9.57E+00	9.86E+00	9.48E+00	8.82E+00	9.47E+00
Ni	6.67E-01	6.41E-01	6.91E-01	6.17E-01	6.10E-01	6.71E-01
P	< 1.0E-01	< 1.0E-01	< 1.0E-01	< 1.0E-01	< 1.0E-01	< 1.0E-01
Pd	< 1.0E-01	< 1.0E-01	< 1.0E-01	< 1.0E-01	< 1.0E-01	< 1.0E-01
Rh	n.m.	n.m.	n.m.	n.m.	< 1.0E-01	< 1.0E-01
Ru	n.m.	n.m.	n.m.	n.m.	< 1.0E-01	< 1.0E-01
S	1.13E-01	1.19E-01	1.37E-01	1.19E-01	9.73E-02	9.58E-02
Si	2.54E+01	2.57E+01	2.43E+01	2.53E+01	2.46E+01	2.42E+01
Sn	< 1.0E-01	< 1.0E-01	< 1.0E-01	< 1.0E-01	< 1.0E-01	< 1.0E-01
Ti	< 1.0E-01	< 1.0E-01	< 1.0E-01	< 1.0E-01	< 1.0E-01	< 1.0E-01
Zn	< 1.0E-01	< 1.0E-01	< 1.0E-01	< 1.0E-01	< 1.0E-01	< 1.0E-01
Zr	1.65E-01	1.62E-01	1.34E-01	1.33E-01	1.62E-01	1.64E-01

n.m. = not measured

3.3.3 SRAT/SME Product Supernatant Elemental Composition

Supernate elemental results for the SRAT and SME products GN80 through GN83 are given in Table 3-7 and Table 3-8. There is good agreement between the soluble components from run to run, and this is expected for runs where the same feed slurry and acid additions were used. In general, the glycolic acid dump increased the solubility of elemental components, with the exception of components such as sodium and manganese, which were already nearly completely soluble in the SRAT products.

Table 3-7. Major SRAT Product Supernate Elements, mg/L

analyte	GN80	GN81	GN82	GN83
Al	9.05E+02	8.36E+02	5.25E+02	4.72E+02
B	6.07E+02	5.93E+02	5.72E+02	5.74E+02
Ba	< 1.0E+00	< 1.0E+00	< 1.0E+00	< 1.0E+00
Ca	2.27E+03	2.30E+03	1.94E+03	1.84E+03
Cr	2.54E+00	2.42E+00	2.46E+00	2.62E+00
Cu	2.80E+01	2.69E+01	2.61E+01	2.47E+01
Fe	4.62E+02	3.77E+02	3.65E+02	4.35E+02
K	4.34E+02	4.23E+02	3.99E+02	3.88E+02
Li	1.06E+01	1.01E+01	< 1.0E+01	< 1.0E+01
Mg	5.24E+02	5.17E+02	5.06E+02	4.94E+02
Mn	1.35E+04	1.40E+04	1.29E+04	1.22E+04
Na	3.22E+04	3.27E+04	3.34E+04	3.22E+04
Ni	1.00E+03	9.68E+02	1.01E+03	1.06E+03
P	< 1.0E+01	< 1.0E+01	< 1.0E+01	< 1.0E+01
Pb	1.25E+00	1.31E+00	1.32E+00	1.38E+00
Pd	n.m.	n.m.	< 1.0E+00	< 1.0E+00
Rh	1.00E+02	9.93E+01	9.57E+01	9.27E+01
Ru	6.13E+02	6.02E+02	5.91E+02	5.70E+02
S	8.94E+02	8.81E+02	8.54E+02	8.42E+02
Si	1.33E+02	1.23E+02	1.25E+02	1.30E+02
Sn	9.09E+00	9.26E+00	8.49E+00	7.69E+00
Ti	5.69E-01	5.46E-01	6.67E-01	7.51E-01
Zn	1.20E+01	1.16E+01	1.16E+01	1.31E+01
Zr	< 1.0E-01	< 1.0E-01	< 1.0E-01	< 1.0E-01

n.m. = not measured

Table 3-8. Major SME Product Supernate Elements, mg/L

analyte	GN80		GN81		GN82	GN83
	SME product	acid dump	SME product	acid dump		
Al	5.69E+02	1.69E+03	7.37E+02	2.03E+03	3.74E+02	3.43E+02
B	6.67E+02	6.46E+02	7.19E+02	6.79E+02	6.59E+02	6.34E+02
Ba	1.04E+00	3.45E+00	1.15E+00	3.60E+00	< 1.0E+00	1.16E+00
Ca	2.27E+03	2.66E+03	2.36E+03	2.88E+03	1.99E+03	1.79E+03
Cr	2.60E+00	7.52E+00	2.65E+00	7.62E+00	2.33E+00	2.34E+00
Cu	2.81E+01	5.48E+01	2.60E+01	5.50E+01	2.49E+01	2.59E+01
Fe	2.64E+02	7.61E+03	2.50E+02	7.76E+03	2.66E+02	3.24E+02
K	4.68E+02	4.70E+02	4.77E+02	4.33E+02	4.65E+02	4.39E+02
Li	1.03E+02	1.23E+02	2.30E+02	2.59E+02	1.02E+02	1.01E+02
Mg	5.70E+02	6.59E+02	5.96E+02	6.69E+02	5.70E+02	5.46E+02
Mn	1.43E+04	1.32E+04	1.55E+04	1.43E+04	1.42E+04	1.36E+04
Na	3.53E+04	3.22E+04	3.79E+04	3.45E+04	3.75E+04	3.77E+04
Ni	1.16E+03	3.30E+03	1.15E+03	3.51E+03	1.23E+03	1.33E+03
P	< 1.0E+01	5.76E+01	< 1.0E+01	6.06E+01	< 1.0E+01	< 1.0E+01
Pb	1.47E+00	2.10E+01	1.36E+00	2.11E+01	1.61E+00	1.54E+00
Pd	n.m.	n.m.	n.m.	n.m.	< 1.0E+00	< 1.0E+00
Rh	1.06E+02	1.35E+02	1.10E+02	1.35E+02	9.87E+01	9.85E+01
Ru	6.62E+02	7.35E+02	6.87E+02	7.40E+02	6.56E+02	6.12E+02
S	9.67E+02	9.25E+02	1.03E+03	9.30E+02	9.80E+02	9.33E+02
Si	1.37E+02	2.53E+02	1.26E+02	2.90E+02	1.46E+02	1.46E+02
Sn	9.56E+00	1.03E+01	1.03E+01	1.08E+01	8.76E+00	8.30E+00
Ti	6.15E-01	1.34E+01	5.26E-01	1.35E+01	6.99E-01	7.69E-01
Zn	1.47E+01	4.58E+01	1.35E+01	4.61E+01	1.51E+01	1.67E+01
Zr	< 1.0E-01	2.43E-01	< 1.0E-01	1.45E-01	< 1.0E-01	< 1.0E-01

n.m. = not measured

3.3.4 SRAT/SME Product Anion Composition

Table 3-9 and Table 3-10 list the anion content of the SRAT and SME slurries, respectively. Table 3-11 and Table 3-12 list the anion content of the SRAT and SME supernatant liquid, respectively. As with the elemental results, there is obvious similarity between the four runs performed. Most anions in the slurries match well between the four runs. There appears to be differences between the anions in the supernate from the chronologically first two runs (GN80 and GN81) when compared with the other two runs. The slightly higher nitrate, oxalate, and glycolate in the earlier runs are within the experimental uncertainty. Sulfate appears to be greater in the GN80 and GN81 SME product supernate versus GN82 and GN83 at

levels outside of the typical analytical uncertainty. The additional glycolic acid dump appears to contribute to larger soluble oxalate concentrations, which is likely due to the lower final pH.

Table 3-9. SRAT Product Anions, mg/kg slurry

analyte	GN80	GN81	GN82	GN83
Cl^-	1.10E+03	1.10E+03	1.13E+03	1.05E+03
NO_2^-	< 5.0E+02	< 5.0E+02	< 5.0E+02	< 5.0E+02
NO_3^-	6.21E+04	6.35E+04	6.11E+04	6.32E+04
SO_4^{2-}	1.97E+03	2.00E+03	1.99E+03	1.92E+03
$C_2O_4^{2-}$	2.25E+03	2.46E+03	2.67E+03	2.80E+03
HCO_2^-	3.48E+02	3.56E+02	3.57E+02	3.88E+02
$C_2H_3O_3^-$	5.13E+04	5.29E+04	4.96E+04	4.93E+04

Table 3-10. SME Product Anions, mg/kg slurry

analyte	GN80		GN81		GN82	GN83
	SME product	acid dump	SME product	acid dump		
Cl^-	9.47E+02	8.83E+02	9.59E+02	8.70E+02	8.91E+02	9.27E+02
NO_2^-	< 5.0E+02	< 5.0E+02	< 5.0E+02	< 5.0E+02	< 5.0E+02	< 5.0E+02
NO_3^-	5.33E+04	5.14E+04	5.48E+04	5.08E+04	5.13E+04	5.31E+04
SO_4^{2-}	1.70E+03	1.46E+03	1.76E+03	1.45E+03	1.63E+03	1.68E+03
$C_2O_4^{2-}$	2.75E+03	2.52E+03	2.89E+03	2.50E+03	3.04E+03	3.17E+03
HCO_2^-	3.25E+02	4.52E+02	3.11E+02	4.29E+02	3.09E+02	3.44E+02
$C_2H_3O_3^-$	4.28E+04	8.51E+04	4.38E+04	8.48E+04	4.14E+04	4.23E+04

Table 3-11. SRAT Product Supernate Anions, mg/L

analyte	GN80	GN81	GN82	GN83
Cl^-	1.46E+03	1.53E+03	1.31E+03	1.28E+03
NO_2^-	< 5.00E+02	< 5.00E+02	< 5.00E+02	< 5.00E+02
NO_3^-	8.21E+04	8.52E+04	7.60E+04	7.67E+04
SO_4^{2-}	2.18E+03	2.37E+03	1.31E+03	1.39E+03
$C_2O_4^{2-}$	2.34E+03	1.34E+03	2.19E+03	2.17E+03
HCO_2^-	3.04E+02	2.94E+02	2.55E+02	2.70E+02
$C_2H_3O_3^-$	6.23E+04	6.35E+04	5.69E+04	5.59E+04

Table 3-12. SME Product Supernate Anions, mg/L

analyte	GN80		GN81		GN82	GN83
	SME product	acid dump	SME product	acid dump		
Cl^-	1.70E+03	1.44E+03	1.75E+03	1.47E+03	1.48E+03	1.40E+03
NO_2^-	< 5.00E+02	< 5.00E+02	< 5.00E+02	< 5.00E+02	< 5.00E+02	< 5.00E+02
NO_3^-	9.61E+04	8.80E+04	1.09E+05	8.32E+04	8.78E+04	8.26E+04
SO_4^{2-}	2.63E+03	2.43E+03	2.75E+03	2.49E+03	1.45E+03	1.54E+03
$C_2O_4^{2-}$	1.50E+03	4.61E+03	1.45E+03	4.28E+03	2.52E+03	2.40E+03
HCO_2^-	3.71E+02	4.56E+02	3.60E+02	4.39E+02	2.99E+02	3.08E+02
$C_2H_3O_3^-$	6.78E+04	1.16E+05	7.61E+04	1.12E+05	6.28E+04	5.74E+04

3.3.5 SRAT/SME Product Soluble and Insoluble Components

By comparing the slurry and supernate data, and knowing the solids information, an evaluation can be made to determine which components are fully soluble in the SRAT and SME products versus which components are present in the solid phase. Table 3-13 contains the data for the percent of each analyte that can be attributed to the aqueous phase for the SRAT products ("SRAT"), the SME products ("SME") and the materials after the additional glycolic acid dump ("dump"). Analytes with values of 100% are fully soluble in the aqueous phase of the slurry, values of 0% are completely in the solid phase, and intermediate values are a partially soluble. Chloride, nitrate, and sulfur are completely soluble in the SRAT and SME products. There is a discrepancy between the sulfur and sulfate results; it is likely that sulfate is almost completely soluble as well. Large fractions of the calcium, potassium, magnesium, manganese, sodium, oxalate, formate, and glycolate are soluble in the SRAT products.

Although the glycolic acid dump is not an intended part of the nitric-glycolic flowsheet, comparison of the acid dump results to the SME product results provides insight into solubility changes with additional glycolic acid. The additional glycolic acid dump contributed to a thirty-fold increase in the soluble iron concentration when compared with the soluble iron concentration in the SME product. However, only about 16.5% of the total iron was soluble after the glycolic acid dump. The percentage of iron that was soluble after the acid dump (~16.5%) is greater than the percentage of the iron that was soluble in the pH adjusted SRAT product from the actual waste testing of the 80:20 glycolic:formic flowsheet (2.22% soluble at pH = 1).[11] However, the increase in the solubility of iron when the acid dump was performed is not expected to impact the criticality controls in DWPF because it could only decrease the Fe:Pu by a maximum of 16.5%. Also, the form of iron species in laboratory-prepared sludge simulants are typically more reactive (faster to dissolve) than the species in the actual waste. The form of iron in the laboratory-prepared simulant is typically goethite while the form in the actual waste sludge is typically hematite.

The glycolic acid dump also contributed to a three-to-four-fold increase in the soluble nickel and a doubling of the soluble aluminum. After the glycolic acid dump, the oxalate in the material became nearly fully soluble. The glycolic acid dump did not appear to increase the solubility of the major frit components.

Table 3-13. Selected SRAT and SME product supernate analytes, % of total

analyte	GN80			GN81			GN82		GN83	
	SRAT	SME	dump	SRAT	SME	dump	SRAT	SME	SRAT	SME
Al	4.5%	2.4%	7.8%	4.0%	3.0%	9.3%	2.7%	1.6%	2.5%	1.5%
B	73%	6.3%	6.4%	72%	6.0%	5.8%	--	6.4%	--	7.0%
Ca	75%	66%	94%	74%	67%	95%	61%	64%	59%	59%
Cr	1.3%	1.0%	3.0%	1.2%	0.9%	3.0%	1.1%	0.8%	1.3%	0.8%
Fe	1.0%	0.5%	16.5%	0.8%	0.5%	16.4%	0.8%	0.5%	0.9%	0.6%
K	134%	60%	65%	127%	60%	62%	132%	62%	135%	61%
Li	4.0%	0.7%	0.9%	3.5%	1.5%	1.7%	--	0.7%	--	0.8%
Mg	82%	74%	95%	78%	75%	94%	80%	73%	80%	71%
Mn	92%	91%	90%	92%	89%	96%	92%	89%	88%	87%
Na	89%	54%	54%	87%	56%	57%	99%	60%	93%	63%
Ni	22%	26%	82%	21%	24%	89%	22%	28%	23%	31%
S	109%	127%	124%	103%	110%	121%	110%	143%	115%	153%
Si	2.2%	0.1%	0.2%	1.9%	0.1%	0.2%	1.9%	0.1%	2.2%	0.1%
Cl^-	103%	102%	94%	107%	102%	97%	90%	93%	93%	87%
NO_3^-	103%	102%	99%	103%	112%	94%	96%	96%	93%	90%
SO_4^{2-}	86%	87%	96%	91%	88%	98%	51%	50%	55%	53%
$C_2O_4^{2-}$	81%	31%	106%	42%	28%	98%	63%	46%	59%	44%
HCO_2^-	68%	65%	58%	63%	65%	59%	55%	54%	53%	52%
$C_2H_3O_3^-$	94%	90%	79%	92%	98%	76%	89%	85%	86%	78%

3.3.6 SRAT/SME Product Calculated Loss of Anions

The SRAT and SME product anions and a mass balance were used to calculate the loss of glycolate, nitrite, and nitrate. The result of this comparison is contained in Table 3-14. Results for similar 4L runs GN73 and GN75 are presented for comparison because the same acid stoichiometry and simulant was used.[4] As is typical in runs with adequate added acid, the nitrite decomposition is complete. The various reactions destroying the nitrite produce NO, N_2O, NO_2, and nitrate. In a typical nitric-formic flowsheet experiment, approximately 33% of the nitrite is converted to nitrate. In runs GN80 through GN83, the nitrite to nitrate conversion was much higher, ranging from 51% to 64%. This higher nitrite-to-nitrate conversion observed for GN80 through GN83 is on the upper end of the range of nitrite-to-nitrate conversions expected for the nitric-glycolic flowsheet.

The loss of glycolate in the SRAT cycles ranged from 13% to 19% for runs GN80 though GN83. This is consistent with the previous 4-L runs with the same simulant and acid stoichiometry, runs GN73 and GN75.

Table 3-14. Changes in major anions

	GN73	GN75	GN80	GN81	GN82	GN83
SRAT Glycolate Loss	17.8%	13.6%	15.4%	12.8%	18.2%	18.7%
SRAT Nitrite Loss	100%	100%	100%	100%	100%	100%
SRAT Nitrite-to-nitrate	44.4%	51.8%	56.5%	63.9%	51.1%	62.2%

Results are susceptible to the analytical uncertainties in the IC measurements of anions in the SRAT and SME product samples as well as to uncertainty in the SRAT and SME product masses. Particularly in these recent runs, there is additional uncertainty in the SME product mass data, which contributes directly to the SME glycolate and nitrate losses.

3.3.7 SME Product Waste Loading Calculation

Waste loadings were calculated by two different methods. The first method compared the iron concentration of the SME product to the SRAT product. The second method compared the Li concentration in SME product and frit 418 (nominally 8% LiO_2). These results are summarized in Table 3-15. The waste loading target was 36%. The calculation on the iron basis showed the slurries to be close to the target waste loading, with GN82 slightly low. The calculation on the lithium basis showed the waste loading for all runs to be higher than expected, indicating either a frit lot that was lower than the nominal concentration of lithium or an analytical anomaly was encountered. The waste loading results based on iron concentration in the SME and SRAT products was closer to the target expected based on a mass balance.

Table 3-15. Waste Loading of SME Products

Run	Fe, wt%	Li, wt%
GN80	34.8%	40.0%
GN81	37.7%	40.8%
GN82	32.3%	41.3%
GN83	36.2%	44.3%

3.4 Condensate and Ammonia Scrubber Analysis

3.4.1 Condensate Analysis

Samples of the condensate removed during SRAT and SME dewatering were analyzed for elemental composition, anions, and pH. Table 3-16 contains the results for the components in the condensate identified in some of the samples at above detectable levels. All samples measured below the detection limit of 0.1 mg/L for Al, Ba, Ca, Cr, Cu, Fe, Mg, Mn, Ni, P, Ti, Zn, and Zr; 1.00 mg/L for K, Li, Na, and S; 10.0 mg/L for Sn; and 100 mg/L for F, Cl, NO_2, $C_2H_3O_3$, SO_4, HCO_2, C_2O_4, and PO_4.

Table 3-16. Condensate analysis from SRAT and SME cycles

SRAT Dewater Composite				
	GN80	GN81	GN82	GN83
pH	0.89	0.80	1.02	1.14
NO_3 (mg/L)	6830	8140	3470	3890
Si (mg/L)	91.7	148.4	38.9	65.0
Hg (mg/L)	48.7	9.44	17.8	15.6
SME Canister Decontamination Dewater				
	GN80	GN81	GN82	GN83
pH	3.27	3.42	3.91	3.62
NO_3 (mg/L)	<100	<100	<100	<100
Si (mg/L)	116	16.4	138	104
Hg (mg/L)	3.88	2.86	2.57	<1.00
SME Frit Dewater				
	GN80	GN81	GN82	GN83
pH	3.3	3.28	3.60	3.57
NO_3 (mg/L)	<100	<100	<100	<100
Si (mg/L)	275	269	205	137
Hg (mg/L)	1.97	2.00	1.26	<1.00

As expected, the SRAT dewater tends to have lower pH and higher Hg concentration than the SME dewater. The SME frit dewater has the highest Si concentration. Condensate samples were not analyzed for ammonium or antifoam degradation products.

3.4.2 Ammonia Scrubber Analysis

Samples ammonia scrubber solutions from after the SRAT and SME cycles were analyzed for anions. Table 3-17 contains the results for nitrate in the ammonia scrubber solutions, which was the only anion at above the detectable level. All samples measured below the detection limit of 100 mg/L for F, Cl, NO_2, $C_2H_3O_3$, SO_4, HCO_2, C_2O_4, and PO_4. A dilute nitric acid solution was used as the medium in the ammonia scrubber.

Table 3-17. Nitrate concentration in the ammonia scrubber (mg/L)

(mg/L)	GN80	GN81	GN82	GN83
NO_3 post-SRAT	13700	13000	7950	16200
NO_3 post-SME	14200	13300	7630	15800

3.5 Offgas Analysis

Gas samples were taken from the exit of the FAVC for analysis by GC, MS, and FTIR. The results of the analysis are discussed below. Note that the offgas had to pass through the condenser, ammonia scrubber, FAVC, and Perma Pure Nafion® gas dryer prior to analysis to remove water, ammonia, solids, and nitric acid prior to analysis. The FTIR was used for only runs GN80 and GN82.

3.5.1 Hydrogen Generation

Hydrogen is one of the minor offgas species based on the small amount generated, but hydrogen is important because it is a flammable gas. The quantification of hydrogen is the primary objective of this set of tests. The hydrogen results included in this section are based on the initial instrument calibration and adjustments for the helium tracer measurements. In Section 4.2, the hydrogen results are reprocessed to include uncertainty, which included a more conservative approach to account for the drift in the calibration during the run. Thus some results in this section do not match the precise values or the significant digits reported in Section 4.2.

Figure 3-3 through Figure 3-6 show the hydrogen released during the SRAT and SME testing. Hydrogen concentration is in volume % and the time is based off the end of acid addition. The slurry temperature is also provided as a reference to the processing stage. The temperature gives an indication of when boiling is achieved. The periods between the SRAT and SME cycles, and periods during the canister decontamination water and frit additions can be identified by spikes lower in temperature. Acid addition periods at the start of the SRAT run and at the start of the glycolic acid dump (after the SME for GN80 and GN81) correspond to periods held at 93 °C. For runs with periods of simmering, the simmering can be identified as the periods of steady slightly lower temperatures (around 100 °C) as compared to the periods of boiling at temperatures of 101 to 103 °C.

The solid black line, when not zero or vertical, indicates the offgas hydrogen concentration as measured by the GC at above the detectable level. The blue circles are individual measurements of hydrogen by the MS. The measurement of hydrogen by MS is considerably more noisy than the measurement by the GC.

For this reason, the red line is also included, representing a twenty measurement moving average for the MS results for hydrogen.

In general, hydrogen production was low in this set of nitric-glycolic CPC tests when compared with the baseline nitric-formic flowsheet. Hydrogen was not seen with the GC at above detectable levels for the first approximately 24 hours of the 36-to-64-hour SRAT cycles. Subsequently, hydrogen concentration slowly increased up to and through the SME cycle, though generation rates were generally lower in the SME cycle. Examining both the GC and MS data for hydrogen, generation and release of hydrogen is reduced during periods of simmering when compared to the boiling conditions. This difference is often enough for the hydrogen concentration to be below the detection limit for the GC during periods of simmering.

At the end of the SME cycle, a glycolic acid dump was performed for runs GN80 and GN81 with the thought that small amounts (<1%) of formic acid contained in the glycolic acid might contribute to hydrogen production. While this additional glycolic acid was added and afterwards as the SME products were heated back to boiling and refluxed for more than an hour, no hydrogen was observed at above detectable levels with the GC. The introduction of additional glycolic acid at this point in the process appeared to lower the rate of hydrogen generation that was occurring at the end of the SME. Continued testing of the impacts of the glycolic acid dump on the maximum hydrogen levels is not recommended because these results indicated that additional glycolic acid addition to the SME does not increase the generation of hydrogen.

Several peaks in hydrogen concentration are noted in the MS results that are not evident in the GC results. These are thought to be associated with interactions of the antifoam degradation products within the MS and should not be considered as hydrogen for these results. See the explanation in Section 3.5.2.

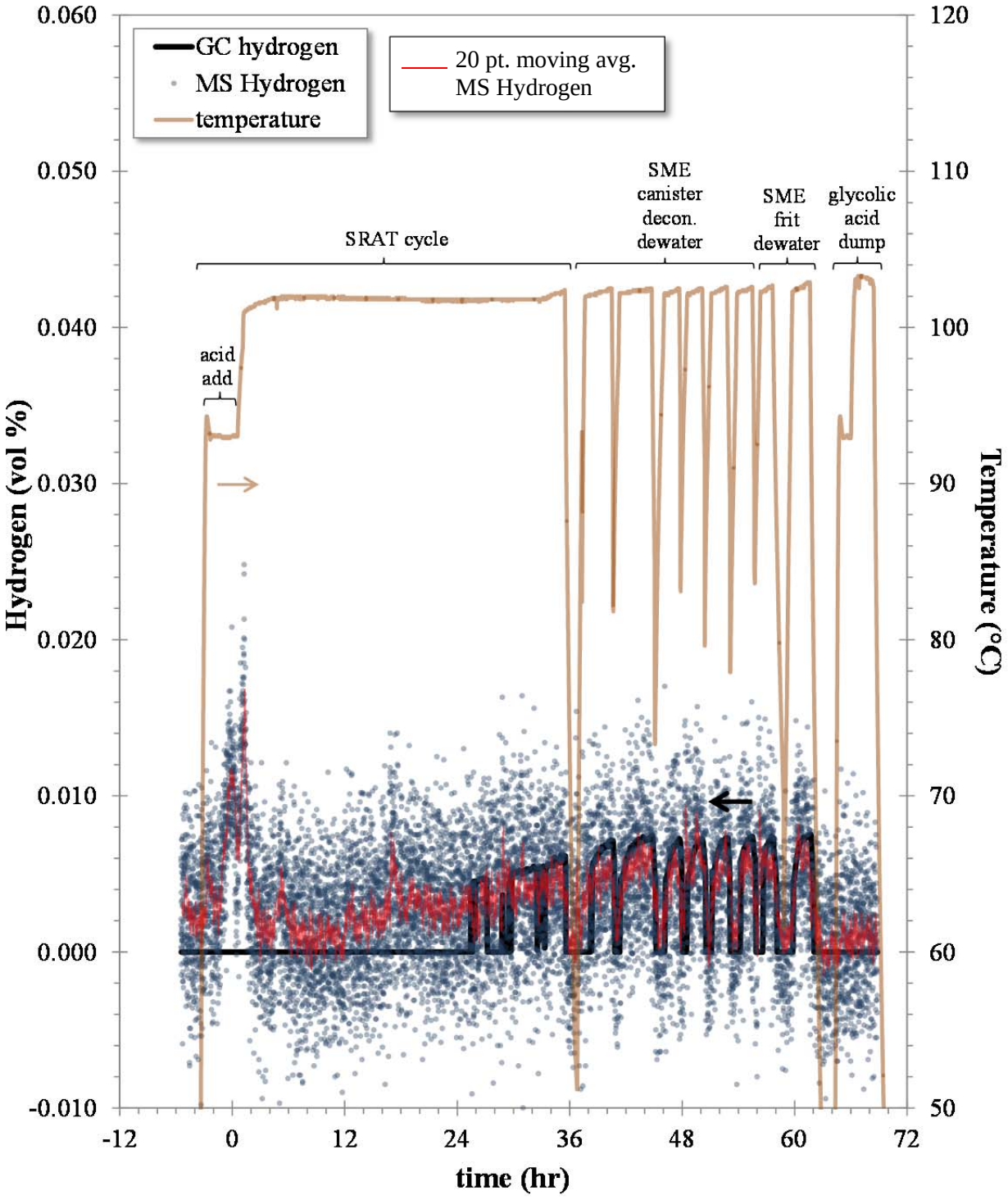

Figure 3-3. Hydrogen Produced During GN80

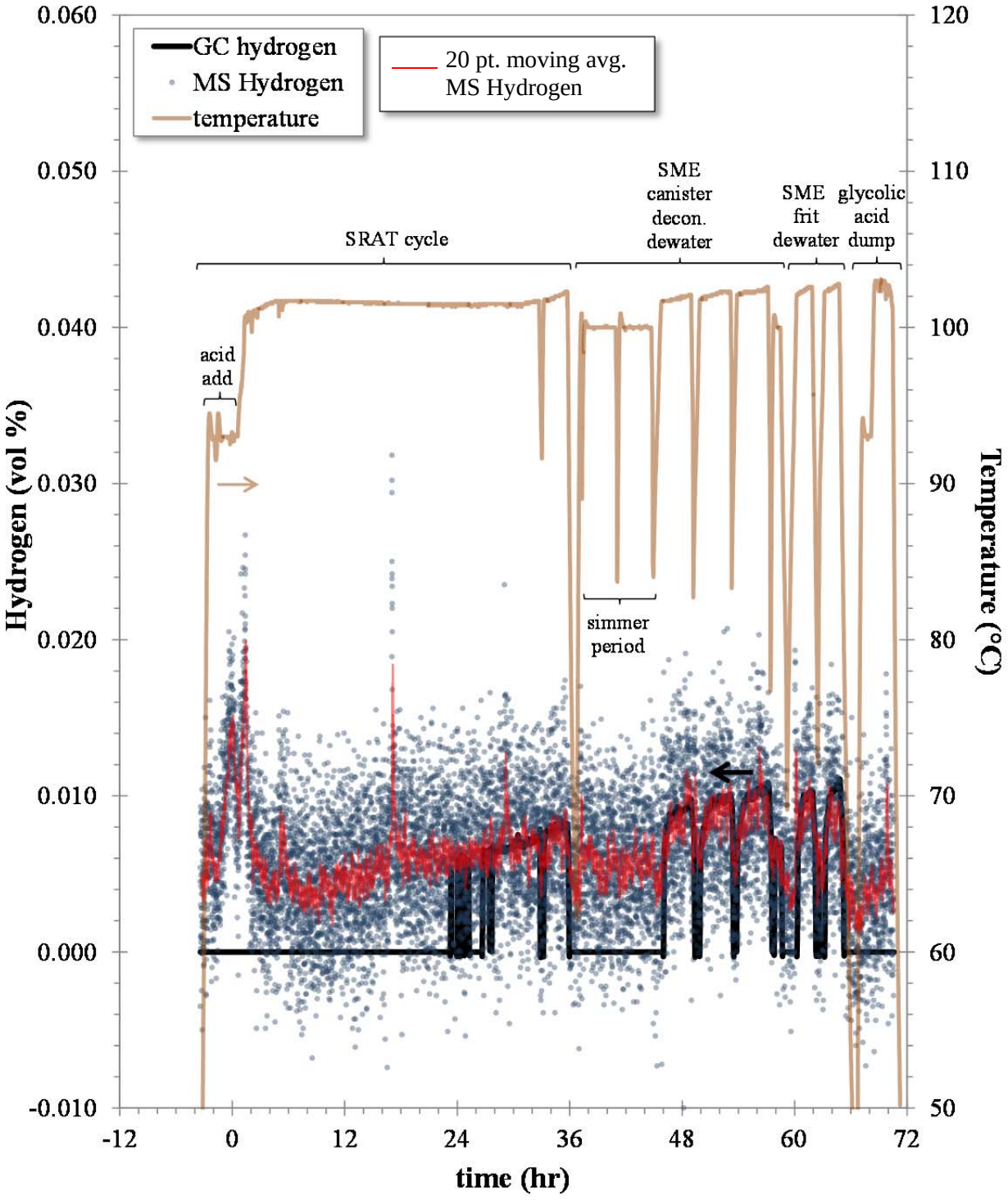

Figure 3-4. Hydrogen Produced During GN81

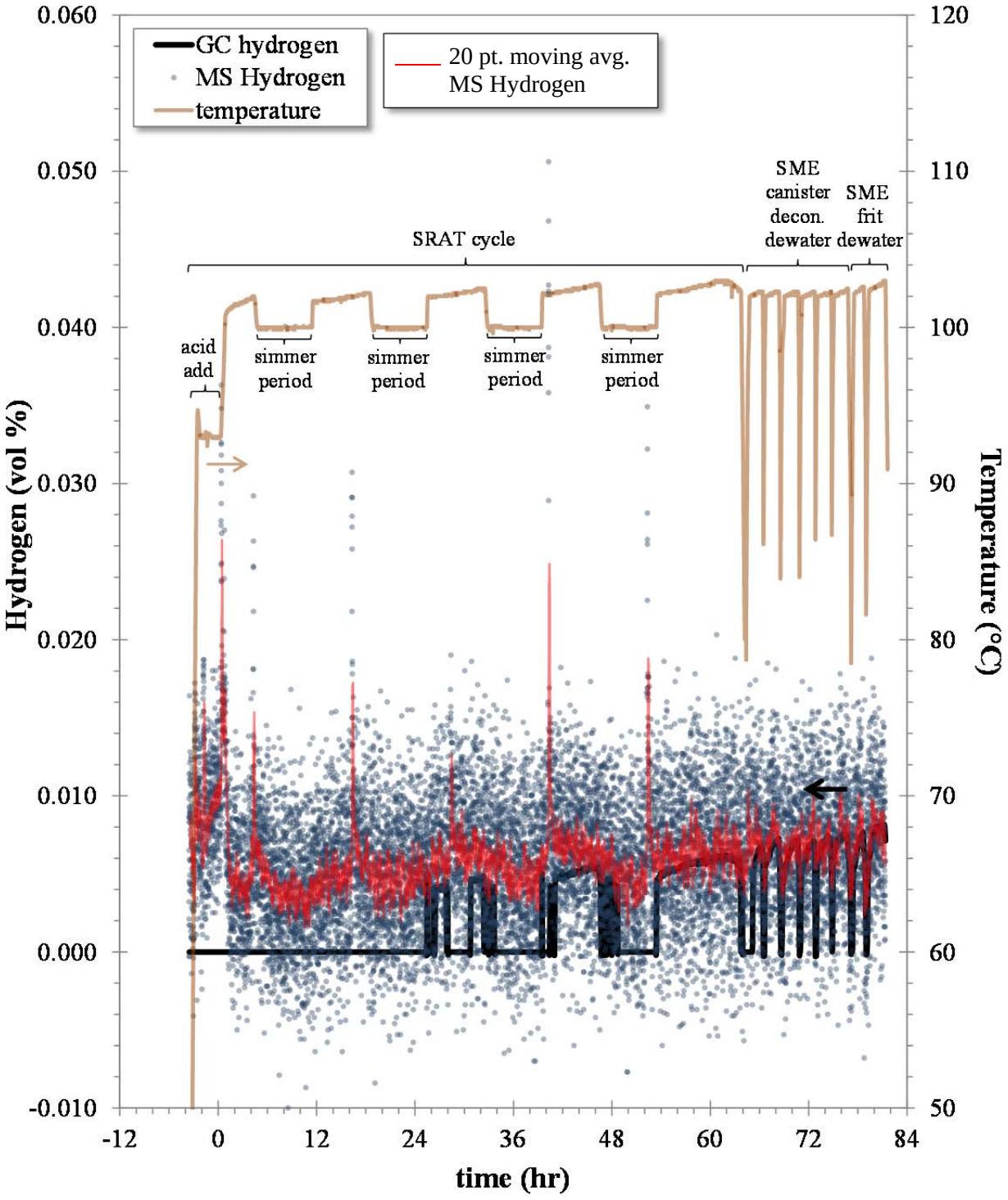

Figure 3-5. Hydrogen Produced During GN82

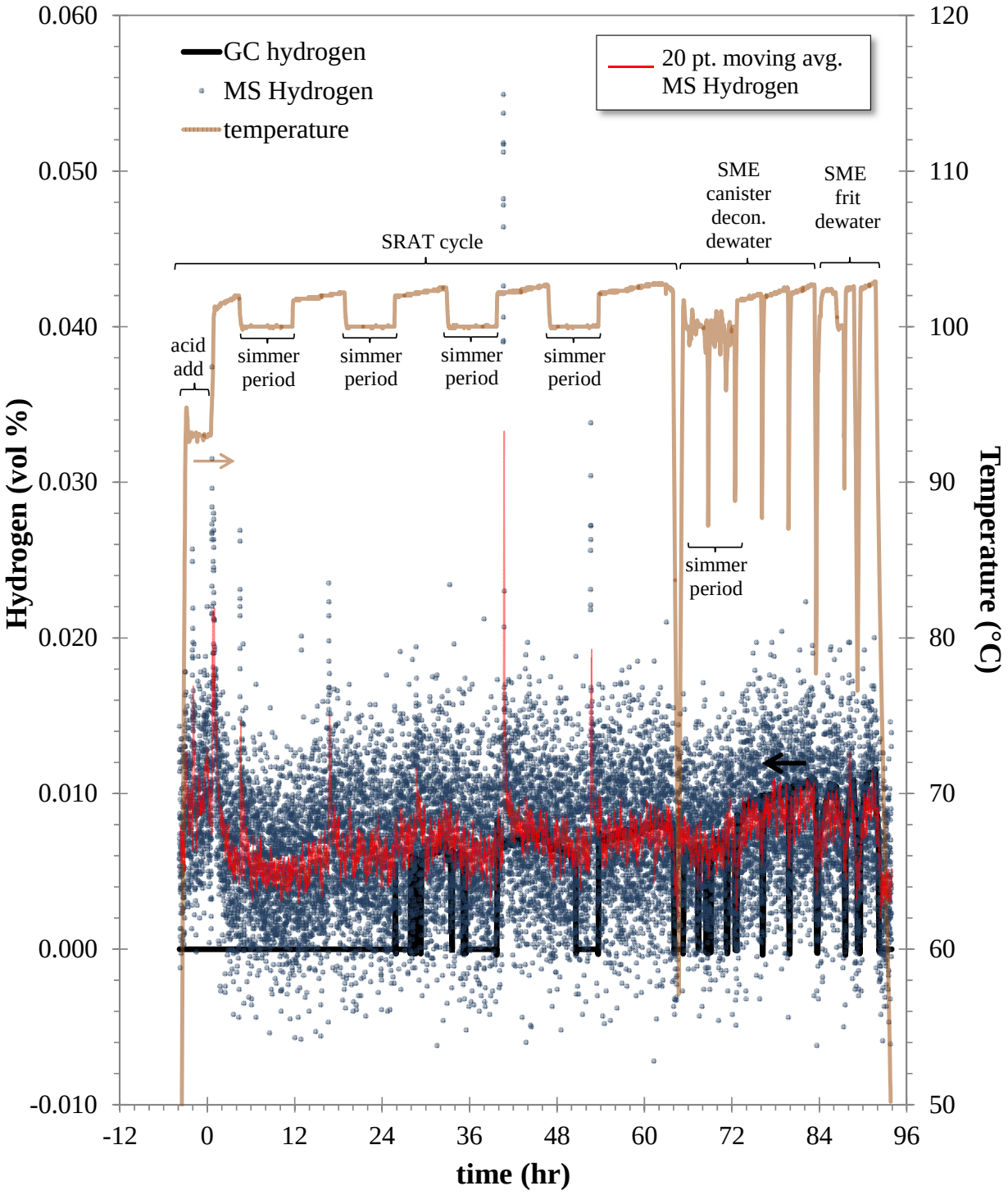

Figure 3-6. Hydrogen Produced During GN83

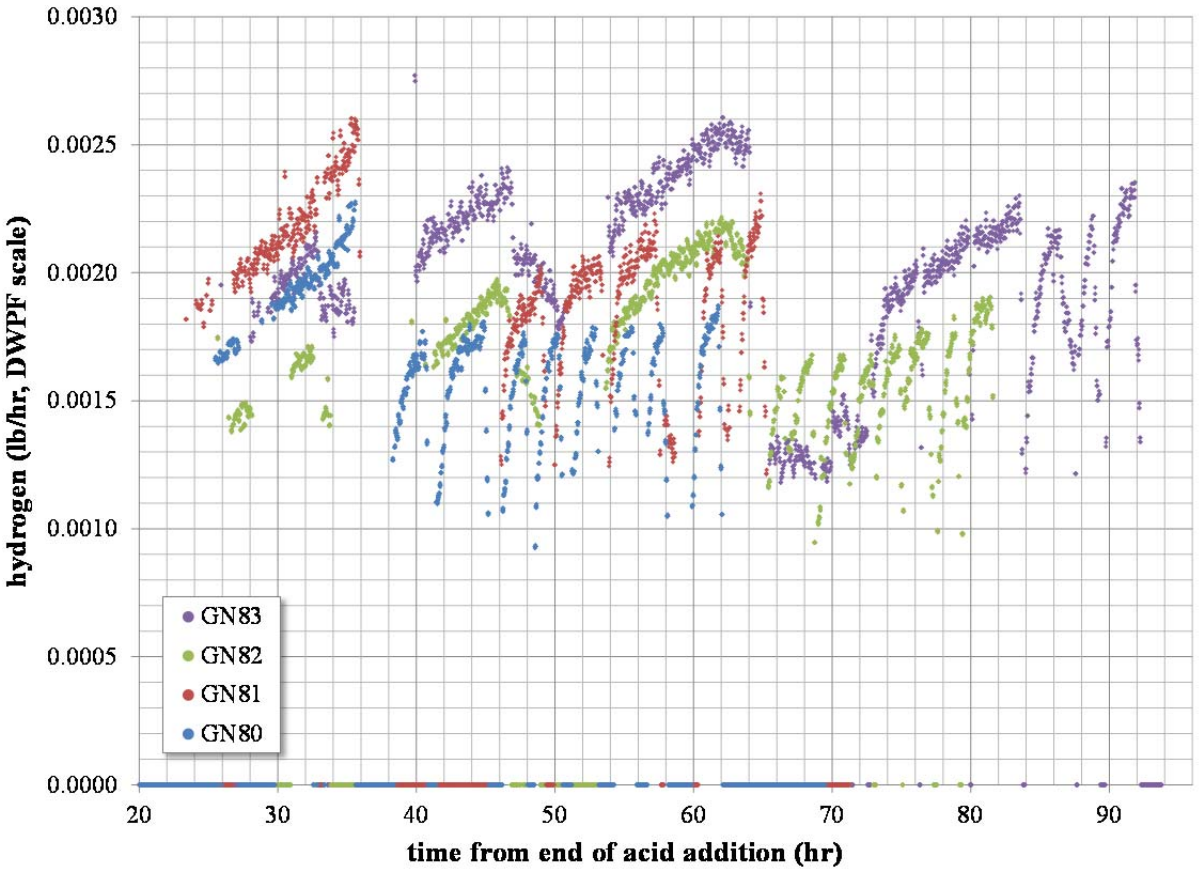

Figure 3-7. Hydrogen measurements late in the SRAT cycles and for the entire SME cycles

Figure 3-7 contains the hydrogen concentrations for all four tests as measured by GC. Because two tests were run in parallel, two GCs were used in this testing. The GC that was used for GN80 and GN82 had a slightly lower detection limit for hydrogen than the GC used for GN81 and GN83. Concurrently, GN80 and GN82 also had lower peak hydrogen levels than GN81 and GN83. This difference in hydrogen production is even noted for the SRAT portions of the test, where the pairs of tests performed concurrently (GN80 with GN81 and GN82 with GN83) were duplicated precisely. Thus, a component of the hydrogen production could not be reproduced between two nearly identical CPC simulation apparatuses. This difference appears be a function of slight differences in measuring low levels of hydrogen by the two separate GC instruments based on the proximity of the hydrogen peak to the helium tracer peak. It is recommended to use the data sets with larger hydrogen measurements in order to bound the catalytic hydrogen created in the CPC process. See the hydrogen measurement uncertainty discussion in Section 4.2.

One reason for performing some of these tests with periods of simmering after acid addition instead of straight boiling was to determine if a higher peak of hydrogen would be encountered when resuming boiling after an intentional simmering period or unintentional cooling of the vessel. One such increased peak was identified during the SRAT period of run GN83. The highest hydrogen concentration in the SRAT cycle of GN83 by GC was seen immediately after resuming boiling at about the 40 hour period (see Figure 3-7). The MS data was consistent with the GC data for this peak during GN83. The GN83 peak in hydrogen as measured by GC did not correspond to an antifoam addition. For the other three tests, the highest hydrogen concentration during the SRAT cycle was encountered at the end of the cycle.

Table 3-18. Maximum concentrations of hydrogen as measured by GC

Run	SRAT maximum H_2 (volume %)	SME maximum H_2 (volume %)	SRAT lb H_2/hr DWPF scale	SME lb H_2/hr DWPF scale
DWPF Limit			0.65	0.223
GN80	0.0062%	0.0075%	0.0023	0.0019
GN81	0.0080%	0.0106%	0.0026	0.0023
GN82	0.0062%	0.0081%	0.0022	0.0019
GN83	0.0082%	0.0110%	0.0028	0.0024

Table 3-18 lists the maximum hydrogen concentrations from the measurements made by GC. The peak hydrogen concentrations occurred during the SME cycle for all cases. The purge rate in the SME cycle (scaled to 74 scfm) is less than the purge rate in the SRAT (scaled to 93.7 scfm). When compared on the basis of the same purge rate, the maximum hydrogen release rates are very similar between the SRAT and the SME. Not only are the purge rates different, but the DWPF limits for hydrogen are also different for the SRAT and the SME. This testing showed that the hydrogen production and release rate was approximately 0.4% of the SRAT limit and approximately 1.1 % of the SME limit.

3.5.2 Other Flammable Offgas Species

Ammonia and HDMSO are the other potential flammable offgas species encountered in this testing. These components will be discussed below. Ammonia was not detected in the offgas by the FTIR for runs GN80 and GN82. The FTIR was not employed in runs GN81 and GN83.

HMDSO is a degradation fragment of Antifoam 747 as the molecule breaks into two pieces. HMDSO is tracked by the FTIR. Any addition of antifoam can be noted by a spike on the FTIR corresponding to HMDSO almost immediately after addition. It is important to consider the HMDSO released from antifoam decomposition because HMDSO can contribute to the composite flammability limit for the CPC.[12] Subsequent to this testing, it was determined that the peaks of HMDSO greater than 20 ppmv were due to the degradation of antifoam after dilution with water and before addition to the CPC vessel.[13] Additional antifoam degradation products were identified during the subsequent testing (trimethylsilanol and propanal), but no attempt was made to quantify these species in the offgas or the condensate during this testing.

Figure 3-8 and Figure 3-9 show the concentration of HMDSO released throughout the SRAT and SME cycles for GN80 and GN82, respectively, plotted along with SRAT vessel temperature. The peaks in HMDSO concentration correspond to each antifoam addition and to the initial boiling after completion of glycolic acid addition. Run GN82 had larger peak HMDSO concentrations than run GN80. Overall, the largest peak in HMDSO concentration measured by the FTIR was during the SRAT cycle of run GN82, which was 2020 ppmv or 14.0 mol/hr on the DWPF scale. The boric acid dewater during the SRAT cycle for GN82 was performed with alternating periods of boiling at 101 to 103 °C and “simmering” at 100 °C. When the antifoam was added during one of the 100 °C simmering periods (time of ~52.3 hrs), the majority of the HMDSO release occurred similarly to the HMDSO release for additions when the SRAT was boiling. The HMDSO peaks for GN82 were significantly larger during the SRAT compared with the SME even though the antifoam additions were the same for both operations and the purge rate is lower in the SME (this difference was not as pronounced for GN80). For SME canister decontamination dewater

additions, there are small HMDSO peaks (<10 ppm) when the SME is brought back to boiling when additional antifoam was not added. There is no record of how long the antifoam was diluted before each addition.

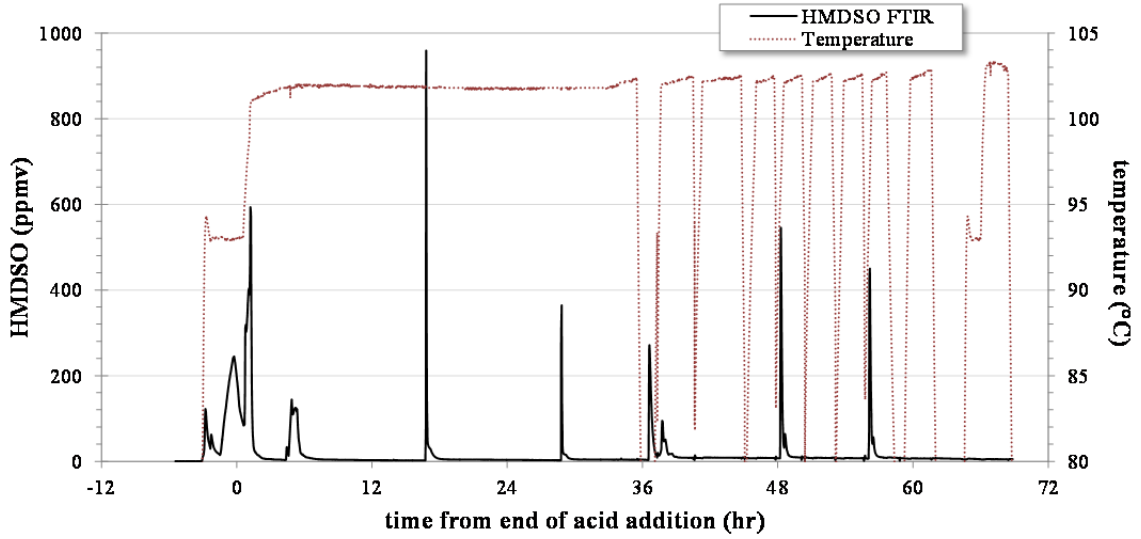

Figure 3-8. HMDSO by FTIR from GN80

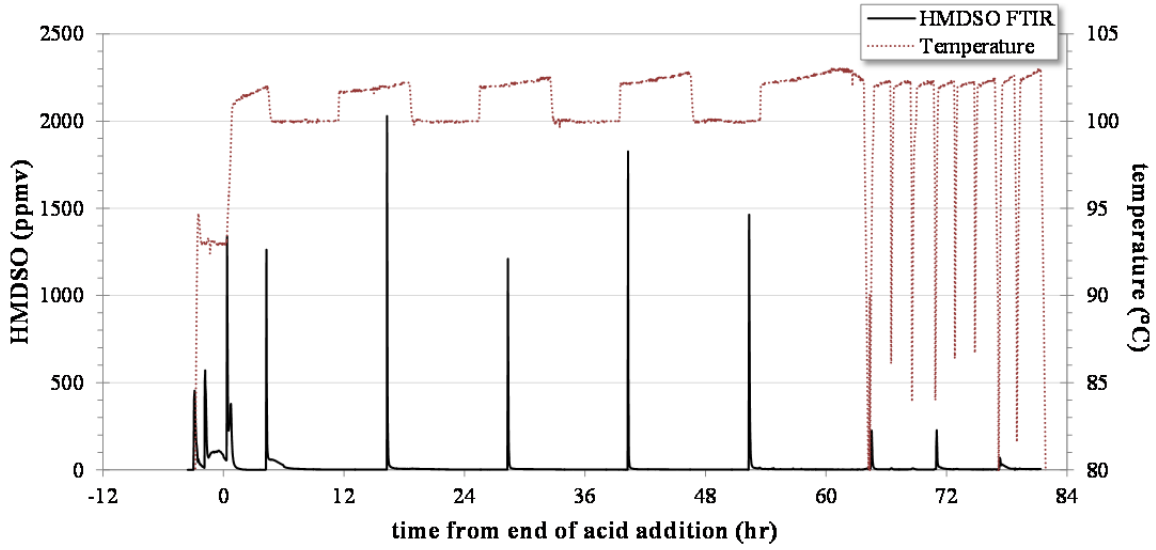

Figure 3-9. HMDSO by FTIR from GN82

3.5.3 Major Offgas Species

The major offgas species (CO_2, O_2, NO, NO_2, and N_2O) along with air components (N_2 and O_2) are shown in Figure 3-10 for the early part of the SRAT cycle of GN80. The later portion of the SRAT cycle and SME cycle for all runs are similar with declining concentrations of CO_2 and NO_x species.

The figure also contains information on the trend of temperature and pH over this time period. The pH crosses pH of 7 at approximately the time that the temperature reaches 93 °C. Acid addition and heating were initiated near the -3.6 hour point of Figure 3-10, where time zero is the end of glycolic acid addition.

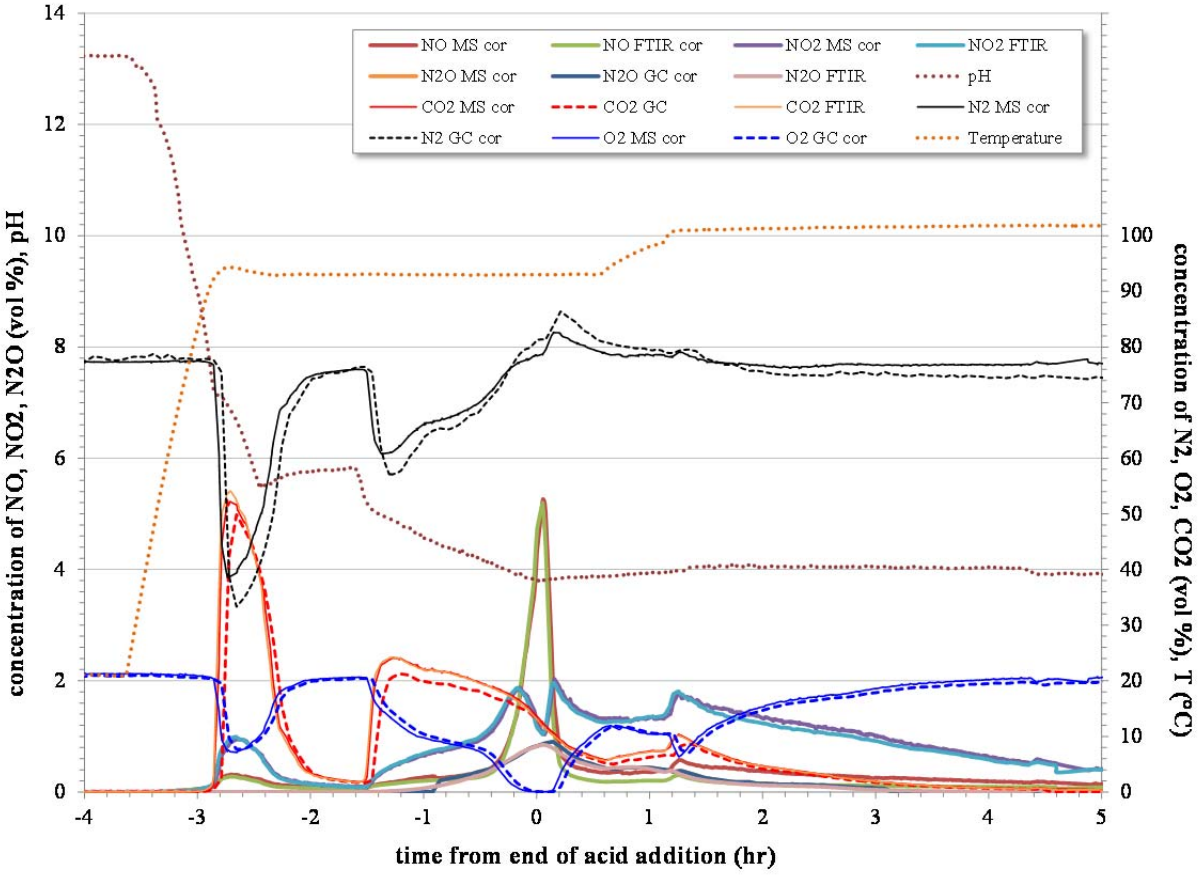

Figure 3-10. Gases emitted early in the SRAT cycle of GN80

There was excellent agreement between all three gas analyzers as can be seen from the graph. The other three runs had very similar concentration profiles. The profiles for GN81 through GN83 are contained in Appendix A (Figure A-1 through Figure A-8). For all tests, there is a period near time zero (near the end of glycolic acid addition and extending just afterwards) where the oxygen concentration in the SRAT offgas is reduced to zero. The lower SRAT cycle purge rate for the nitric-glycolic flowsheet (compared with the nitric-formic flowsheet) is at least partially responsible for this period of low O_2 and NO_2 and high NO and N_2O at the end of acid addition.

Table 3-19. Nitrogen Species Production Measured by Offgas Analyzers, mol% N

Generated Nitrogen Offgas Species	GN80	GN81	GN82	GN83
MS NO	31.3%	25.9%	19.8%	30.3%
MS NO_2	59.7%	56.5%	68.1%	51.6%
GC N_2O	18.1%	17.6%	12.1%	18.1%

The predominant nitrogen species measured by the offgas instruments is nitrogen. Nitrogen is largely introduced by the air purge and does not participate in the reactions. As a result, the other nitrogen offgas species will be the focus of the discussion. The predominant reactive nitrogen offgas species is NO_2. NO comprised approximately 20-30% of the reactive nitrogen moles, N_2O comprised 10-20% and NO_2 comprised 50-70%. Data for all runs is summarized in Table 3-19.

NO, N_2O and NO_2 are all produced through reactions destroying nitrite and by nitrate reactions. The profile of nitrogen species early in the SRAT cycles are indicated in Figure 3-10, Figure A-3, Figure A-5, and Figure A-7 in the Appendix. At the period where the oxygen concentration goes to zero at the end of the glycolic acid addition, the NO_2 concentration shows a decrease and the NO and N_2O concentrations show an increase. As oxygen concentration again increases, the N_2O concentration is sharply decreased. No NH_3 was detected by the FTIR or MS.

The predominant carbon offgas species is CO_2. CO_2 is produced through the reduction of carbonate (the first CO_2 peak). The reduction of mercury and the reaction to destroy nitrite comprise the second peak. The CO_2 slowly decreases while the nitrite is destroyed and manganese is reduced during acid addition and the beginning of the boiling segment of the SRAT cycle.

3.6 REDOX

Table 3-20 contains a summary of the REDOX measurements. Scatter is apparent between some of the individual glasses measured for REDOX. Averaged data is presented except for the cases where scatter was noted. The raw data from all REDOX measurements is contained in the Appendix in Tables A-1 and A-2.

Limited sample volume was collected from the SME product from runs GN80 and GN81 prior to the remaining material receiving the glycolic acid dump. Thus, only two portions of glass for REDOX measurement was prepared for the SME products of GN80 and GN81 without the glycolic acid dump. The results of the REDOX measurements on the two glasses for each of those runs were varied, 0.062 and 0.306 for GN80 and 0.085 and 0.297 for GN81. Ideally, additional glasses would be prepared and measured for those SME products. However, insufficient SME product remained from GN80 and GN81 to prepare additional glass for REDOX measurement. The lower of the REDOX values for GN80 and GN81 SME products are more consistent with the overall set of REDOX data.

All glass preparation for this work was performed by the Closed Crucible with Hot insertion (CC_{hot}) method, which involved the placement of the sealed crucible with dried slurry into the 1150 °C furnace.[14] Evaluation of the glass viscosity was not performed as part of this procedure. Many of the replicates of the resulting REDOX measurements of the SME product glasses performed by this method were more oxidized than the target of 0.14. The initial REDOX measurements for the previous tests GN73, GN75, GN77 and GN78 were performed using an alternative method of Closed Crucible with Ramped heat

treatment (CC_{ramp}), where the sealed crucible was placed into the furnace at a lower temperature and ramped to the final temperature of 1150 °C. The CC_{ramp} method was used to set the acid ratio for the target REDOX of 0.14. Subsequent CC_{hot} measurements for GN73, GN75, GN77 and GN78 were more consistent with the GN80 though GN83 REDOX values (at a slightly higher acid ratio) that showed that the glass was more oxidized than the target.[4] REDOX prediction for the nitric-glycolic flowsheet is still being investigated and the results of that work will be documented in a separate report.

As expected, the GN80 and GN81 materials after the glycolic acid dump produced glass that was highly reduced.

Table 3-20. Summary of REDOX measurements of glass made from SME products

run	Fe^{2+} / total Fe
GN80	0.062, 0.306
GN81	0.085, 0.297
GN82	0.056
GN83	All Fe^{+3}
GN80 acid dump	0.976 – all Fe^{2+}
GN81 acid dump	0.773 – all Fe^{2+}

3.7 Rheology

Flow curves for the SRAT and SME products were obtained by using a Haake RS600 rheometer and the current DWPF simulant rheology protocol.[6] The up and down curves were fit to a Bingham plastic model to determine yield stress and consistency. Table 3-21 contains a summary of the rheology data for GN80 through GN83. The DWPF design basis rheology is included for comparison.[15] All of the SRAT and SME products from runs GN80 through GN83 were below the lower limit of the DWPF design basis for yield stress and consistency. These low rheologies are consistent with previous testing with this range of acid stoichiometry.[4] As seen in Table 3-15, however, the waste loading of the SME products as estimated by comparing the iron content of the SME and SRAT products were distributed around the target waste loading of 36%. This means that in spite of the thin rheology of the SME products, the mixing during sampling was adequately keeping the frit suspended in the slurry. It may be possible to increase the consistency and/or yield stress to within the DWPF design basis range by increasing the insoluble solids concentration in the slurry.

Rheological changes were noted for the SME materials after they received the additional glycolic acid dump. The yield stress for GN80 and GN81 were very near the lower limit of the DWPF design basis and the consistencies were within the design basis.

Figure 3-11, Figure 3-12 and Figure 3-13 contain the flow curves that graphically represent the rheology data gathered on the SRAT products, SME products, and glycolic acid dump materials, respectively. A linear fit of the SRAT product rheology of GN80 and GN81 were virtually indistinguishable. Likewise, the SRAT product rheology of GN82 and GN83 were virtually indistinguishable with a slightly higher yield stress and consistency than GN80 and GN81. SME products from all four runs showed similar results, with shear thickening evident above 150 rotations per second. The higher shear rate data was not

used in the regression of the yield stress and consistency in Table 3-21. The glycolic acid dump material from GN80 and GN81 had higher consistency and yield stress than the corresponding SME products, but the flow curves had a very gradual increase

Table 3-21. SRAT and SME product rheology summary

Run	Insoluble Solids (wt %)	Up Yield Stress (Pa)	Down Yield Stress (Pa)	Up Consistency (cP)	Down Consistency (cP)
SRAT Design Basis[15]		1.5-5		5-12	
GN80 SRAT	12.5%	0.16	0.10	3.39	3.44
GN81 SRAT	13.1%	0.17	0.11	3.53	3.59
GN82 SRAT	12.9%	0.29	0.22	4.03	4.14
GN83 SRAT	13.0%	0.29	0.24	4.14	4.19
SME Design basis[15]		2.5-15		10-40	
GN80 SME	35.4%	0.91	0.59	6.12	6.77
GN81 SME	35.6%	0.88	0.60	7.34	7.11
GN82 SME	37.1%	1.01	0.60	6.15	6.88
GN83 SME	34.3%	0.98	0.56	6.24	7.09
GN80 Acid Dump	32.4%	1.94	1.52	17.4	17.2
GN81 Acid Dump	33.0%	2.94	2.44	26.7	28.5

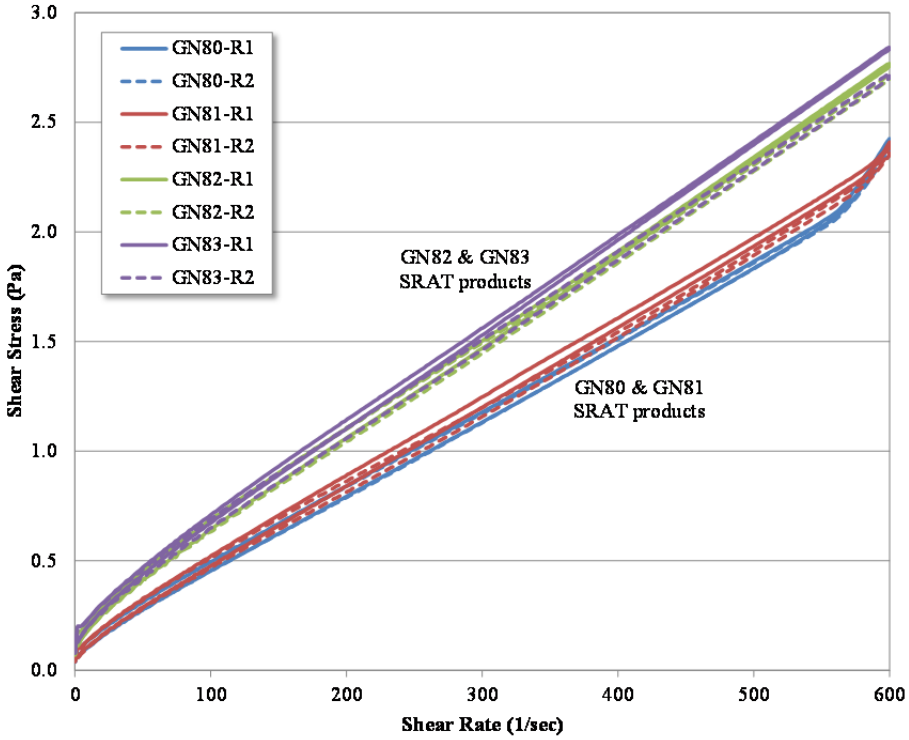

Figure 3-11. SRAT Product Rheology Curves

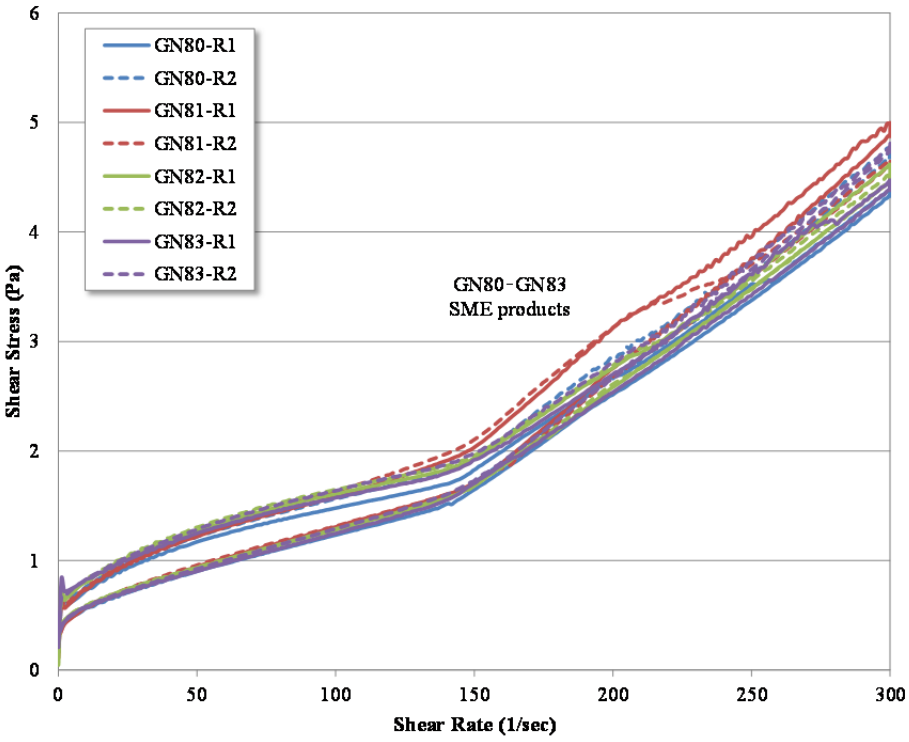

Figure 3-12. SME Product Rheology Curves

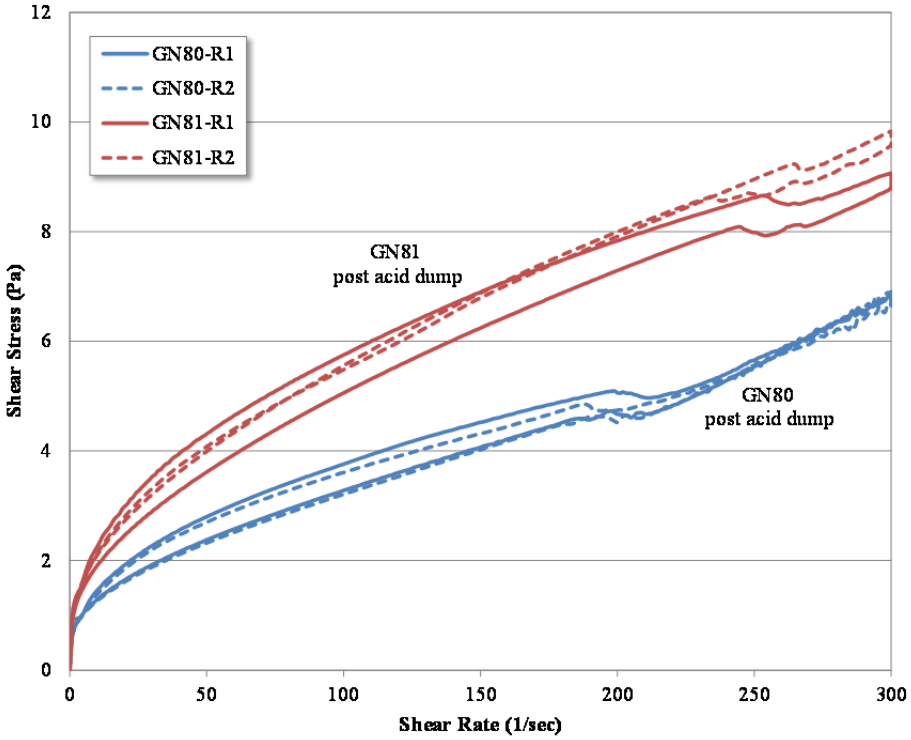

Figure 3-13. Rheology Curves for SME Products that Received Additional Glycolic Acid

3.8 Influence of Cold Temperatures on the Formation of White Precipitates

From previous testing, there was concern that crystallization of glycolate species could occur. The characterization and evaluation of impacts of calcium and manganese glycolate species crystallization has been summarized in a recent memorandum.[16] The SRAT product from run GF28 had white clumps or crystals that could be easily distinguished from the dark reddish brown sludge slurry.[17,18] These clumps appeared to be forming or congregating at the wall of the poly bottle. Similar white solids were seen on the bottom of several of the drums of SRAT product that Harrell produced for the Cold-cap Evaluation Furnace (CEF) testing.[19] The material was described as somewhat thick and lard-like. Subsequent analysis of the CEF feed material revealed that the white precipitated material may have been calcium glycolate. For the scaled demo run GN78, which used the same sludge simulant and had the same acid stoichiometry as runs GN80 though GN83, some of the early intermediate samples pulled from the SRAT cycle showed similar white solids forming on the sides of the bottle.[4] A hypothesis was formed that storage at cold temperatures is causing a precipitate that possibly contains glycolate.

No separate areas of white solids were noted in the SME product slurries for runs GN80 though GN83 within approximately one month from the end of the testing. During this period, the archived materials were stored at laboratory temperature. Figure 3-14 is a photograph of the archived materials from GN80 through GN83. GN80 and GN81 received the additional glycolic acid dump. Note that there are no white spots evident in the supernatant or settled portions of the slurry.

Immediately after the photograph in Figure 3-14 was taken, the archived products from GN80 through GN83 were stored in a refrigerator at approximately 5 °C. When checked after several days, small amounts of white solids were evident at the inner sides of the bottle in contact with the settled sludge layer of GN82 and GN83 SME products. Figure 3-15 contains two photographs of the materials from GN80 through GN83 after the bottles were removed from the refrigerator after fourteen days. Many small white dots are evident at the sides of the container below the surface of the settled sludge for GN82 and GN83. A few of the small areas of white solids are indicated by the yellow circles overlaid on the photographs. There may be some white dots for the post glycolic acid dump samples of GN80 and GN81, but there are much fewer. Although we did not perform chemical analysis, due to the constancy of the appearance we suspect the white solids in GN82 and GN83 SME products to be the same or similar to the white material noted in GF28 SRAT product, CEF feed, and GN78 intermediate SRAT samples.

For these samples, the precipitation appeared to be reversible. After storage at laboratory temperature again for several weeks, the white precipitates had disappeared. Figure 3-16 contains two photographs taken two months after removal of GN80 through GN83 from the refrigerator. There are no white precipitates evident in the samples shown in Figure 3-16.

Figure 3-14. GN80 through GN83 materials after storage at room temperature

Figure 3-15. GN80 through GN83 materials after storage for 2 weeks at ~5 °C

Figure 3-16. GN80 through GN83 materials after again storage at room temperature

4.0 Discussion

4.1 Comparison of Hydrogen Generation with Previous Tests

Runs GN80 through GN83 were performed with parameters chosen to maximize the generation of hydrogen for expected nitric-glycolic flowsheet conditions (high concentration of noble metals, high stoichiometric excess acid).[3] When compared to the nitric-formic flowsheet, hydrogen production remained relatively low for runs GN80 through GN83. Converted to the DWPF scale, the maximum hydrogen generation rate was 0.0028 lb/hr in the SRAT and 0.0024 lb/hr in the SME. From this testing, the peak hydrogen production and release rate was 0.43% of the current SRAT limit and 1.1 % of the current SME limit. There were no heating rod temperature excursions during this testing.

Table 4-1 contains a summary of peak hydrogen generation results from tests with glycolic acid as the sole reducing acid and tests with 80:20 mixtures of glycolic and formic acids as the reducing acid. For inclusion in the table, the runs needed to have glycolic acid corresponding to at least 80% of the reducing acid and hydrogen measurement by GC must have been attempted. The table includes three metrics of the acid use: the percent of KMA, the total moles of acid added per kg of slurry, and the ratio of reducing acid to total acid. The table lists the key elemental components that are known to influence catalytic hydrogen generation from formic acid, including mercury and the noble metals: silver, palladium, rhodium and ruthenium. Element concentrations are given on the basis of weight percent of the total dried solids in the sludge fed to the SRAT vessel.

Peak hydrogen concentrations measured by the GC during each SRAT and SME cycle are listed as calculated on the rate of generation on the DWPF scale. When hydrogen was not measured above the detection limit during the cycle, "b.d.l." for below detection limit is included in the table. Many of the runs only had a SRAT cycle and did not have a SME cycle, and in those cases "N/A" for not applicable is included in the table. For the SME portion of the back-to-back runs (GN65-GN68), "N/A" is included for the SRAT cycles.

Runs listed in the table prior to GN34 (renamed from GF34) had an 80:20 mixture of glycolic and formic acids, with the exception of run GN8 (renamed from GF8). Run GN8 and all runs starting with run GN34 had glycolic acid as the only reducing acid. Starting with run GN43, formic acid was not added during frit addition. Runs prior to GN43 which included SME cycles included 1.5 wt% formic acid added during frit addition. The majority of the runs were performed on an apparatus with a roughly 4 L volume. The exceptions are the actual-waste demonstration (SC-13), which was performed with 1 L of sludge slurry, and the scaled demonstration, which was performed in vessels with approximately 22 L (GN76 and GN77) and 220 L (GN78 and GN79) volumes.

The following is a discussion of each set of nitric-glycolic hydrogen generation data grouped by reference.

The initial CPC simulations for the nitric-glycolic-formic flowsheet with an 80:20 ratio of glycolic to formic acid produced a maximum hydrogen generation rate of 0.11 lb/hr in the SRAT and 0.17 lb/hr in the SME at DWPF scale.[20] This hydrogen generation rate was high relative to the rest of the set and was the only run in the set that did not include mercury in the feed, which is not a realistic situation for actual-waste sludge processing in DWPF. The highest peak hydrogen generation rate amongst the 80:20 glycolic:formic runs with mercury present was 0.024 lb/hr in the SRAT and 0.049 lb/hr in the SME at a relatively high 200% KMA. Run GN8, which did not include formic acid, had no detectible hydrogen from the SRAT cycle.

Run SC-13 was an approximate replicate the SRAT cycle of the 80:20 glycolic:formic run GF6 but with actual Sludge Batch 5 Tank 51H waste. Where run GF6 had a peak hydrogen of 0.013 lb/hr, the actual waste run SC-13 had catalytic hydrogen production below the GC detection limit of 0.001 lb/hr.[11]

The CPC simulations for the nitric-glycolic-formic flowsheet sludge matrix test with sludge simulants produced a maximum hydrogen generation rate of 0.0046 lb/hr at DWPF scale.[17] Because formic acid was added as a part of the reducing acid during the sludge matrix study, it is understandable that hydrogen was produced at a higher rate from some of those tests than was produced in GN80 through GN83.

Table 4-1. Summary of hydrogen generation from nitric-glycolic CPC testing

Run [g]	% KMA	Total Acid mol/kg slurry	Acid Ratio reducing/total	Hg wt%	Ag wt%	Pd wt%	Rh wt%	Ru wt%	SRAT H_2 Peak lb/hr DWPF scale	SME H_2 Peak lb/hr DWPF scale	Ref.	Note
GF2	125%	1.60	0.619	0	0.014	0.079	0.038	0.217	1.1E-01	1.7E-01	20	a,c
GF3	125%	1.64	0.617	3.263	0.014	0.079	0.038	0.217	6E-03	4E-03	20	a,c
GF4	125%	1.89	0.637	3.263	0.014	0.079	0.038	0.217	4E-03	3E-03	20	a,c
GF5	150%	1.97	0.594	3.263	0.014	0.079	0.038	0.217	8.0E-03	1.3E-02	20	a,c
GF6	100%	1.31	0.670	3.263	0.014	0.079	0.038	0.217	1.3E-02	1.2E-02	20	a,c
GF7	200%	2.62	0.602	3.263	0.014	0.079	0.038	0.217	2.4E-02	4.9E-02	20	a,c
GN8	125%	1.64	0.572	3.263	0.014	0.079	0.038	0.217	b.d.l.	N/A	20	
GF13	100%	1.30	0.508	3.263	0.014	0.079	0.038	0.217	b.d.l.	N/A	20	a
GF14	100%	1.30	0.588	3.263	0.014	0.079	0.038	0.217	8.0E-03	N/A	20	a
GF15	100%	1.30	0.549	3.263	0.014	0.079	0.038	0.217	5.0E-03	N/A	20	a
GF16	100%	1.30	0.628	3.263	0.014	0.079	0.038	0.217	6.0E-03	N/A	20	a
SC-13	100%	1.17	0.600	1.94	0.0121	0.00321	0.0201	0.0926	b.d.l.	N/A	11	f
GF26	100%	1.41	0.571	1.5	0.001	0.0003	0.0026	0.101	3.7E-03	N/A	17	a
GF27	150%	2.11	0.512	1.5	0.001	0.0003	0.0026	0.101	2.8E-03	N/A	17	a
GF28	100%	1.43	0.609	1.5	0.001	0.0003	0.0026	0.101	3.1E-03	N/A	17	a
GF29	150%	2.15	0.537	1.5	0.001	0.0003	0.0026	0.101	b.d.l.	N/A	17	a
GF30	100%	1.31	0.580	1.5	0.001	0.0003	0.0026	0.101	4.6E-03	N/A	17	a
GF31	150%	1.96	0.518	1.5	0.001	0.0003	0.0026	0.101	b.d.l.	N/A	17	a
GF32A	100%	1.33	0.606	1.5	0.001	0.0003	0.0026	0.101	b.d.l.	N/A	17	a
GF33A	150%	1.99	0.535	1.5	0.001	0.0003	0.0026	0.101	b.d.l.	N/A	17	a
GN34	104%	1.54	0.631	1.5	0.0014	0.079	0.038	0.217	b.d.l.	5.6E-03	21	c
GN34B	104%	1.54	0.631	1.5	0.0014	0.079	0.038	0.217	b.d.l.	N/A	21	
GN34C	104%	1.54	0.631	1.5	0.0014	0.079	0.038	0.217	b.d.l.	N/A	21	
GN35	100%	1.05	0.569	1.5	0.0014	0.079	0.038	0.217	b.d.l.	4.0E-03	21	c
GN36	106%	1.53	0.593	1.5	0.0014	0.079	0.038	0.217	b.d.l.	1.11E-02	21	c
GN36B	106%	1.53	0.593	1.5	0.0014	0.079	0.038	0.217	b.d.l.	N/A	21	
GN36C	106%	1.53	0.593	1.5	0.0014	0.079	0.038	0.217	b.d.l.	N/A	21	
GN37	100%	1.33	0.604	1.5	0.0014	0.079	0.038	0.217	b.d.l.	1.57E-02	21	b,c
GN37B	100%	1.33	0.604	1.5	0.0014	0.079	0.038	0.217	b.d.l.	N/A	21	
GN38	125%	1.66	0.590	1.5	0.0014	0.079	0.038	0.217	b.d.l.	N/A	21	
GN40	134%	1.85	0.537	1.5	0.0144	0.0033	0.0192	0.0877	2.9E-03	1.8E-03	21	c
GN41	130%	1.90	0.537	1.5	0.0144	0.0033	0.0192	0.0877	3.2E-03	b.d.l.	21	c
GN60	110%	1.41	0.548	1.34	0.0012	0.0706	0.0339	0.194	b.d.l.	N/A	23	
GN61	110%	1.41	0.548	1.34	0.0012	0.0706	0.0339	0.194	b.d.l.	N/A	23	
GN62	110%	1.41	0.548	1.34	0.0012	0.0706	0.0339	0.194	b.d.l.	N/A	23	
GN63	110%	1.41	0.548	1.34	0.0012	0.0706	0.0339	0.194	b.d.l.	N/A	23	
GN64	110%	1.41	0.548	1.34	0.0012	0.0706	0.0339	0.194	b.d.l.	N/A	23	
GN65	110%	1.41	0.548	1.34	0.0012	0.0706	0.0339	0.194	N/A	4.1E-03	23	
GN66	110%	1.41	0.548	1.34	0.0012	0.0706	0.0339	0.194	N/A	4.9E-03	23	b
GN67	110%	1.41	0.548	1.34	0.0012	0.0706	0.0339	0.194	N/A	7.6E-03	23	b
GN68	110%	1.41	0.548	1.34	0.0012	0.0706	0.0339	0.194	N/A	3.9E-03	23	b
GN70	100%	1.19	0.583	2.14	0.0164	0.0034	0.0175	0.083	4.2E-03	2.2E-03	4	
GN71	125%	1.49	0.550	2.14	0.0164	0.0034	0.0175	0.083	1.4E-01	b.d.l.	4	b
GN72	100%	1.19	0.521	2.14	0.0164	0.0034	0.0175	0.083	b.d.l.	b.d.l.	4	
GN73	110%	1.31	0.522	2.14	0.0164	0.0034	0.0175	0.083	b.d.l.	b.d.l.	4	
GN74	100%	1.19	0.545	2.14	0.0164	0.0034	0.0175	0.083	b.d.l.	b.d.l.	4	
GN75	110%	1.31	0.522	2.14	0.0164	0.0034	0.0175	0.083	b.d.l.	b.d.l.	4	
GN76	100%	1.20	0.583	2.14	0.0164	0.0034	0.0175	0.083	b.d.l.	b.d.l.	4	d
GN77	110%	1.31	0.522	2.14	0.0164	0.0034	0.0175	0.083	b.d.l.	b.d.l.	4	d
GN78	110%	1.31	0.522	2.14	0.0164	0.0034	0.0175	0.083	b.d.l.	4.9E-03	4	e
GN79	100%	1.19	0.545	2.14	0.0164	0.0034	0.0175	0.083	b.d.l.	7.2E-03	4	e
GN80	110%	1.30	0.542	1.00	0.0164	0.0034	0.0475	0.2713	2.3E-03	1.9E-03		
GN81	110%	1.30	0.542	1.00	0.0164	0.0034	0.0475	0.2713	2.6E-03	2.3E-03		
GN82	110%	1.30	0.542	1.00	0.0164	0.0034	0.0475	0.2713	2.2E-03	1.9E-03		
GN83	110%	1.30	0.542	1.00	0.0164	0.0034	0.0475	0.2713	2.8E-03	2.4E-03		

b.d.l. = below the GC detection limit for hydrogen; N/A = Not Applicable due to cylcle not being performed; n.r. = not reported

a = reducing acid was 80:20 mixture of glycolic:formic; b = heating rod fouling, temperature excursions, or heat transfer issues were encountered;

c = 1.5 wt% formic acid added with frit; d = 22 L scale; e = 220 L scale; f = actual waste 1 L run with 80:20 glycolic:formic

g = in this report, GN is used as a prefex when formic acid was not present (some such runs were labeled as GF in orignial reports)

CPC simulation sludge matrix tests were performed using the nitric-glycolic flowsheet.[21] The tests with the highest peak hydrogen generation during the SRAT cycle were GN40 and GN41 at 0.00287 and 0.00324 lb/hr at DWPF scale, respectively. The feeds for these tests with the most hydrogen had a relatively high total acid added with respect to the %KMA due to the relatively high supernatant sodium salt content. The other tests in this set had hydrogen generation during the SRAT cycle at <0.0014 lb/hr at DWPF scale. The SME cycles (when performed) during this testing included formic acid in the frit additions and had hydrogen generation as high as 0.0157 lb/hr at DWPF scale. Run GN37, which had the highest hydrogen generation during the SME cycle, also had heating rod fouling. Heating rod fouling has been seen in other testing to lead to higher heating rod temperatures and correlate with increased hydrogen generation.[22] The steam heading in DWPF would not lead to increased coil temperatures in fouled sections of the coil and thus would not be expected to contribute to increased hydrogen generation. The SME cycle for run GN36 has the highest hydrogen generation rate at DWPF scale (0.0111 lb/hr) amongst all nitric-glycolic flowsheet runs when only considering runs in which heating rod fouling did not occur. The GN36 SME product had a hydrogen generation rate approximately 5-times the SME hydrogen generation rate in run GN83 (the highest SME hydrogen generation rate amongst runs GN80 through GN83). Run GN36 did have 1.5 wt% formic acid included in the frit addition, which falls outside of the conditions that the nitric-glycolic flowsheet will be run. Thus, it may be over-conservative to use the SME cycle hydrogen production from GN36 as a basis for the anticipated nitric-glycolic flowsheet without the introduction of formic acid during the frit addition.

Eight additional nitric-glycolic flowsheet tests (GN43-GN50) were performed with offgas measurement but they were not documented and they are not included in Table 4-1. Two of the eight tests had measureable hydrogen generation but also had major rheology issues that lead to very poor mixing and poor heat transfer. Due to the data integrity issues, it is not recommended to use the hydrogen data from these runs.

Subsequent CPC simulations studied the influence of batch heels by performing five back-to-back SRAT cycles and four back-to-back SME cycles.[23] SRAT cycle hydrogen generation was below the detection limit, corresponding to <0.0005 lb/hr at DWPF scale. SME cycle peak hydrogen generation ranged from 0.0039 to 0.0071 lb/hr at DWPF scale. All SME cycles except GN65 encountered heating rod fouling, which may have contributed to higher hydrogen generation rates.

With two exceptions, the hydrogen generation rates encountered during the CPC scaled demonstration with simulants were within the rates of runs GN80 through GN83.[4] The exceptions are scaled rates of 0.0042 lb/hr for run GN70 and 0.14 lb/hr for run GN71. The hydrogen produced during run GN71 was coincident with heating rod fouling, with a temperature excursion of the heating rod exceeding 550 °C. The high hydrogen produced during run GN71 is not representative of hydrogen production from the nitric-glycolic flowsheet due to the temperature excursion well outside of the range that is possible to attain in DWPF. The hydrogen generation rates for the SME cycles of the 220-L runs GN78 and GN79 were also not within the rates of runs GN80 through GN83.[4] Of these two runs, GN79 had the higher SME hydrogen generation rate of 0.0078 lb/hr at DWPF scale.

The factors that were thought to impact the hydrogen generation most strongly were manipulated in this study, including high concentration of noble metals and high acid stoichiometry for the nitric-glycolic flowsheet. The hydrogen generation data for runs GN80 through GN83 would be acceptable to use for the maximum hydrogen production during CPC processing under normal DWPF heating conditions. However, as seen in the discussion above, runs GN80 through GN83 did not produce the highest hydrogen generation rates. It would be more appropriate to use the higher runs from the entire set of data when considering the maximum hydrogen production during CPC processing with nitric-glycolic flowsheet. Runs GN41 and GN70 produced the highest hydrogen generation rates in the SRAT (0.00324 lb/hr and 0.00042 lb/hr, respectively). Run GN36 produced the highest valid hydrogen generation rate in

the SME (0.0111 lb/hr), but formic acid was added with the frit addition. Run GN79 produced the highest valid hydrogen generation rate in the SME (0.0072 lb/hr) for which formic acid was not added.

It is recommended that hydrogen concentration continue to be measured for non-radioactive and actual waste CPC simulations for future sludge batches. However, measurement of hydrogen at the low levels produced in the nitric-glycolic flowsheet is challenging and improvements in the analytical measurement may be necessary.

4.2 Hydrogen Measurement Uncertainty

An uncertainty analysis was performed to place an upper bound (with 95% confidence) on the reported maximum hydrogen concentrations and generation rates encountered during individual nitric-glycolic flowsheet runs. The focus of this uncertainty analysis was runs GN80 through GN83, plus the runs summarized in Table 4-1 that had the maximum hydrogen production without temperature excursions.

Several factors contribute to uncertainty in the hydrogen measurements and generation rates. The factors considered in this analysis include the following:

- Uncertainty in the air purge flowrate
- Uncertainty in the helium tracer flowrate
- Uncertainty in the hydrogen and nitrous oxide concentrations in the GC calibration gasses
- Uncertainty due to variance in GC measurements
- Bias due to drift in the calibration during the run

The MKS flow meter / flow controllers used for the flow rates of the air purge and helium tracer had tolerances of 2% of full scale and were tracked in the M&TE program. The standards used to calibrate GC for concentration of hydrogen, helium, and other gasses have a NIST certification to 5% of the reported concentrations. The variance in the GC measurements is estimated from the data collected during the instrument calibration check. The bias due to the calibration drift is handled by processing the calibration of the GC in a manner to provide conservatively large hydrogen generation measurements. The pre- and post-run calibration-check information is compared, and the sets of calibration data are used that would maximize the instrument-measured hydrogen and nitrous oxide concentrations and minimize the helium tracer concentration.

Uncertainty can be applied to the maximum hydrogen concentration and the corresponding helium concentrations by Equations 3 and 4, respectively. The concentrations of hydrogen and helium (C_{H2} and C_{He}) are in mole fraction. These equations are the GC responses (e.g., $area_{H2}$ and $area_{He}$) multiplied by the GC response factor and the targeted to actual purge flow. The GC response is in terms of an area. Gas of known concentration (calibration gas) is run through the GC. A response factor of known concentration/known area is then used to determine concentration of gasses in the SRAT and SME offgas. A response factor is determined as the relationship between the integrated chromatogram area with the concentration in the gas standard. $F_{SRNL\text{-}purge}$ is the target SRNL purge rate; and F_{air} and F_{He} are the flow rates of air and helium purges at lab scale. While the ratio ($F_{SRNL\text{-}purge}$ / (F_{air} + F_{He})) is by definition equal to 1 (the sum of the He and air flow rates are set to equal the SRNL purge rate), these terms allow accounting for the uncertainty in the He and air flow controllers.

$$C_{H_2} = area_{H_2}\left(\frac{C_{H_2}^{std}}{area_{H_2}^{std}}\right)\left(\frac{F_{\text{SRNL-purge}}}{F_{\text{air}} + F_{\text{He}}}\right) \quad [3]$$

$$C_{\mathrm{He}} = area_{\mathrm{He}} \left(\frac{C_{\mathrm{He}}^{std}}{area_{\mathrm{He}}^{std}} \right) \left(\frac{F_{\mathrm{SRNL\text{-}purge}}}{F_{\mathrm{air}} + F_{\mathrm{He}}} \right) \quad [4]$$

The value calculated by Equation 5 is the DWPF-scale generation rate of hydrogen, in lb/hr, scaled from the results for mole fraction concentrations calculated by Equations 3 and 4. The DWPF-scale purge flow rates ($F_{DWPF\text{-}purge}$) are based on 93.7 scfm purge in the SRAT and 74 scfm purge in the SME. MW is the molecular weight of H_2 and $A_{constant}$ is a combination of multiple unit conversions. The helium tracer concentration is used to correct the offgas data for the unknown total offgas flowrate.

$$\mathrm{H}_{2(\mathrm{DWPF\text{-}scale})}(\mathrm{lb/hr}) = \frac{C_{\mathrm{H}_2}}{C_{\mathrm{He}}} * F_{He} * \frac{F_{\mathrm{DWPF\text{-}purge}}}{F_{\mathrm{SRNL\text{-}purge}}} * MW_{\mathrm{H}_2} * A_{\mathrm{constant}} \quad [5]$$

The inputs were processed using the statistical package GUM Workbench[24] to propagate the uncertainty in the measurements to the calculated results. Table 4-2 and Table 4-3 contain the results of the uncertainty analysis for the DWPF-scale maximum concentrations and generation rates, respectively. The expanded uncertainties are the half-widths of the two sided 95% confidence intervals on the average analytical measurements and adjusted to DWPF scale when necessary. The upper 95% bounds are the sum of the averages and the half-widths of the confidence intervals. Thus, these upper 95% bounds are the maximum values adjusted for the uncertainty based on the nitric-glycolic flowsheet scaled demonstration. Uncertainty analysis could not be performed effectively for the SME cycle of run GN36, but that run would not be representative of the planned nitric-glycolic flowsheet SME cycle because formic acid was added during the frit addition. Because the reprocessing of the hydrogen concentration and generation rate data included a more conservative approach to account for the drift in the calibration during the run, some results in Table 4-2 and Table 4-3 do not match the precise values or the significant digits reported in Section 3.5.1.

Table 4-2. Maximum concentrations of hydrogen encountered in runs GN80 through GN83, GN41 SRAT, and GN36 and GN79 SME

	maximum concentration (vol%)	expanded uncertainty (vol%)	maximum concentration upper 95% bound (vol%)
GN80 SRAT H_2	0.0066	0.0062	**0.0128**
GN81 SRAT H_2	0.0080	0.0028	**0.0108**
GN82 SRAT H_2	0.006	0.014	**0.020**
GN83 SRAT H_2	0.0082	0.0041	**0.0123**
GN41 SRAT H_2 [21]	0.009	0.013	**0.022**
GN70 SRAT H_2 [4]	0.0114	0.0079	**0.0193**
GN80 SME H_2	0.0080	0.0063	**0.0143**
GN81 SME H_2	0.0105	0.0028	**0.0133**
GN82 SME H_2	0.008	0.014	**0.022**
GN83 SME H_2	0.0110	0.0041	**0.0151**
GN36 SME H_2 [21]	0.062	n.d.	**n.d.**
GN79 SME H_2 [4]	0.0306	0.0074	**0.0380**

n.d. = not determined

Table 4-3: DWPF-scale generation rates of hydrogen from runs GN80 through GN83, GN41 SRAT, and GN36 and GN79 SME

	DWPF-scale rate (lb/hr)	expanded uncertainty (lb/hr)	DWPF-scale rate upper 95% bound (lb/hr)
GN80 SRAT H_2	0.0024	0.0016	**0.0040**
GN81 SRAT H_2	0.0026	0.0008	**0.0034**
GN82 SRAT H_2	0.0022	0.0044	**0.0066**
GN83 SRAT H_2	0.0028	0.0013	**0.0041**
GN41 SRAT H_2 [21]	0.0028	0.0038	**0.0066**
GN70 SRAT H_2 [4]	0.0042	0.0024	**0.0066**
GN80 SME H_2	0.0024	0.0013	**0.0037**
GN81 SME H_2	0.0028	0.0007	**0.0035**
GN82 SME H_2	0.0023	0.0036	**0.0059**
GN83 SME H_2	0.0029	0.0010	**0.0039**
GN36 SME H_2 [21]	0.011	n.d.	**n.d.**
GN79 SME H_2 [4]	0.0072	0.0015	**0.0087**

n.d. = not determined

Including uncertainty, the highest peak DWPF-scale hydrogen generation rate in the SRAT cycle was 0.0066 lb/hr encountered in three separate tests (GN41, GN70, and GN82). For runs GN41 and GN82, the majority of this rate was attributable to the high uncertainty, while run GN70 had the highest rate prior to inclusion of uncertainty. Including uncertainty, the highest peak DWPF-scale hydrogen generation rate in the SME cycle was 0.0087 lb/hr for 220-L scaled run GN79.

For runs without formic acid addition in the SRAT or the SME that did not have temperature excursions due to heating rod fowling, run GN79 had the highest overall peak hydrogen concentration of 0.038 vol % at the upper 95% confidence interval of the analytical measurement. This corresponds to 0.95% of the lower flammability limit of hydrogen in air, which is 4.0 vol%.[25] For comparison, the peak hydrogen concentration for GN36 of 0.062 vol%, for which formic acid was added during frit addition, corresponds to 1.6 % of the lower flammability limit of hydrogen in air. Based on these results, the peak levels of hydrogen produced during the glycolic-nitric flowsheet testing were reliably and significantly less than 25% of the lower flammability limit of hydrogen in air.

The largest source of uncertainty in the hydrogen results is the estimated variance in the hydrogen measurement. The variance in the hydrogen measurements were determined by the absolute variance in the calibration standard readings for hydrogen. Applying the absolute variance in the calibration standard measurement directly to the measurements at lower hydrogen concentrations is conservative. Potential improvements can be made to the estimation of hydrogen measurement variance if an additional standard with lower hydrogen concentration is used for nitric-glycolic flowsheet testing. After the measurement

variance, the next largest sources of uncertainty in the hydrogen results are typically the calibration gas concentrations, the purge air flow, and the helium flow.

This uncertainty analysis is primarily based on the analytical method. There are some uncertainties that are not being addressed by this analysis. The CPC process simulation was performed on a sludge simulant based on Sludge Batch 8 composition and this uncertainty analysis does not take into account any potential differences between the material used in the simulation and the material that is actually processed in DWPF.

There is an additional bias based on the separation of helium and hydrogen in both the calibration gas and the process offgas samples. Based on how the GC was calibrated and the chromatogram integration was performed, the hydrogen measurements are conservatively large. For additional conservatism, it is recommended to not correcting for this bias.

Figure 4-1 and Figure 4-2 contain examples of the portions of the GC chromatograms during the time that helium and hydrogen are eluted (approximately 0.56 minutes through 0.64 minutes). The data shown are from the points in time where the highest hydrogen concentrations were noted for runs GN80 and GN83. The first peak on each chromatogram, which corresponds to the 0.5 wt% of helium used as a tracer, is much larger than the second peak, which corresponds to the hydrogen formed in the process. The hydrogen measurements at low concentration are biased high due to contribution from the tail of the helium peak. For the hydrogen concentrations measured for GN80 through GN83, this bias appeared to contribute a factor of 2 to 4 to the hydrogen concentration. This bias is illustrated in and as the difference in integrating for the hydrogen peak based on the baseline prior to the helium peak (left chromatogram) and the tangential baseline that removes the helium tail (right chromatogram) This bias would approach zero as the concentration of hydrogen increases to the concentration of the 1% hydrogen standard.

Figure 4-1 and Figure 4-2 also show that slight differences in the separation of helium and hydrogen between the two separate GCs can be considered as the main cause of the apparent variation between the hydrogen generation rates provided by the two experimental setups. The GC used on the experimental setup for runs GN80 and GN82 had a better separation of helium and hydrogen than the GC used on the experimental setup for runs GN81 and GN83. Thus, the bias explained in the previous paragraph was less pronounced for runs GN 80 and GN82 than for runs GN81 and GN83. The difference in this bias may be the sole difference noted between the four runs performed.

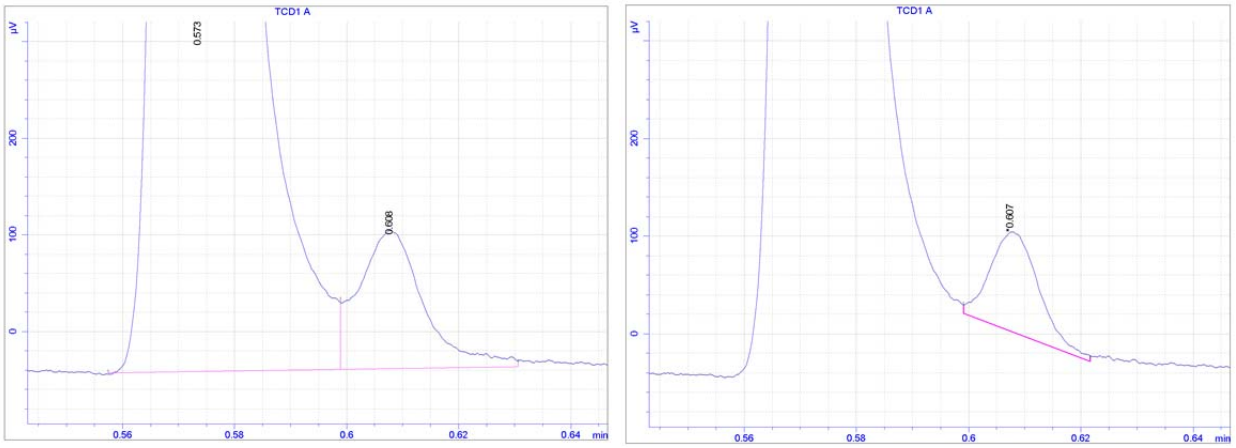

Figure 4-1. Example GC chromatogram for He and H_2 during GN80

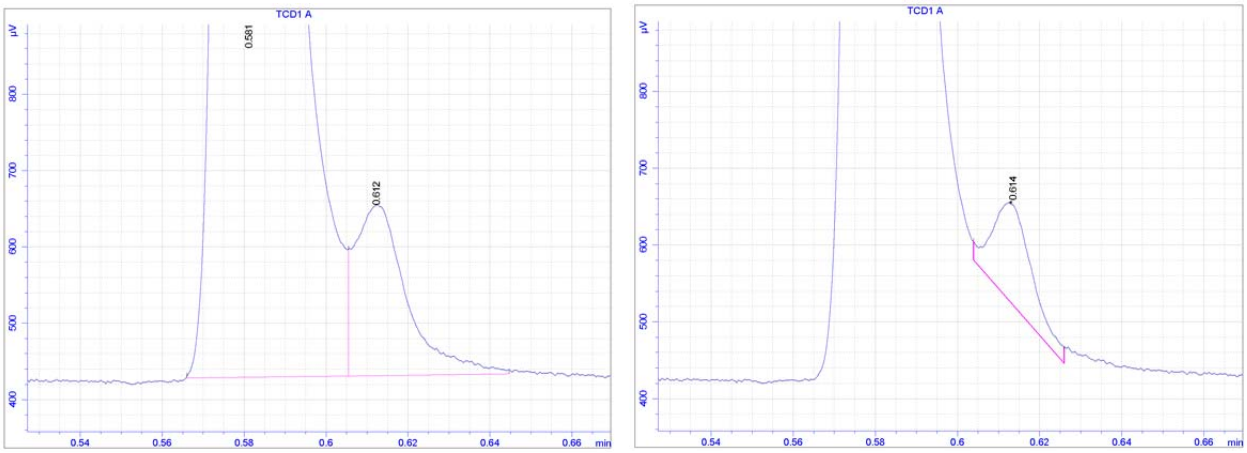

Figure 4-2. Example GC chromatogram for He and H_2 during GN83

The following are examples of some additional factors do not need to be included in the hydrogen measurement uncertainty. The small variation in volume and pressure of individual GC injections introduce error that is bounded by the other factors that are considered to influence the hydrogen measurement uncertainty. The unknown loss offgas from the system is mitigated by use of the helium tracer and adjustment of the hydrogen measurement values when losses are noted.

The high bias in the hydrogen measurement due to the influence of the helium tracer on the integration of small hydrogen peaks greatly outweighs the other uncertainties and potential low biases in this testing. We do not adjust for the high bias of the hydrogen measurement from the influence of the helium tracer to keep the hydrogen measurement conservatively high. This bias decreases as the hydrogen concentration increases.

4.3 Hydrogen Generation Mechanisms and Chemistry

With the nitric-glycolic flowsheet, a small amount of hydrogen is formed and released late in the CPC process. Hydrogen concentration was below the detectable level by GC in the first approximately 24 hours of the SRAT runs. Hydrogen was then apparent for the remainder of the SRAT and SME cycles (as long as boiling was maintained).

One potential explanation for the production of small amounts of hydrogen late in the CPC process is the catalytic decomposition of formate by ruthenium.[26] This is one of the mechanisms at play in the nitric-formic flowsheet, and may be occurring in the nitric-glycolic flowsheet at much lower rates due to the greatly reduced concentration of formate in the process.

4.4 False Peaks in MS Measurements of Hydrogen

As seen in Figure 3-3 through Figure 3-6, there are sharp peaks of hydrogen measured by the MS that are not reflected in the GC measurements. Additionally, there is hydrogen apparent by MS at the beginning of the CPC cycle that is not evident by GC. It is hypothesized that these peaks in the MS for m/z = 2 are not due to hydrogen in the CPC vessel but rather are due to an analytical interference. As currently tuned, the quadrupole M/S is apparently susceptible to false m/z = 2 readings for periods when too many m/z=1

fragments are encountered. This is noted in MS data both at the beginning of the CPC cycle and just after antifoam addition.

Figure 4-3 and Figure 4-4 contain comparisons of the HMDSO and hydrogen concentrations for runs GN80 and GN82, respectively. The peaks in HMDSO concentration correspond to each antifoam addition and to the initial boiling after completion of glycolic acid addition. The MS data contain spikes in hydrogen that correspond to each HMDSO peaks. These hydrogen spikes that correlate with HMDSO concentration are not seen by the GC. Our hypothesis is that these apparent increases in hydrogen coincident with antifoam addition do not reflect actual CPC offgas concentrations of hydrogen. Rather, some interaction of the HMDSO within the MS is contributing to high hydrogen (m/z = 2) measurements by the MS.

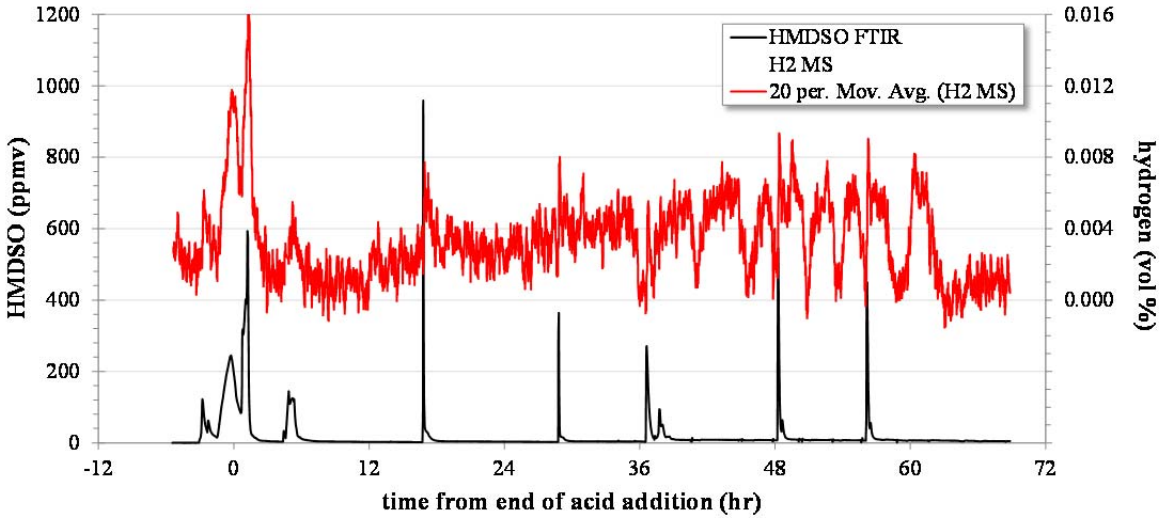

Figure 4-3. HMDSO by FTIR and hydrogen by MS from GN80

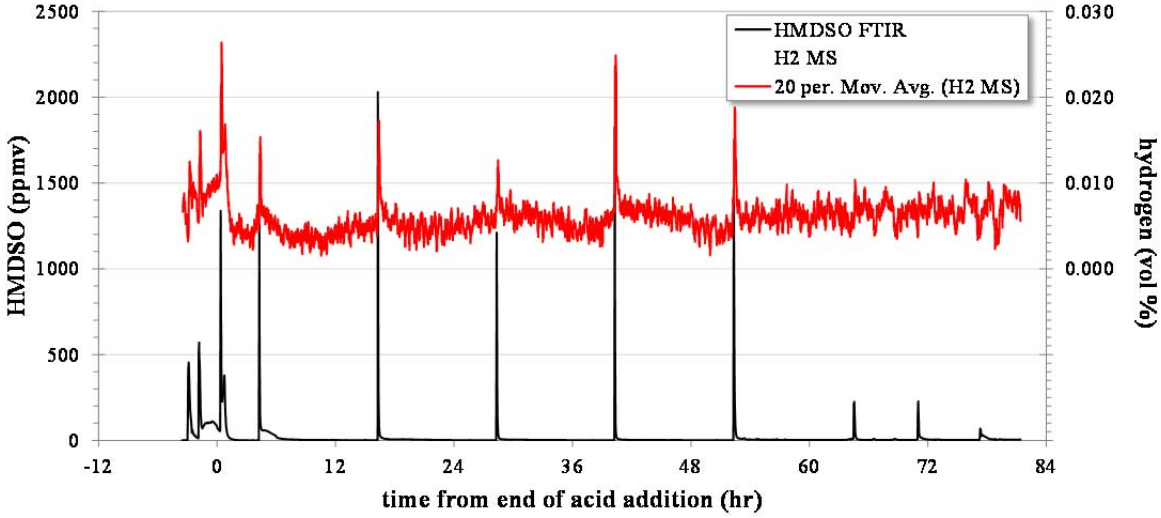

Figure 4-4. HMDSO by FTIR and hydrogen by MS from GN82

Figure 4-5 contains a plot of hydrogen by MS and HMDSO by FTIR for a previous run, GN77. During GN77, no hydrogen was seen by GC. Figure 4-6 is data for run GN77 focused on the time around 36.5 hours. The hydrogen peak shown in Figure 4-6 was measured by the MS over a period of greater than 3 minutes. This time period is long enough that at least one gas sample taken by the GC should have captured a hydrogen concentration above the GC detection limit. This supports that the hydrogen peaks apparent by MS that are coincident with HMDSO peaks are not due to hydrogen in the CPC process but rather are due to some other factor such as an interference.

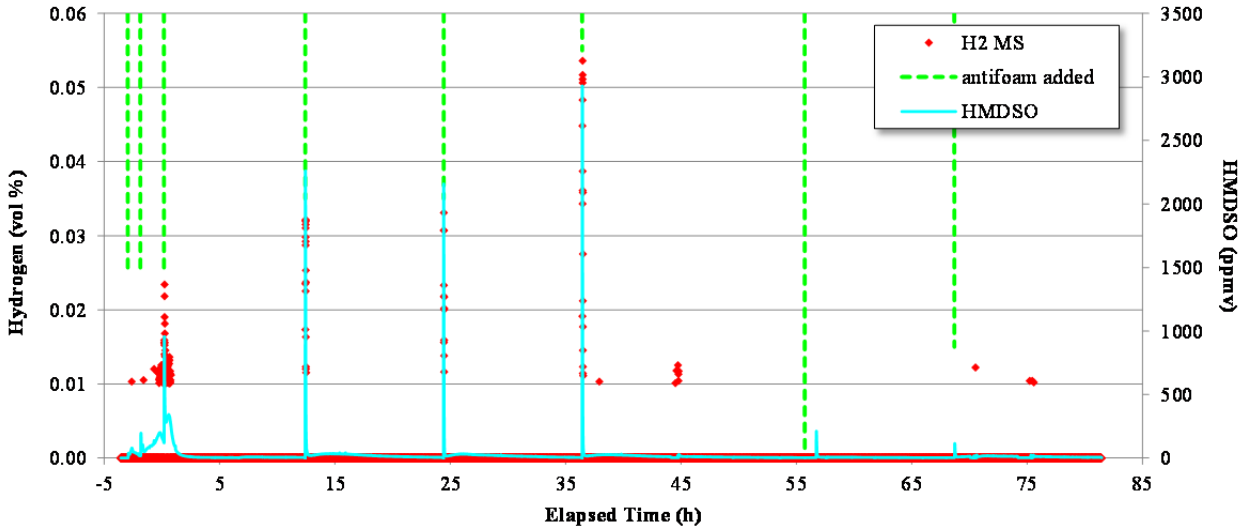

Figure 4-5. Comparison of HMDSO by FTIR and hydrogen by MS from GN77

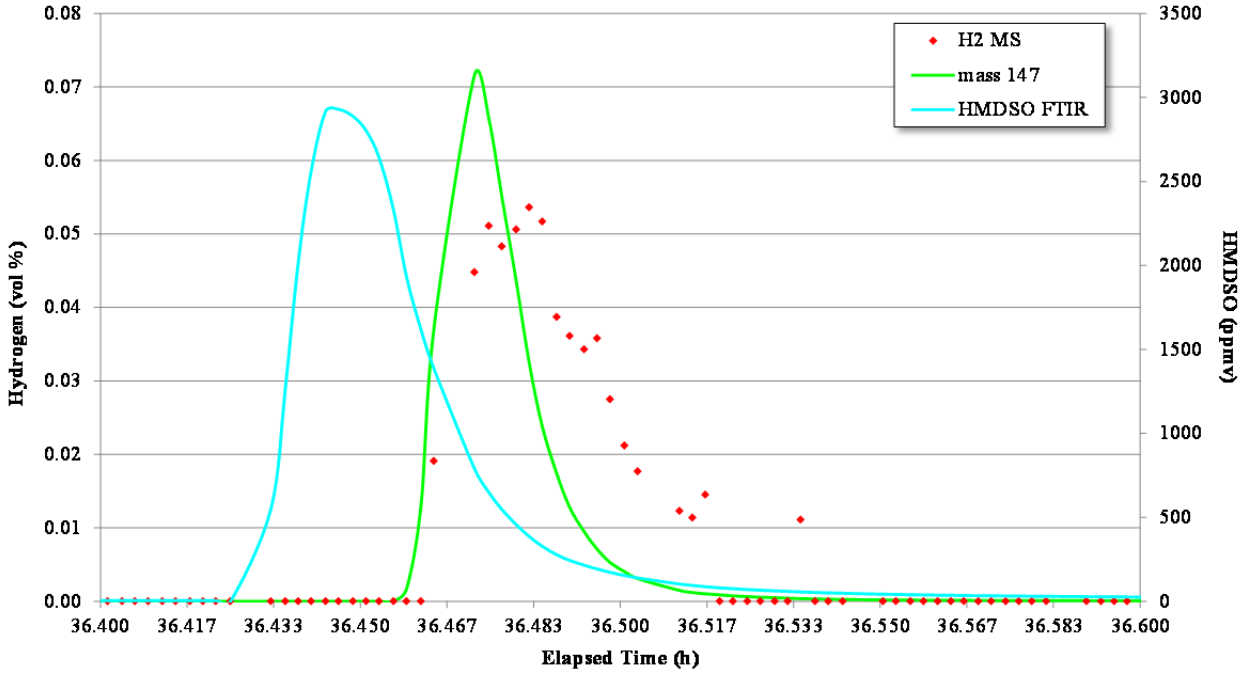

Figure 4-6. HMDSO and hydrogen results for peak near 36.5 hours of run GN77

5.0 Quality Assurance

Data are recorded in the SRNL electronic notebook system in experiments c7605-00021-08 and A6583-00142-05 and various PSAL notebooks.

Requirements for performing reviews of technical reports and the extent of review are established in manual E7 2.60. SRNL documents the extent and type of review using the SRNL Technical Report Design Checklist contained in WSRC-IM-2002-00011, Rev. 2.

6.0 Acknowledgements

The authors acknowledge the efforts of many other chemists, engineers, and technicians that supported this work. Dan Lambert wrote a white paper that laid out the optimal experimental plan for gathering this data. The CPC apparatus was constructed by Gary Dobos and Curt Sexton of the SRNL Glass Apparatus Laboratory. The CPC apparatus was setup and operated by Jon Duval, Vickie Williams, Phyllis Workman, Kim Wyszynski and Wanda Matthews. Other support staff included Holly Hall, Frances Williams, Mike Stone, and Dan Lambert. Sample analysis by PSAL was supervised by Whitney Riley and David Best and supported by Kim Wyszynski and Beverly Wall. Jack Zamecnik and John Pareizs were involved with the setup and data processing for the offgas equipment. Tommy Edwards was instrumental in application of uncertainties to the hydrogen offgas data.

7.0 Conclusions

The following are key observations from this work:

1. When compared to the nitric-formic flowsheet, hydrogen production remained very low for these nitric-glycolic flowsheet tests. For laboratory results converted to the DWPF scale but without including measurement uncertainty, the maximum hydrogen production and release rate for the current runs was 0.0028 lb/hr in the SRAT and 0.0024 lb/hr in the SME. For this testing, the maximum hydrogen production and release rate was 0.43% of the current SRAT limit of 0.65 lb/hr and 1.1 % of the current SME limit of 0.223 lb/hr.

2. Reviewing current and previous nitric-glycolic flowsheet runs for which formic acid was not added and heat transfer or heating rod temperature issues were not encountered, the highest peak DWPF-scale hydrogen generation rate in the SRAT cycle including measurement uncertainty was 0.0066 lb/hr (at the upper bound of the 95% confidence interval) in three separate tests (GN41, GN70, and GN82). Similarly, the highest peak DWPF-scale hydrogen generation rate in the SME cycle including measurement uncertainty was 0.0087 lb/hr (at the upper bound of the 95% confidence interval) for 220-L scaled run GN79. Run GN36 produced the highest valid hydrogen generation rate in the SME (0.0111 lb/hr), but formic acid was added with the frit addition and difficulties with the measurement prevent estimation of the measurement uncertainty.

3. Run GN79 had the highest overall peak hydrogen concentration measured for the runs that did not have formic acid addition in the SRAT or the SME and that did not have temperature excursions or heat transfer issues. The SME cycle of GN79 had a peak hydrogen concentration of 0.038 vol% (including measurement uncertainty), which is only 0.95% of the lower

flammability limit of hydrogen in air. The peak levels of hydrogen produced during the nitric-glycolic flowsheet testing were reliably and significantly less than 25% of the lower flammability limit of hydrogen in air.

4. For two runs in this testing, additional glycolic acid was introduced at the end of the SME cycle. The glycolic acid dump appeared to lower the rate of hydrogen generation that was occurring at the end of the SME cycle. The biggest impact of the glycolic acid dump was the increase in the amount of metal cations in solution, specifically iron, aluminum, and nickel. After the glycolic acid dump, the oxalate in the SME product became nearly fully soluble. An increase in rheological properties and foaming during processing were encountered after the glycolic acid dump.

5. The pH measurements of the SRAT products were approximately 4.5 and remained at nearly this level through the SME cycle. The additional glycolic acid dump performed on two of the runs further reduced the pH of the SME material to approximately 3.

6. The loss of glycolate in the SRAT cycles was ranged from 13% to 19% and the nitrite-to-nitrate conversion ranged from 51% to 64%. These values are in line with previous nitric-glycolic flowsheet testing.

7. The largest peak in hexamethyldisiloxane concentration from the decomposition of diluted antifoam was 2020 ppmv for a very short duration during a SRAT cycle. This concentration corresponds to a peak generation or release rate of 14.0 mol/hr on the DWPF scale.

8.0 Recommendations

When performing CPC simulations on non-radioactive simulants and actual waste samples, SRNL should continue quantifying the hydrogen production using GC methods. SRNL should consider replacing the helium used as a tracer gas in the SRAT and SME with another gas in order to improve the quantification of the lower levels of hydrogen produced by the alternate reductant flowsheet. A standard containing a lower concentration of hydrogen should be used to optimize the GC calibration for the alternate reductant flowsheet and potentially improve the uncertainty analysis.

The post-SME glycolic acid dump does not need to be included in future testing if the purpose of the testing is to quantify the maxim hydrogen generation rate. In these tests, the acid dump was shown to cease the formation of hydrogen at the end of the SME cycle. Future testing with extra glycolic and nitric acid may be warranted to understand the increased solubility of some metals, although no safety impacting observations of metal dissolution were indicated in this work.

9.0 References

[1] E. W. Holtzscheiter, "Bounding Alternate Reductant Testing/Chemistry and REDOX Definition," X-TTR-S-00024, Revision 0, August 21, 2014.

[2] C. J. Martino, "Task Technical and Quality Assurance Plan for Bounding Hydrogen Tests of the Nitric-Glycolic Flowsheet," SRNL-RP-2014-01045, Revision 0, November 12. 2014.

[3] D. P. Lambert, "White Paper: Bounding Hydrogen Testing Program for the Nitric-Glycolic Acid Flowsheet," SRNL-L3100-2014-00139, Revision 1, September 30, 2014.

[4] D. P. Lambert, J. R. Zamecnik, J. D. Newell and C. J. Martino, "Impact of Scaling on the Nitric-Glycolic Acid Flowsheet," SRNL-STI-2014-00306, Revision 0, February 2016.

[5] T. L. White, D. P. Lambert, J. R. Zamecnik and W. T. Reiley, "Ion Chromatography (IC) Analysis of Glycolate in Simulated Waste," SRNL-STI-2015-00049, Revision 0, May 2015.

[6] D. C. Koopman, "Rheology Protocols for DWPF Samples," WSRC-RP-2004-00470, Revision 0, October 4, 2004.

[7] D. C. Koopman, "Preparation, Characterization, and Preliminary SRAT/SME Testing of a Simulant for the Hydrogen and Rheology Modifiers Program," SRNL-PSE-2007-00191, September 11, 2007.

[8] M. E. Stone, "Lab-scale CPC Equipment Setup," SRNL-L3100-2011-00127, Rev. 2, June 11, 2012.

[9] "Laboratory Scale Chemical Process Cell Simulations," Manual L29, Procedure ITS-0094, Revision 7, June 20, 2012.

[10] J. D. Newell, "Glycolic/Nitric Acid Scale SRAT/SME Testing," Experiment C7605-00021-07, SRNL E-Notebook 2014.

[11] D. P. Lambert, J. M. Pareizs and D. R. Click, "Demonstration of the Glycolic-Formic Flowsheet in the SRNL Shileded Cells," SRNL-STI-2011-00622, Revision 0, November 2011.

[12] J. R. Zamecnik and J. D. Newell, "Antifoam Degradation in the DWPF Chemical Process Cell," SRNL-L3100-2015-00088, Revision 0, May 14, 2015.

[13] D. P. Lambert, J. R. Zamecnik, J. D. Newell and M. S. Williams, "Antifoam Degradation Testing," SRNL-STI-2015-00352, Revision 0, August 20, 2015.

[14] "Heat Treatment of Waste Slurries for REDOX ($Fe^{2+}/\Sigma Fe$) and Chemical Composition Measurement," Manual L29, Procedure ITS-0052, Revision 4, December 19, 2014.

[15] "Technical Data Summary for the Defense Waste Processing Facility Sludge Plant, Part 10, Item 230," DPSTD-80-38, Revision 2, September 1982.

[16] C. J. Martino, "Analysis of Precipitated White Solids from Nitric-Glycolic Flowsheet Chemical Processing Cell Products," SRNL-L3100-2016-00004, Revision 0, February 4, 2016.

[17] D. P. Lambert and D. C. Koopman, "Glycolic-Formic Acid Flowsheet Sludge Matrix Study," SRNL-STI-2011-00275, June 30, 2011.

[18] D. P. Lambert, M. E. Stone, J. D. Newell, D. R. Best and W. T. Riley, "Glycolic-Nitric Flowsheet Demonstration," Presentation to the SRNL/SRR Plan of the Month, January 19, 2012.

[19] F. C. Johnson, M. E. Stone and D. H. Miller, "Alternate Reductant Cold Cap Evaluation Furnace Phase II Testing," SRNL-STI-2014-00157, Revision 0, September 2014.

[20] D. P. Lambert, B. R. Pickenheim, M. E. Stone, J. D. Newell and D. R. Best, "Glycolic - Formic Acid Flowsheet Final Report for Downselection Decision," SRNL-STI-2010-00523, Revision 1, March 9, 2011.

[21] D. P. Lambert, M. E. Stone, J. D. Newell, D. R. Best and J. R. Zamecnik, "Glycolic-Nitric Acid Flowsheet Demonstration of the DWPF Chemical Process Cell with Sludge and Supernate Simulants," SRNL-STI-2012-00018, Revision 1, August 2012.

[22] D. P. Lambert and J. R. Zamecnik, "Flowsheet Testing for Strip Effluent to Slurry Mix Evaporator Modifications at the Defense Waste Processing Facility," SRNL-STI-2015-00002, Revision 0, April 2015.

[23] D. P. Lambert, J. R. Zamecnik and D. R. Best, "FY13 Glycolic-Nitric Acid Flowsheet Demonstrations of the DWPF Chemical Process Cell with Simulants," SRNL-STI-2013-00343, Revision 0, March 2014.

[24] Metrodata GmbH, "GUM Workbench: User Manual for Version 1.2, 2.3, and 2.4,"

[25] H. F. Coward and G. W. Jones, "Limits of Flammability of Gases and Vapors," US Bureau of Mines Bulletin 503, 1953.

[26] D. C. Koopman, "Noble Metal Chemistry and Hydrogen Generation during Simulated DWPF Melter Feed Preparation," WSRC-STI-2008-00002, Revision 0, June 2008.

Appendix A.

Table A-1. REDOX measurements of glass made from SME products

	Fe^{2+}	tot.Fe	Fe^{2+}/tot.Fe
GN80-1	0.021	0.322	0.065
	0.019	0.321	0.059
GN80-2	0.116	0.381	0.304
	0.117	0.381	0.307
GN81-1	0.111	0.374	0.297
	0.111	0.374	0.297
GN81-2	0.030	0.359	0.084
	0.031	0.360	0.086
GN82-1	0.026	0.484	0.054
	0.026	0.485	0.054
GN82-2	0.021	0.437	0.048
	0.021	0.435	0.048
GN82-3	0.027	0.412	0.066
	0.027	0.414	0.065
GN83-1	<0.010	0.415	All Fe^{3+}
	<0.010	0.416	All Fe^{3+}
GN83-2	<0.010	0.393	All Fe^{3+}
	<0.010	0.394	All Fe^{3+}
GN83-3	<0.010	0.442	All Fe^{3+}
	<0.010	0.440	All Fe^{3+}

Table A-2. REDOX measurements of glass made from glycolic acid dump products

	Fe^{2+}	tot.Fe	Fe^{2+}/tot.Fe
GN80-1	0.557	0.570	0.977
	0.558	0.573	0.974
GN80-2	0.636	0.637	All Fe^{2+}
	0.634	0.637	All Fe^{2+}
GN80-3	0.710	0.714	All Fe^{2+}
	0.712	0.715	All Fe^{2+}
GN81-1	0.354	0.419	0.845
	0.340	0.417	0.815
GN81-2	0.408	0.571	0.715
	0.409	0.571	0.716
GN81-3	0.490	0.498	All Fe^{2+}
	0.488	0.497	All Fe^{2+}

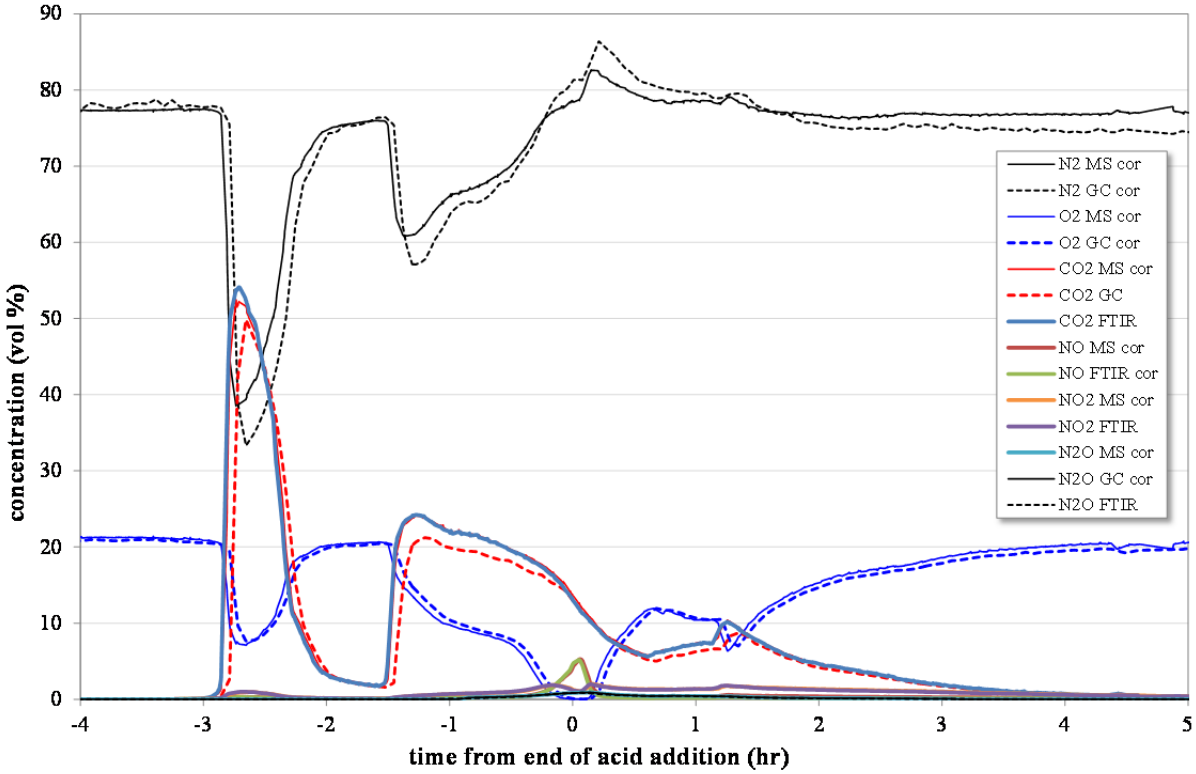

Figure A-1. Gasses emitted early in the SRAT cycle of GN80

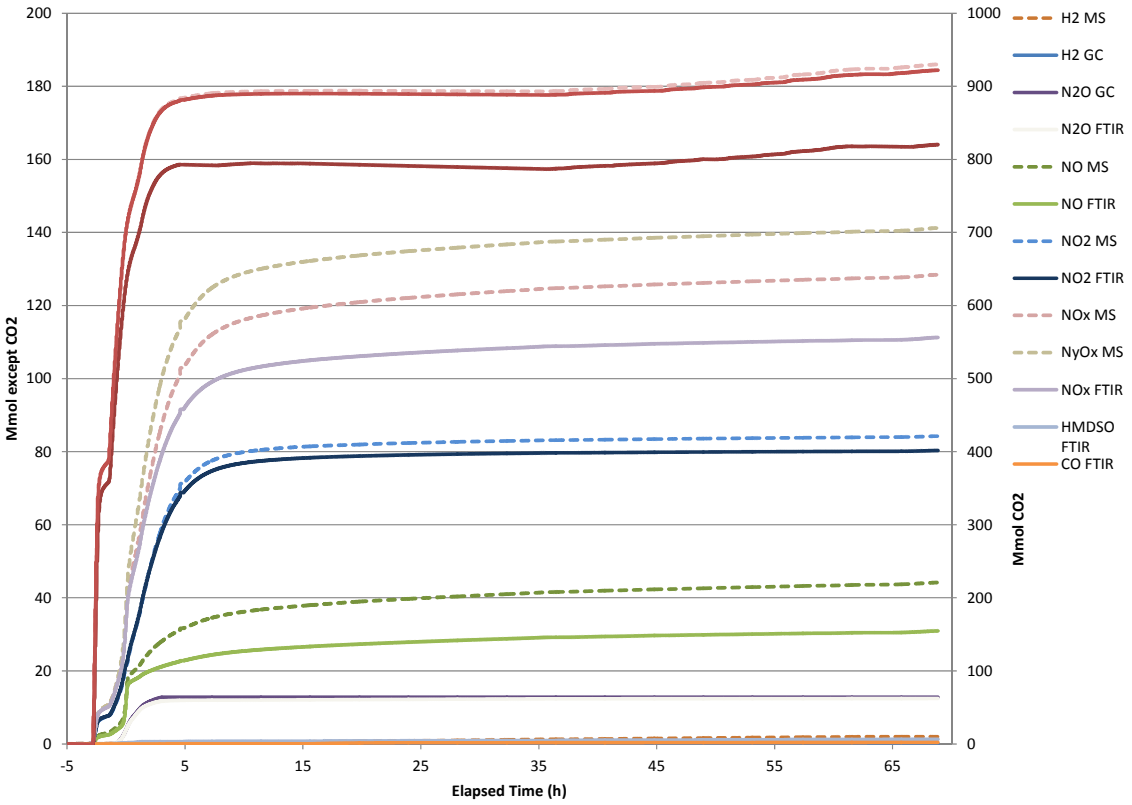

Figure A-2. Cumulative gas emissions from GN80

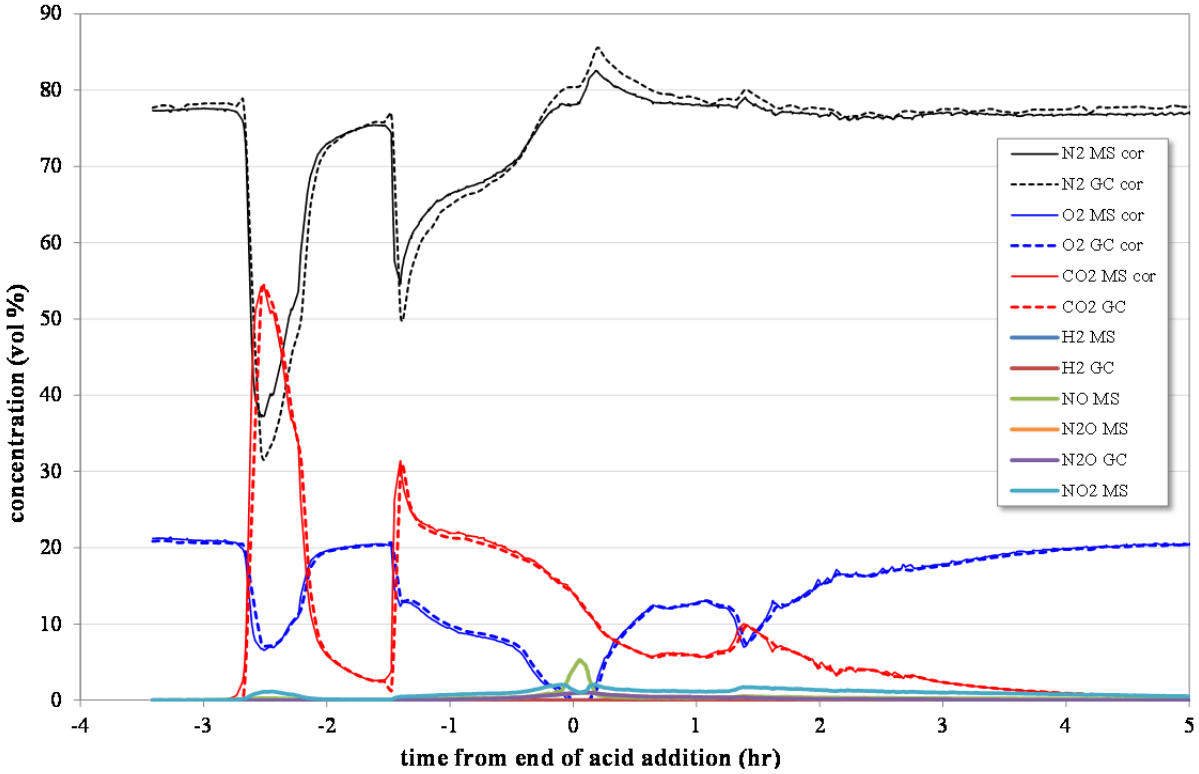

Figure A-3. Gasses emitted early in the SRAT cycle of GN81

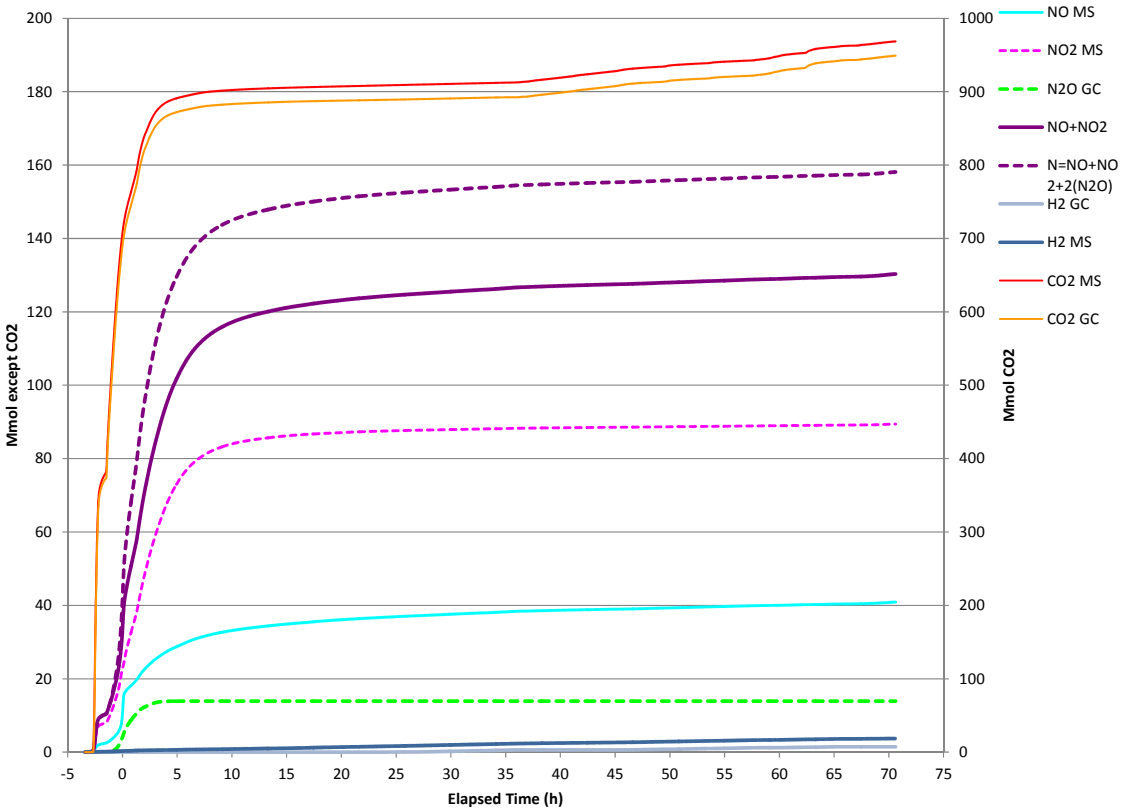

Figure A-4. Cumulative gas emissions from GN81

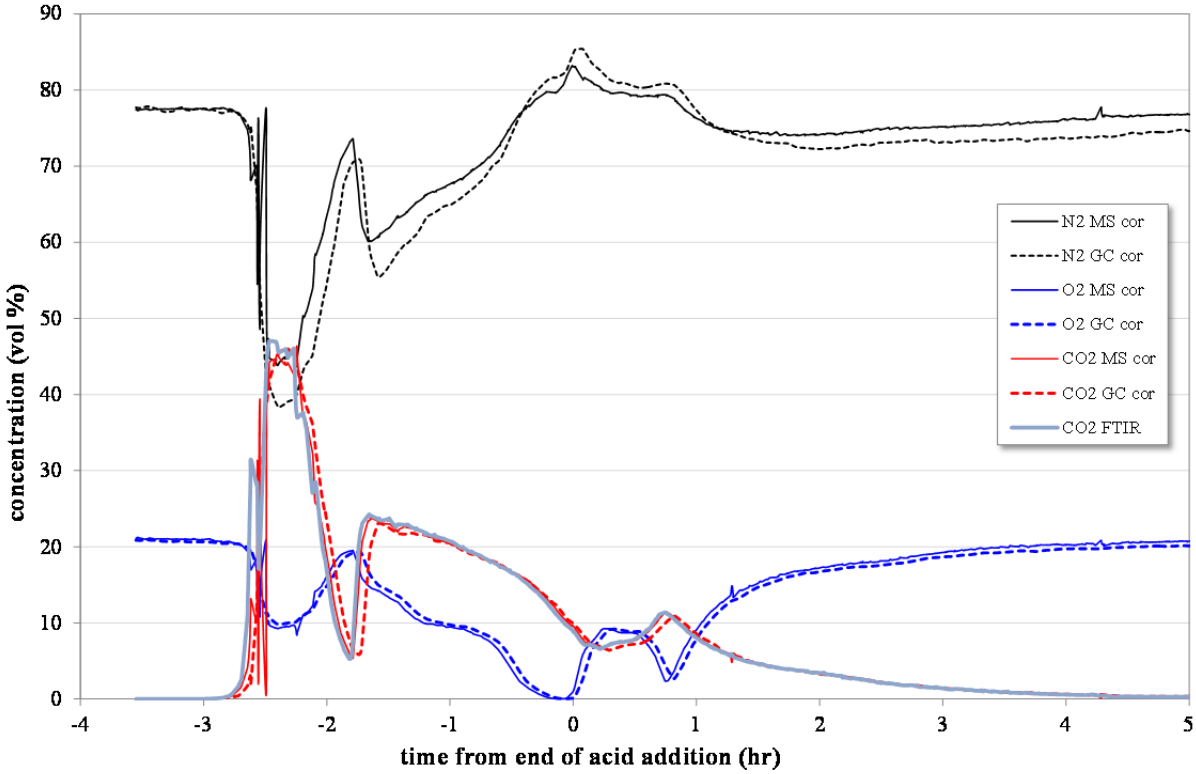

Figure A-5. Gasses emitted early in the SRAT cycle of GN82

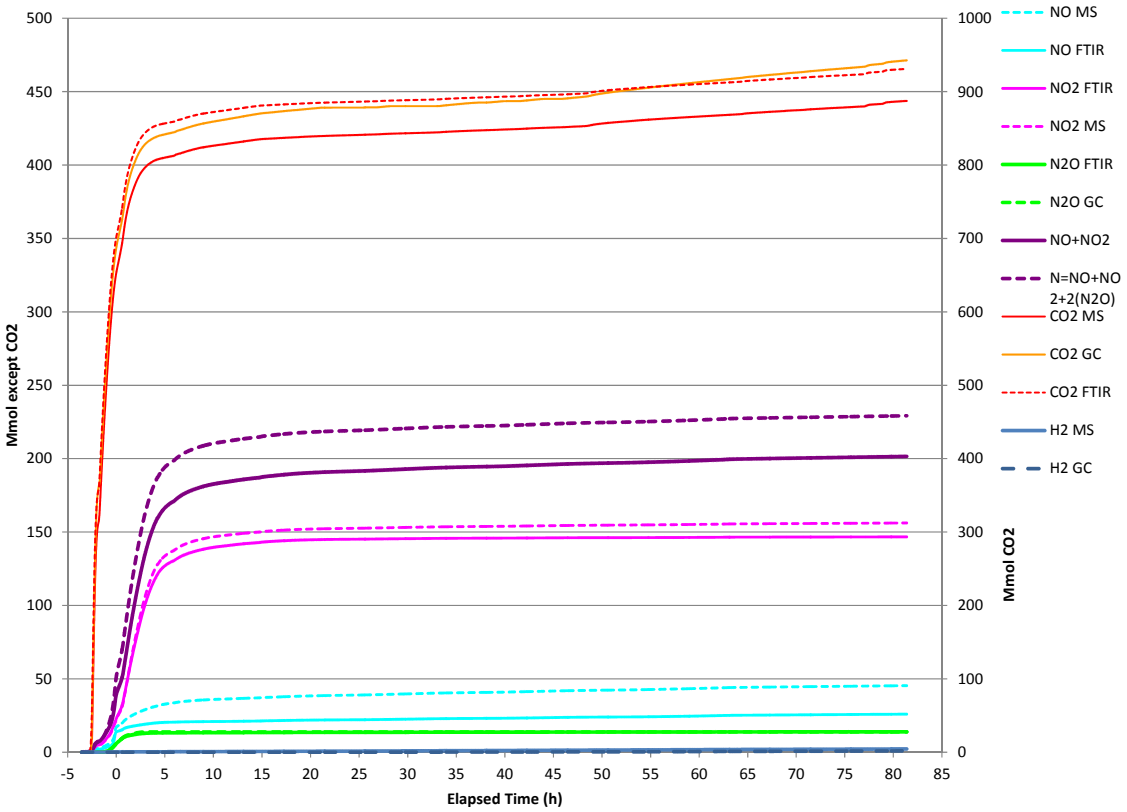

Figure A-6. Cumulative gas emissions from GN82

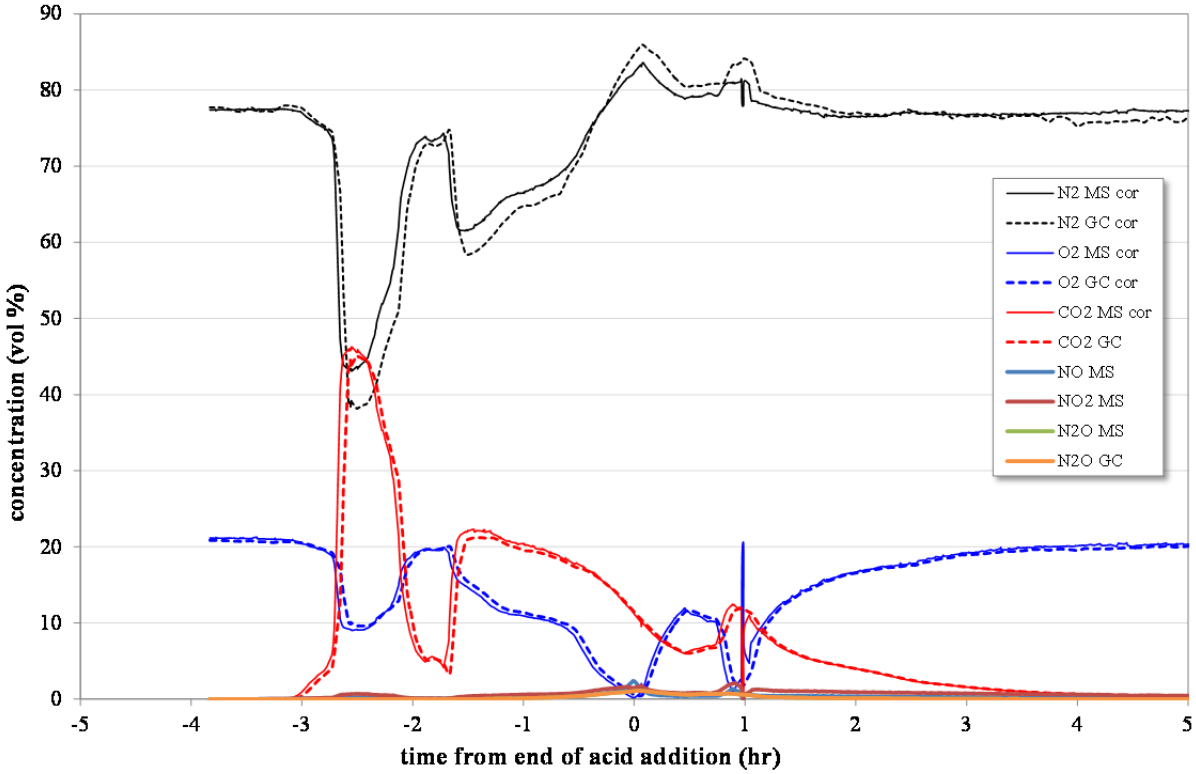

Figure A-7. Gasses emitted early in the SRAT cycle of GN83

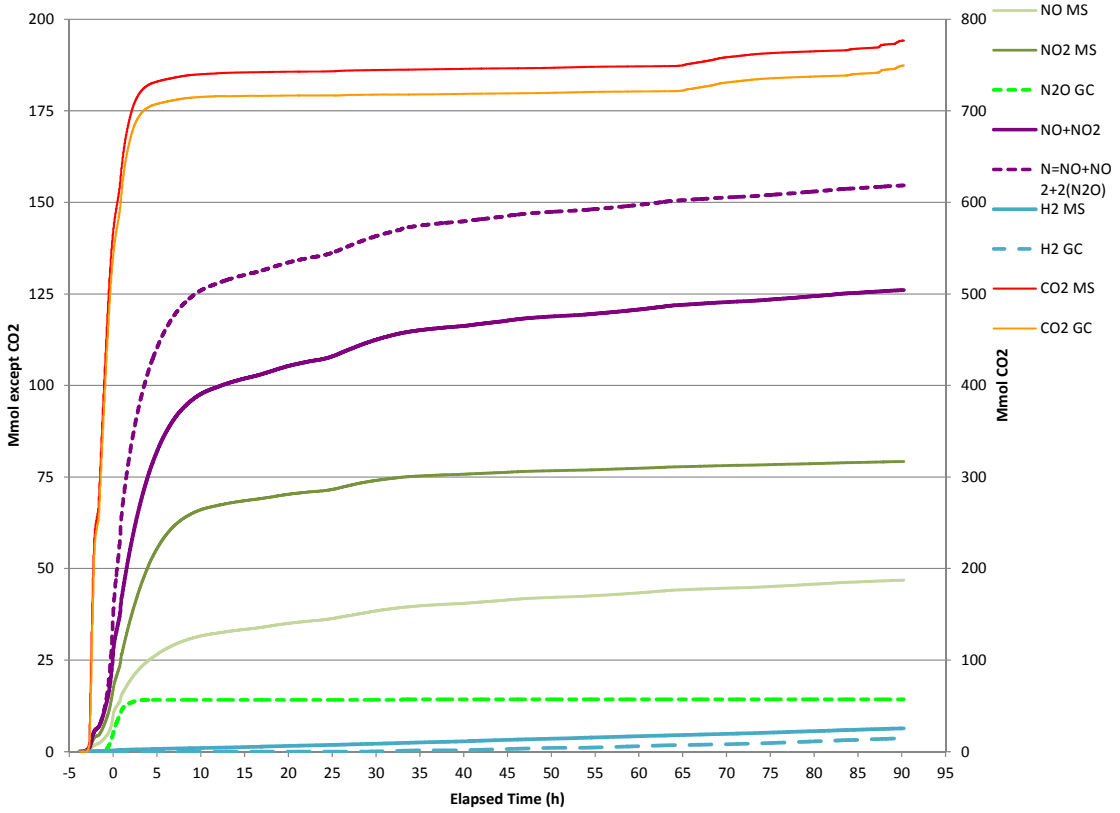

Figure A-8. Cumulative gas emissions from GN83

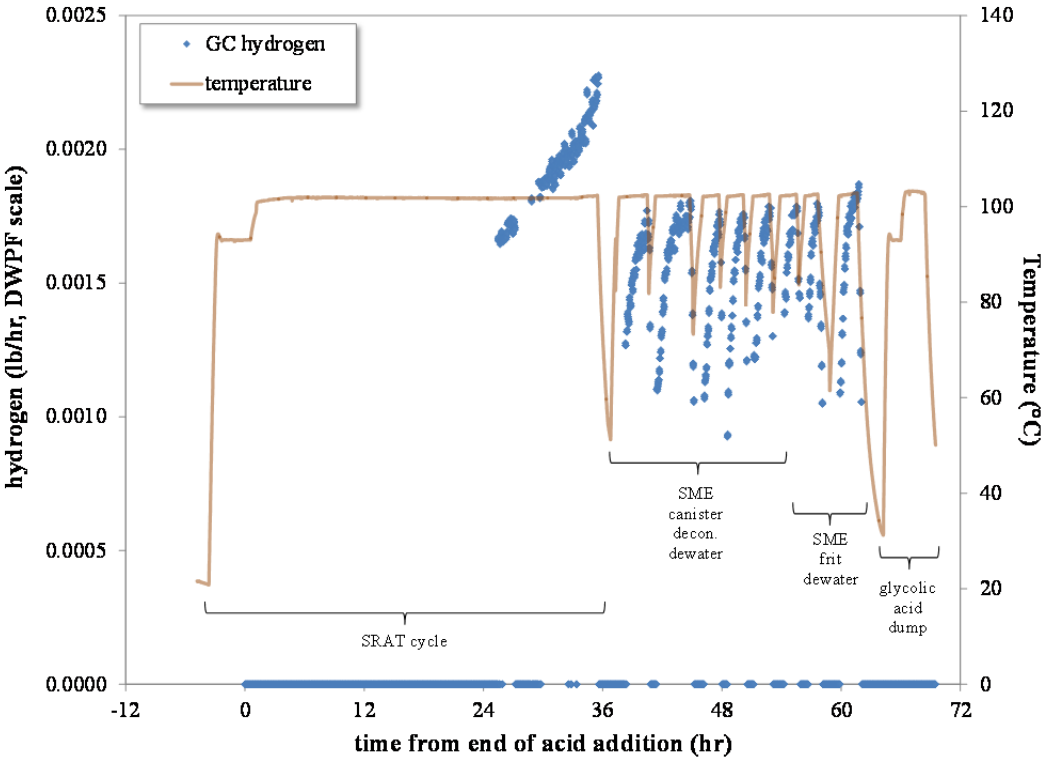

Figure A-9. hydrogen produced during GN80 on the DWPF scale

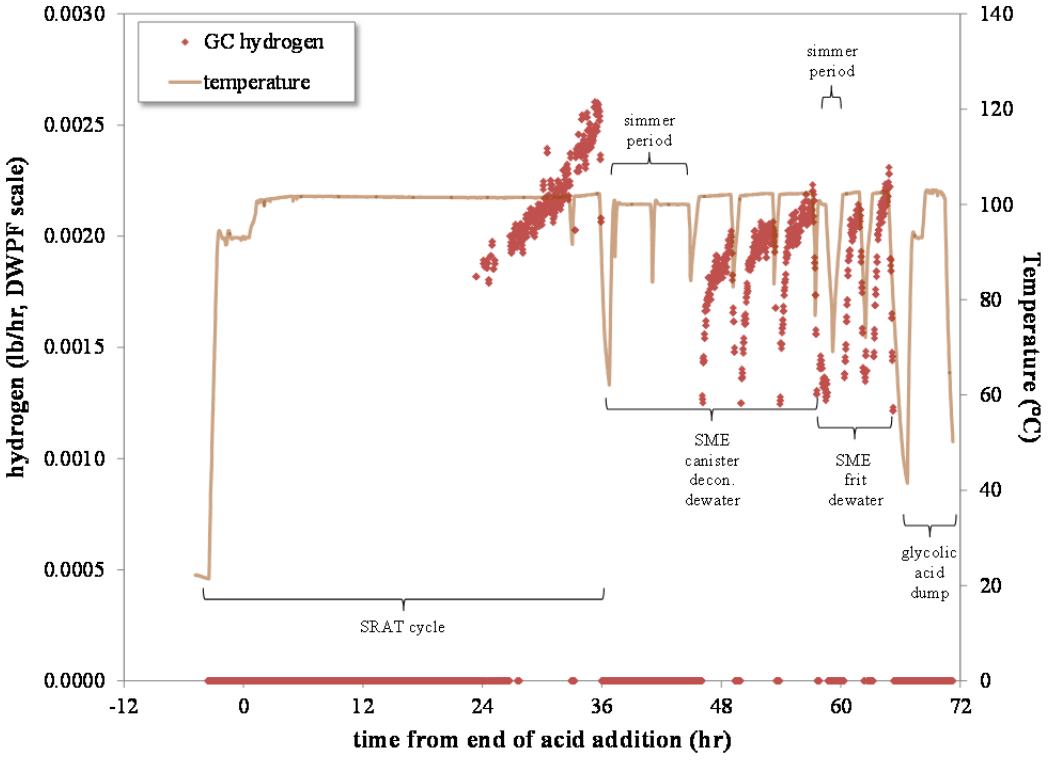

Figure A-10. hydrogen produced during GN81 on the DWPF scale

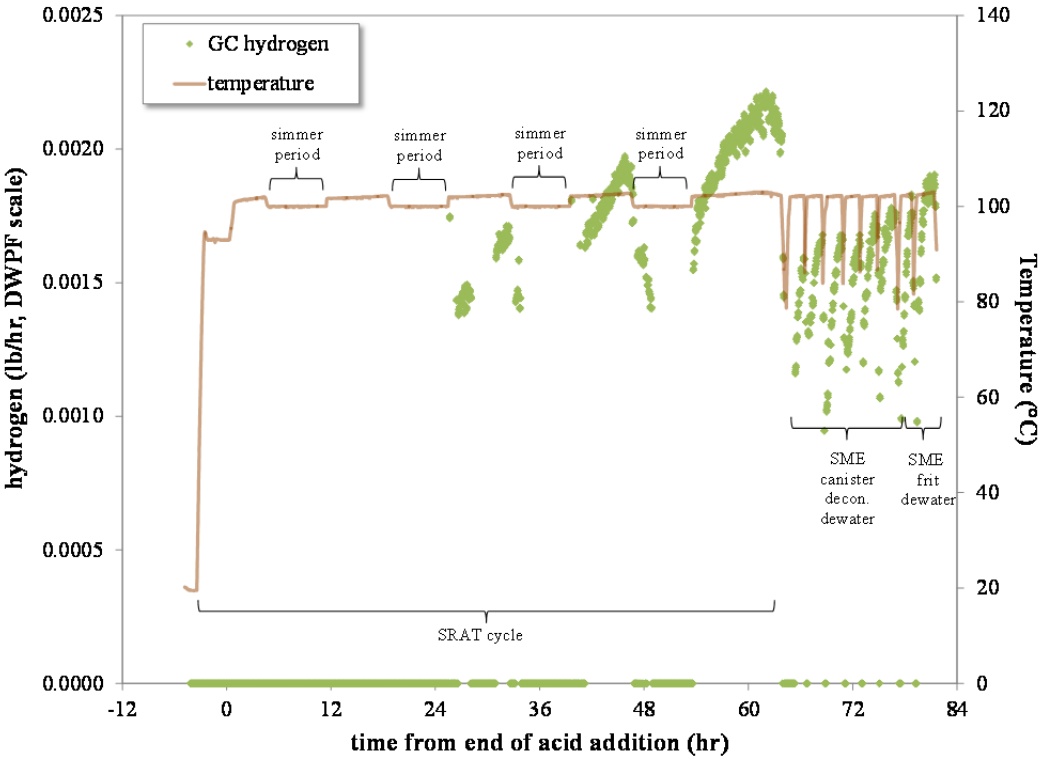

Figure A-11. hydrogen produced during GN82 on the DWPF scale

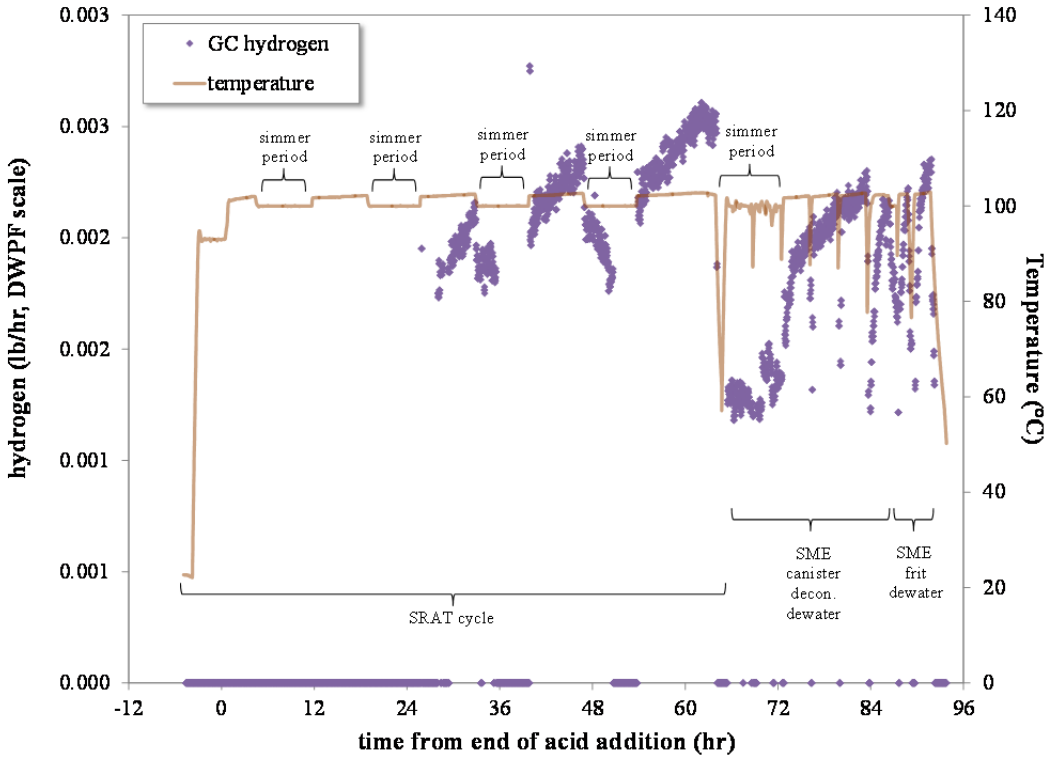

Figure A-12. hydrogen produced during GN83 on the DWPF scale

Distribution:

T. B. Brown, 773-A
M. E. Cercy, 773-42A
D. A. Crowley, 773-43A
D. E. Dooley, 999-W
A. P. Fellinger. 773-42A
S. D. Fink, 773-A
C. C. Herman, 773-A
D. T. Hobbs, 773-A
E. N. Hoffman, 999-W
J. E. Hyatt, 773-A
K. M. Kostelnik, 773-42A
B. B. Looney, 773-42A
D. A. McGuire, 773-42A
T. O. Oliver, 773-42A
F. M. Pennebaker, 773-42A
G. N. Smoland, 773-42A
M. E. Stone, 999-W
B. J. Wiedenman, 773-42A
W. R. Wilmarth, 773-A
Records Administration (EDWS)
H. P. Boyd, 704-27S
J. M. Bricker, 704-S
J. S. Contardi, 704-56H
T. L. Fellinger, 766-H
E. J. Freed, 704-S
J. M. Gillam, 766-H
B. A. Hamm, 766-H
E. W. Holtzscheiter, 766-H
J. F. Iaukea, 704-27S
V. Jain, 766-H
C. J. Martino, 999-W
J. W. Ray, 704-27S
P. J. Ryan, 704-26S
M. A. Rios-Armstrong, 766-H
H. B. Shah, 766-H
D. C. Sherburne, 249-8H
S. T. Isom, 773-67A
T. E. Colleran, 773-67[a]
J. D. Newell, 999-W
D. P. Lambert, 999-W
J. R. Zamecnik, 999-W
M. S. Williams, 999-W
T. E. Smith, 999-W
W. H. Whoodham, 999-W